School of Engineering

Design and Development of a Progressive Cavity Pump for Extrusion Based Bioprinting

Yusuf Furkan Ugurluoglu

Submitted for the degree of Doctor of Philosophy in the School of Engineering, Newcastle University

January 2024

ABSTRACT

Bioprinting is an emerging technology with the ability to fabricate customised tissue constructs. Extrusion-based bioprinting (EBB) attracts considerable attention due to its ability to continuously extrude high-viscous materials with the necessary precision. While currently available EBB methods, mechanical or pneumatic driven syringes-based systems, provide an acceptable extrusion, several limitations remain, such as low accuracy, the ability to retract material from the nozzle and cartridge volume restriction. Recently, progressive cavity pumps (PCPs) have started to be used in the field of bioprinting as an advanced dispensing unit and have shown promising results. However, they require an adaptation for bioprinting needs in terms of easy cleaning, low cost and low dead volume. This study aimed to develop a low-cost, scalable, easy-to-clean extrusion system based on the PCP principle to overcome the mentioned limitations.

PCPs have a long history; however, the working mechanism of the first design and core components have almost never changed. Developing a new product requires extensive research on problem definition and many iterations of possible solutions. Recent developments in the field of additive manufacturing (AM) have led to a renewed interest in the spiral product development process. The spiral development model allows the generation of various concepts quickly with AM's help. Therefore, it was more likely to find an innovative solution for the current drawbacks of dispensing PCPs by obtaining insight from each concept. Consequently, a spiral development model was established in this research. The development process consists of three main phases: initials, concept development and product development.

The initials phase begins with the problem definition: the high cost of PCP and control unit, cleaning difficulty, and scalability of PCPs. Based on the problem definition, background research was conducted, including literature research, user questionnaire and user interview. Subsequently, a commercial syringe pump was evaluated to highlight the limitations of current technology. The syringe pump evaluation step aimed to explore the relationship between extrusion accuracy and syringe features, including plunger rubber compressibility and the amount of volume inside the syringe. The weighing scale and the flow rate sensor

were used to assess the extrusion accuracy. Results showed that the plunger rubber has a negative impact on extrusion accuracy due to its compressibility. Likewise, when the amount of compressed volume inside the syringe increases, the start and stop accuracy of the extrusion decreases. Finally, a conventional PCP design was reverse-engineered to understand better the fundamentals of PCPs, including the design's working principle and essential features. To conclude the initials phase, the collected information was expressed as technical terms and specifications to develop the requirements of the concept development phase.

The key research question of this study was whether or not there is a better unknown PCP mechanism for EBB. Due to the nature of the spiral development process, the concept development phase requires many iterations of PCP designs. Therefore, an application programming interface (API) was developed to enable rapid design iterations of PCP components. Subsequently, various concepts were developed by collecting information from the reverse engineering phase and previous concepts. These concepts were evaluated to produce a better PCP design, either changing the working mechanism or cross-sectional geometry design of the rotor and stator. Consequently, three PCP concepts were designed, prototyped and evaluated to meet the EBB requirements, and the product development phase began with a selected concept.

The selected concept was redesigned and prototyped for validation tests in the product development phase. A previously developed open-source and commercial syringe pumps were used to validate the novel PCP concept. The developed PCP showed better performance than syringe pumps for highly viscous materials. In addition, the aim of the low-cost, scalable and easy-to-clean PCP was successfully developed. The proposed spiral development model has the potential to offer a quick product development methodology. In addition, the developed PCP has excellent potential as an advanced dispensing unit for highly viscous fluids and pastes.

ACKNOWLEDGEMENTS

Thanks to the One who created us, I was able to complete this journey with the permission of the best of creators and planners.

Firstly, I am grateful to Dr Javier Munguia Valenzuela for his comments and guidance since the first days of my PhD. I have learned how I can be a well-qualified researcher from him. Specifically, I would like to thank Dr Piergiorgio Gentile for his unending encouragement from the beginning to the end of this hard journey. I am also grateful to Dr Ana Ferreira-Duarte for her support.

I am also grateful to my dear friends/brothers Azizkhon Afzalov, Halil Gurbuz, Usame Gurbuz, Metin Koyuncu, Fatih Tuysuz, Ali Mese, Nurettin Ayvali, Fatih Cure, Furkan Celiktas, Furkan Tektas, Usame Altuntas, Muhammed Cavus, Emre Ozturk, Oguzhan Kalyon, Umit Demirbaga, Cafer Deniz, Sebih Oruc, Huseyin Ayan, Muhammed Karayagli, Yasin Ozturk, Ibrahim Baktir, Muhammet Erel, Salih Gul, Emre Yurtkuran, Abdülkadir Altunsoy, Furkan Kaya, Furkan Korkmaz, Fatih Gezer, Hasan Tekin, Hasan Ozcan, Ali Akay, and so on.

I would like to thank the Ministry of National Education of the Republic of Turkey for granting me the during my PhD research.

Last and most importantly, I am especially grateful to my wife, Esma, for her unfailing support, incredible patience and continuous encouragement throughout my years of study and through the process of researching and writing this thesis. I am grateful to my dear daughter, Meryem Vera, who grew up with my doctoral thesis, for making this process fun for me. Also, I am grateful to my parents and brothers, who supported me during my life with their prayers.

PUBLICATIONS

1. Ugurluoglu, Y. F., Ferreira, A. M., Gentile, P., & Munguia, J. (2023). Conceptual design and development of a progressive cavity pump for extrusion-based additive manufacturing applications. *CIRP Journal of Manufacturing Science and Technology, 46*, 191–203. doi:10.1016/j.cirpj.2023.08.011

2. Ugurluoglu, Y. F., Gentile, P., Ferreira, A.M., & Munguia, J. (2021), 'Effect of process parameters of the positive displacement pump for extrusion-based bioprinting application', *Journal of Additive Manufacturing Technologies* 1(2), 560-560.

3. Ugurluoglu, Y. F., Gentile, P., Ferreira, A.M., & Munguia, J. (2019), 'Development of a Bioprinting Extrusion System', *Newcastle University Internal Engineering Conference*.

4. Ugurluoglu, Y. F., Gentile, P., Ferreira, A.M., & Munguia, J. (2018), 'Design and Validation of Multi-material 3D Bioprinter', *Newcastle University Internal Engineering Conference*.

5. Munguia, J., Ma, Z., & Ugurluoglu, Y. F. (2018), 'Towards the Digital Hospital: From Implant Design to In-Clinic Bio Fabrication', *International Conference on the Development of Biomedical Engineering in Vietnam*, 341-345.

CONTENTS

LIST OF FIGURES

LIST OF TABLES

NOMENCLATURE

N	Number of lobe
$\vec{r}$	Position vector
$\vec{T}$	Tangent vector
$\vec{K}$	Curvature vector
$\vec{n}$	Unit normal vector
w	Tolerance (design)
r	Generator circle radius (design)
R	Base circle radius (design)
P_s	Stator pitch
P_r	Rotor pitch
A_F	Flow area
A_N	Flow area of N number of lobe
e	Eccentricity (design)
Q	Volumetric flow rate
V	Rotational speed of the rotor (design)
F_p	Theoretical pump factor
L_t	Layer thickness
D_n	Needle diameter
V_p	Printing velocity
ΔP	Pressure difference (Hagen-Poiseuille)
μ	Dynamic viscosity (Hagen-Poiseuille)
L	Needle length (Hagen-Poiseuille)
R	Needle radius (Hagen-Poiseuille)
T	Torque (torque)
d_m	Mean diameter (torque)
f	Coefficient of friction (torque)
l	Lead distance (torque)

LIST OF ABBREVIATIONS

3D	Three-dimensional
AM	Additive Manufacturing
API	Application Programming Interface
CAD	Computer-aided Design
DfAM	Design for Additive Manufacturing
DIW	Direct Ink Writing
EBB	Extrusion Based Bioprinting
ECM	Extracellular Matrix
FDM	Fused Deposition Modelling
FFF	Fused Filament
G-code	Geometric Code
LDW	Laser Direct Writing
LVSP	Large Volume Syringe Pump
MRI	Magnetic Resonance Imaging
PA12	Polyamide 12
PCP	Progressive Cavity Pump
PLA	Polylactic Acid
PMMA	Polymethyl methacrylate
SLA	Stereolithography
SLS	Selective Laser Sintering
STL	Stereolithography File
TE	Tissue Engineering
UV	Ultraviolet

1

INTRODUCTION

1.1 Background

In the last decade, additive manufacturing (AM) has gained significant attention among hobbyists, academia, and industry. AM is defined as the "process of joining materials to make parts from 3D model data, usually layer upon layer, as opposed to subtractive manufacturing and formative manufacturing methodologies" (ISO/ASTM, 2021). AM processes can be classified into seven categories: vat photopolymerisation, binder jetting, powder bed fusion, sheet lamination, direct energy deposition, material jetting and material extrusion (ISO/ASTM), 2015).

In the material extrusion process, the material is dispensed in a controlled manner through a nozzle or orifice to make 3D objects. Material extrusion can be mainly divided into two categories based on the raw material form: fused filament fabrication (FFF) and 3D extrusion (Ligon et al., 2017).

FFF and Fused Deposition Modelling (FDM) use the same material extrusion technology. The term FFF is commonly used in the open-source RepRap community because FDM was patented and trademarked by Stratasys (Crump, 1992). FFF and FDM involve the 3D extrusion of thermoplastic polymers that are mechanically fed into the extrusion print head in a filament form. The extruder is heated to the required processing temperature for the polymer being used and is moved in a controlled manner to produce a 3D object. However, FDM uses a heated chamber during the printing process to reduce problems related to residual stresses and distortion during the printing phase by creating a uniform temperature around the part (Swanson et al., 1999). This feature is particularly useful for high-temperature materials. On the other hand, FFF printers often omit this feature as a means to offer a lower-cost design.

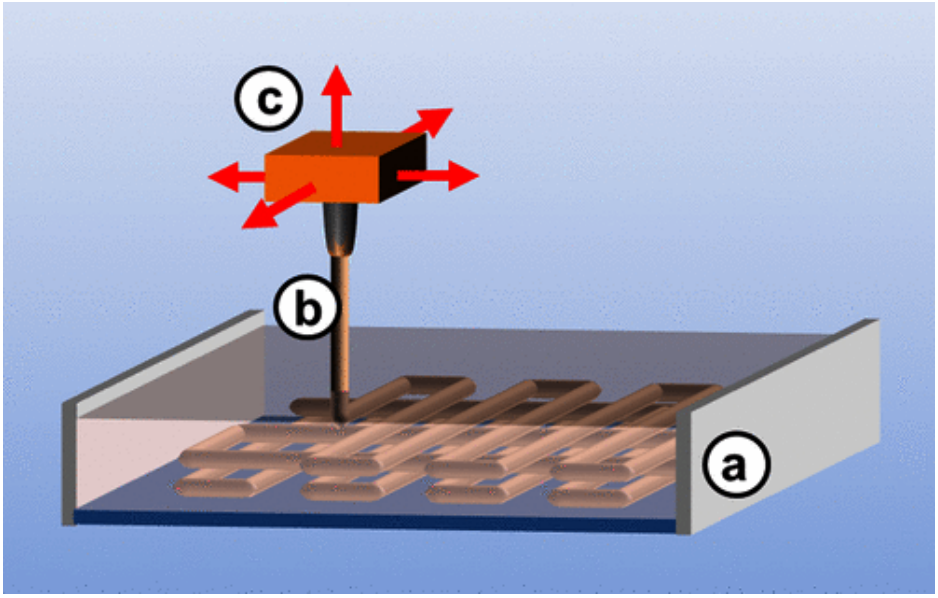

Figure 1.1: Schematic diagram of 3D micro extrusion consists of (a) a build platform in air or immersed in a liquid and (b) a dispensing nozzle coupled to a (c) extrusion head that can move in 3-axis (Ligon et al., 2017).

FFF is restricted to the high-temperature extrusion of thermoplastics, whereas 3D extrusion allows the processing of many other classes of materials, such as thermosets, silicones, organic and inorganic pastes, biomaterials, hydrogels and living cells. Figure 1.1 shows the 3D extrusion process. The extrusion print head consists of a nozzle and a cartridge, and material dispensing is controlled either pneumatically or mechanically. 3D extrusion can be considered a generic name, and it contains the methods of 3D dispensing, 3D plotting, direct-ink-writing (Robocasting) and extrusion-based bioprinting (EBB), a sub-branch of bioprinting.

Bioprinting emerged due to the need for Tissue Engineering (TE), which aims to fabricate artificial tissues or to mimic the real environment of the human body through bioprinting (Li et al., 2016). Bioprinting can employ an additive manufacturing technology to deposit materials known as bio-inks to construct tissue-like structures. There are three types of bioprinting techniques: droplet-based bioprinting, laser-based bioprinting, and extrusion-based bioprinting.

EBB is an in-demand technology, allowing wide material selection (viscosity range from 0.3 to 30$Pa \cdot s$), high manufacturing speed and a controllable printing environment (Murphy et al., 2013; He et al., 2016; Ozbolat and Hospodiuk, 2016). In terms of material driv-

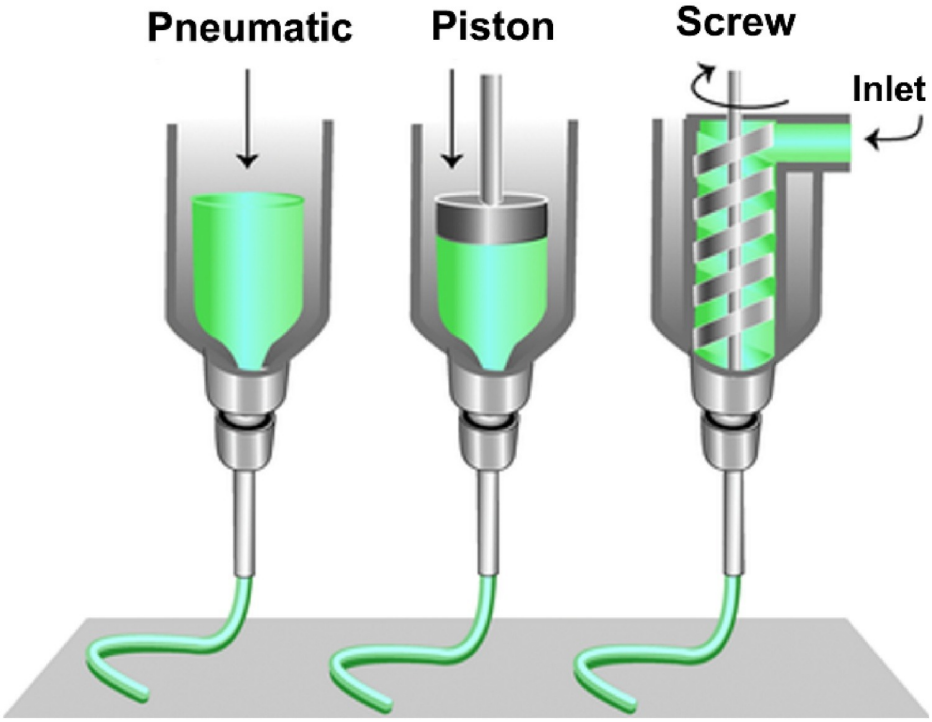

Figure 1.2: Schematic diagram and the working principles of extrusion-based 3D printing technique. (a) Pneumatic-driven, (b) piston-driven, (c) screw-driven (Malda et al., 2013).

ing systems, EBB can be divided into pneumatic-driven, piston-driven, and screw-driven (including an auger screw and progressive cavity pump). Figure 1.2 shows the available designs of EBB technologies, each with advantages and limitations.

In the pressure-driven extrusion, the cartridge's remaining material volume requires various pressure forces and affects the accuracy, and the pressure control unit increases the system cost (Ozbolat and Hospodiuk, 2016). In piston-driven extrusion, high-viscous materials require high force and limit the material selection range. In addition, syringe cartridges restrict the dispensing volume (Li et al., 2017; Pusch et al., 2018). Low viscous materials can leak through the nozzle due to the continuous flow path in the auger screw-driven extrusion. Therefore, it is a suitable method to dispense high-viscous biomaterials, though low-viscous dispensing limitations restrict its usage in bioprinting (Ozbolat and Hospodiuk, 2016). In progressive cavity pumps (PCP), the main limitations can be defined as the high cost of the system, cleaning and assembly difficulty, and large dead volume (Fisch et al., 2020; Wang et al., 2016).

PCP was invented by the French engineer René Moineau in 1930, and it can be referred to in the literature as a progressing cavity pump, progressive cavity pump or Moineau pump

(Moineau, 1930). While much of the current PCP literature is related to high-speed and high-volume fluid pumping, PCPs are also used as advanced pumps in fluid dispensing and have shown promising results (Shakor et al., 2019; Yao et al., 2015; Raval and Patel, 2022; Fisch et al., 2020; Canessa et al., 2017; Li et al., 2017).

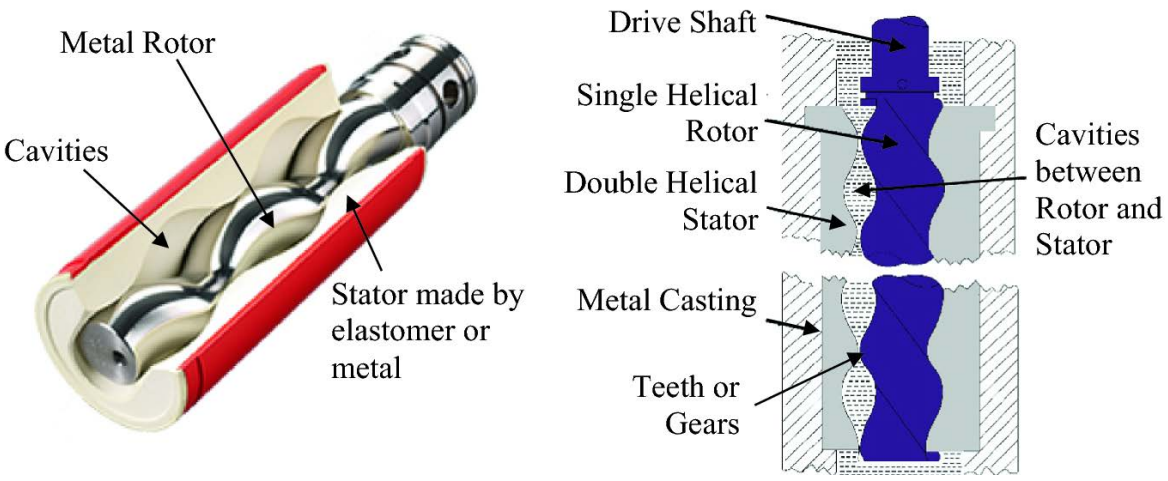

Figure 1.3: Single lobe PCP with metal rotor and elastomer stator (Nguyen, 2020).

Commercially available PCPs have received considerable attention in recent academic research due to their high accuracy in soft material dispensing (Gelber, 2015; Yao et al., 2015; Wang et al., 2016; Li et al., 2017). The PCP mechanism creates cavities that enable the movement of media without causing any deformation. This process enables the transfer of fluid through a series of small, fixed shapes and discrete cavities, as illustrated in Figure 1.3. PCPs have a great potential to provide better dispensing quality than pneumatic and piston-driven methods. Recent studies have shown that PCPs offer a valuable tool to improve the accuracy of EBB (Fisch et al., 2020; Wang et al., 2016; Yao et al., 2015).

While the literature shows promising results of commercial PCPs, it has also been shown that there are several limitations. Fisch et al. (2020) suggested that bioprinting applications benefit from a specifically designed PCP considering the current limitations of the large dead volume, high volume flow and cleaning difficulty. Moreover, several studies using commercially available PCPs have reported potential future works, including the development of an open-source PCP to reduce costs and the adaptation of the technology for multi-material 3D printing (Yao et al., 2015; Wang et al., 2016; Fisch et al., 2020).

Few studies have attempted to develop a PCP for ceramic and pellet extrusion. Canessa et al. (2017) combined the auger screw and PCP mechanism for pellet extrusion. While

the study has shown some successful printing attempts, a full-functional PCP could not be proposed. Maker movement was another community that showed interest in developing an open-source PCP-based ceramic extruder (Verbruggen, 2014). In addition, Unfold has emerged as a leader in the open-source movement to develop a PCP for ceramic extrusion, and the first article was published in the RepRap Magazine (Verbruggen, 2014). Most of their attempts have been to build an extruder using the existing PCP mechanism used in commercial pumps. However, there is not any available PCP proposed by the maker community, and the Unfold (Belgium) company decided to use a commercial PCP (Viscotec, 2016).

In summary, much of the current literature on printing with PCPs pays particular attention to the need for a better PCP for fluid and paste dispensing. While there is a recent advancement in industry and research, a low-cost, scalable, easy-to-clean PCP extrusion unit could not be developed to date. Detailed information on PCP literature can be found in Section 2.3.4.

1.2 Aim and Objectives

This research aimed to develop a novel low-cost fluid dispensing and deposition pump based on a selected technology that responds to technical challenges presented by biomaterials in extrusion-based bioprinting technology.

The research was conducted based on two assumptions, (1) current extrusion technologies could not meet the requirements of bioprinting and (2) making use of a positive-displacement delivery method such as a progressive cavity pump (PCP) could be used as an advanced dispensing pump for an extruder in bioprinting.

The research objectives based on the first assumption were as follows:

1.1 Research current bioprinting extrusion technologies to identify problems and requirements which could be used to develop a novel pump

1.2 Identify existing fluid dispensing pump technologies to highlight known limitations

The research objectives based on the second assumption were as follows:

2.1 Research PCP mechanism to determine pump characteristics and limitations

2.2 Develop a novel and low-cost PCP concept based on identified requirements

2.3 Validate and compare the developed PCP by gathering pump specifications with flow experiments

1.3 Thesis Outline

The outline of the following chapters of the thesis is as follows:

- **Chapter 2: Literature Review**
  Current bioprinting extrusion technologies were investigated, and bio-materials and printability requirements were reviewed. Furthermore, positive displacement pumps were mentioned, and the operation principles and basic cross-section generation methods of PCPs were described.

- **Chapter 3: Methods and Materials**
  An additive manufacturing-enabled spiral product development model was proposed, and the methodology and materials were explained based on the model.

- **Chapter 4: User Questionnaire and User Interview**
  To understand more about bioprinter capabilities and user expectations, a user questionnaire and interviews were conducted. The purpose of this study was to provide information for the product development process in order to create a better extrusion unit.

- **Chapter 5: Syringe Pump Evaluation**
  A large-volume syringe pump was developed and validated. Using the developed pump, an initial investigation of syringe-based pumps was carried out to better understand the limitations of bioprinting.

- **Chapter 6: Design, Prototyping and Implementation of a PCP**
  Design methodology and mathematical modelling of PCPs were explained in detail. Subsequently, an application programming interface was developed in python language to speed up the PCP development process.

- **Chapter 7: PCP Concept Development**

  PCP requirements were highlighted, three PCP concepts were designed, prototyped and evaluated to meet the defined requirements, and the final concept was approved for product prototype development.

- **Chapter 8: Inner Gear Actuated PCP Prototype**

  A selected PCP concept in Chapter 6 was developed. Besides, a syringe pump to feed the PCP was developed and integrated with the PCP. Extrusion unit validation was performed against a commercial and an open-source syringe pump.

- **Chapter 9: Conclusions and Future Works**

  The outcome of this research and novelty was presented by answering the initial questions. In addition, the obtained conclusion from all chapters was drawn, and future works were proposed.

2

LITERATURE REVIEW

2.1 Keywords of Literature Review

This research aims to develop a novel low-cost fluid dispensing and deposition pump that responds to the technical challenges of biomaterials in extrusion-based bioprinting technology. Therefore, the research requires a multidisciplinary approach to the problem and extensive literature research on bioprinting and PCP-related subjects. Bioprinting is a current topic of interest in academia, and there is a wealth of information in the literature. However, PCPs have shown more development in the industry, and there is limited information available in the academic literature regarding PCP design and development.

The literature research keywords are presented in Table 2.1. The research was conducted by searching for these terms separately or together in the Scopus, Web of Science and Science Direct databases and the Google Scholar search engine.

Table 2.1: Keywords used in literature research for bioprinting and progressive cavity pump (PCP).

	Literature Research Keywords
1	Bioprinting
2	3D
3	Extrusion based
4	Positive displacement dispensing or Positive displacement pump
5	Direct ink writing
6	Printing
7	Additive manufacturing
8	Material extrusion
9	Progressive cavity pump or Progressing cavity pump
10	Moineau pump
11	Dispensing
12	Robocasting

2.2 Bioprinting Literature Review

2.2.1 Bioprinting

Tissue engineering is a field that applies the principles and methods of engineering and life sciences to develop biological substitutes that restore, maintain, or improve tissue function (Skalak and Fox, 1988). Tissue engineering is currently used in clinical applications to develop replacements for vessels, skin, bone and cartilage (Mandrycky et al., 2016).

The primary purpose of tissue engineering is to fabricate artificial tissues and organs which can maintain or restore damaged tissues or organs (Langer and Vacanti, 1993). The main components of tissues are cells, a scaffold and a microenvironment that mimics the real environment of the human body. Cells are located in a matrix environment called extracellular matrix (ECM), and a scaffold is used to mimic the ECM of tissues to facilitate cell delivery and proliferation.

There are three strategies used in TE to substitute targeted tissues: (1) the use of cells alone, (2) the use of biomaterials and (3) the use of a combination of both cells and biomaterials (Khademhosseini et al., 2006). Creating tissue-like structures via bioprinting, an additive manufacturing (AM) technique, can be employed in various tissue engineering applications. Bioprinting refers to 3D printing biomaterials with or without cells, providing an accurate, repeatable, high-resolution printing process (Chua and Yeong, 2014).

Bioprinting is a sub-branch of AM, a layer-by-layer fabrication technique using liquid, solid, powder, gel, and paste materials from a digital 3D model. Bioprinting is a popular method for fabricating tissues and organs because of its advanced controlling features of the fabrication environment (Li et al., 2016). Droplet-based bioprinting, laser-based bioprinting, and extrusion-based bioprinting (EBB) employing biomaterials are the major techniques used in bioprinting (Ozbolat and Hospodiuk, 2016). Bioprinting consists of three essential stages, (1) pre-processing, (2) processing, and (3) post-processing, and Figure 2.1 shows the schematic of the processes (Ramadan and Zourob, 2021).

Pre-processing consists of imaging, designing mimicked tissue and determining process parameters. In the imaging stage, a 3D laser scanner and a series of computed tomography (CT) or magnetic resonance imaging (MRI) scans are used to construct or capture a

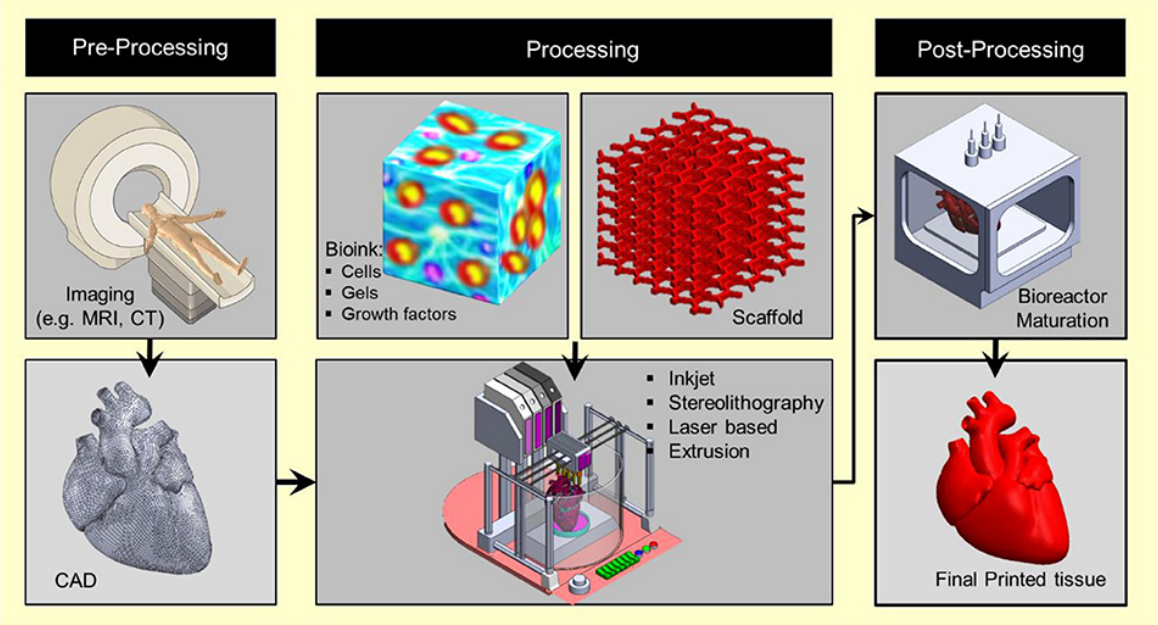

Figure 2.1: Schematic of the bioprinting processes. Pre-processing includes imaging and design. Processing includes material selection and 3D printing. Post-processing includes the removal of the support, post-curing and the application (Ramadan and Zourob, 2021).

computer-aided design (CAD) model from a physical object. In the design stage, the CAD model is transformed into a format that enables computer model virtual slicing, typically in stereolithography (STL) file format. The outward normal of each triangle in Cartesian coordinates is included in the STL file, along with an unordered list of triangular faces. These triangular facets represent a precise CAD model's exterior surface as closely as possible (Dababneh and Ozbolat, 2014). Digital cross-sectional layers of the CAD model are created from an STL file using specialised software. Users of this software can alter the build direction, part size, quantity of copies, and layer thickness of a CAD model. Layer thickness is a crucial slicing element because it influences both model correctness and construction time. Reduced layer thickness improves model accuracy but increases construction time.

Following pre-processing, the digital information of the sliced layers is delivered in sequence to the bioprinter for processing. The 3D printing process is utilized by machine-specific software as there is no available generic software for bioprinting. In the processing stage, biomaterials are properly selected and loaded into the bioprinter, and printing parameters are adjusted through a control system (Mandrycky et al., 2016). The prototype is then constructed layer by layer on top of one previously constructed layer. The bioprinter prints the model physically, often one layer at a time. The workstation where the physical model

has been constructed moves to the next layer after each layer has been completed, a distance equal to the thickness of one layer. Until the entire model is finished, the process is repeated.

The post-processing stage is considered to be of two types in bioprinting: the removal of support structures and the post-curing of the printed object. Second, the application of printed tissue, such as implantation or in-vitro testing (Murphy and Atala, 2014).

A scaffold in tissue engineering refers to a three-dimensional, porous structure which provides a temporary home for cells (seen Figure 2.1). The shape, mechanical properties and strength of the mimicked tissue are maintained using the scaffold, which provides a suitable environment for cell attachment and proliferation (Hutmacher et al., 2004).

The scaffold fabrication technique significantly affects characteristics such as mechanical strength and porosity (Peltola et al., 2008). In extrusion-based bioprinting, scaffolds can be made with organic or synthetic biomaterials which are biocompatible with a body for implantation.

Cell attachment and cell proliferation are essential to mimic a tissue, and it is provided by scaffold by generating necessary features such as shape, size, porosity and interconnectivity. These scaffold features can be fabricated with the advanced specifications of bioprinting, including control accuracy, high resolution, scalability, and cost-effectiveness (Khalil et al., 2005; Khademhosseini et al., 2006; Mandrycky et al., 2016).

2.2.2 Bioprinting Processes

The most common 3D bioprinting methods include extrusion-based bioprinting, inkjet bioprinting, stereolithography-based bioprinting, and laser-assisted bioprinting, as shown in Figure 2.2. Table 2.2 shows the advantages and disadvantages of these strategies.

Inkjet-Based Bioprinting

The inkjet printing manufacturing method is based on the 2D printer method of employing a jet to spray tiny drops of ink onto paper(see Figure 2.3). In the bioprinting process, ink is replaced by liquid biomaterials. These materials are printed as liquid drops that crosslink to form a layer of the part. The benefits of inkjet printing include high accuracy and surface qualities. However, this technique has several disadvantages. One of the main drawbacks is

Table 2.2: The advantages and disadvantages of the most common bioprinting methods.

Bioprinting Methods	Advantages	Limitations	References
Inkjet-based bioprinting	Manufacturing speed, low cost, and the capacity to bioprint numerous biomaterials at once	Limited to low viscosity biomaterials, nozzle clogging, and operation difficulty	(Mandrycky et al., 2016; Boland et al., 2006; Nakamura et al., 2005; Xu et al., 2012)
Stereolithography-based bioprinting	Manufacturing speed, high resolution (ranging between 5-300 μm), smooth surface and edges	Biomaterial must be photopolymers, used photo-crosslinkers are hazardous, and multi-material bioprinting is complicated	(Yue et al., 2015; Raman et al., 2016; Mondschein et al., 2017)
Laser-assisted bioprinting	High resolution (ranging between 10–50 μm), precise cell placement, nozzle free manufacturing	Costly installation, biomaterial limitation, low manufacturing speed, requiring a very high temperature (up to 1400$^{\circ}C$), and operation complexity	(Murphy and Atala, 2014; Kawecki et al., 2018; Guillotin and Guillemot, 2011)
Extrusion-based bioprinting	User-friendly, adaptability, low cost (for syringe-based printers), the possibility of sterilising, and the capability to dispense multiple biomaterials simultaneously	Low resolution due to nozzle diameter restriction (generally over 100μm), cell damage caused by shear stress within the nozzle tip, cartridge volume restriction	(Leberfinger et al., 2017; Nair et al., 2009; Wüst et al., 2011; Ozbolat, 2015)

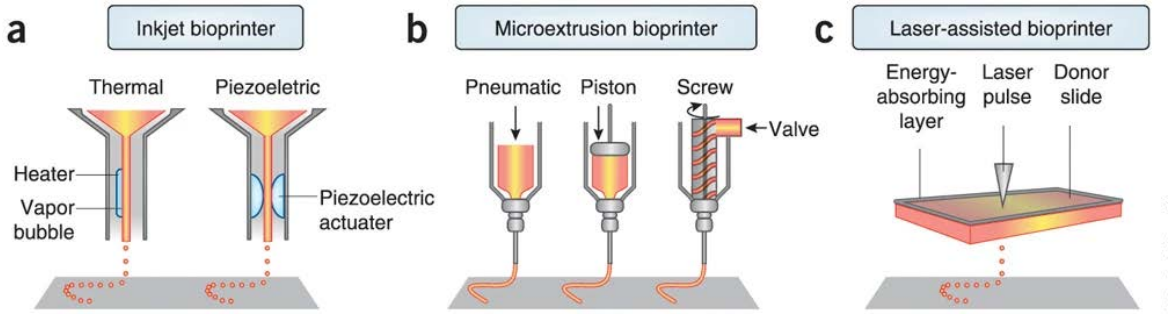

Figure 2.2: Inkjet, microextrusion (extrusion-based) and laser-assisted based bioprinting techniques. (a) Thermal and piezoelectric sources are used to produce droplets. (b) Microextrusion (extrusion-based) techniques can produce continuous beads. Pneumatic uses air pressure, piston and screw use mechanical force to push the material, and the screw-based method can be further divided into the auger and progressive cavity pumps. (c) Laser-assisted bioprinting technique uses laser pulses to produce a desired shape by actuating material substrate (Murphy and Atala, 2014).

the biomaterial's low viscosity upper limit, around $0.1 Pa \cdot s$ (Calvert, 2001). Other limitations and challenges associated with this technique include the amount of material that can be processed in a given amount of time (material throughput), droplet reproducibility, the range of shear forces within the nozzle, cell aggregation and sedimentation in the cartridge reservoir, clogging of the nozzle orifice and the limited number of printed materials in a process (Dababneh and Ozbolat, 2014).

Stereolithography-Based and Laser-Assisted Bioprinting

In laser-based bioprinting, laser energy is used to stimulate the biomaterials and produce exact patterns to regulate the spatial environment of the cellular environment. The most common laser-based systems are stereolithography (SLA) and laser-induced forward transfer (LIFT) (Kumar and Kim, 2020). SLA uses ultraviolet (UV) light to cure the photopolymer. In a vat of liquid photosensitive polymer, a three-dimensional object is traced out in successive cross-sections using a focused UV laser. The polymer solidifies while the laser traces the layer, leaving the liquid in blank spaces (see Figure 2.4). In LIFT, a laser pulse directs a single cell from a source to a substrate. The bubble formed by the shock waves of the laser pulse induces cells to move toward the collecting substrate (see (c) in Figure 2.2).

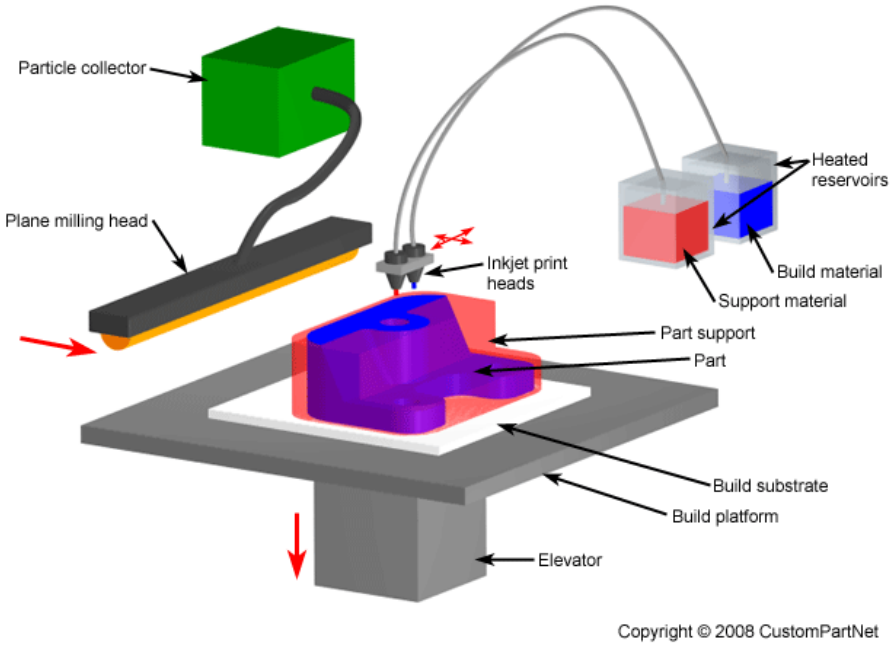

Figure 2.3: Schematic representation of the inkjet additive manufacturing process (CustomPartNet, 2008*a*).

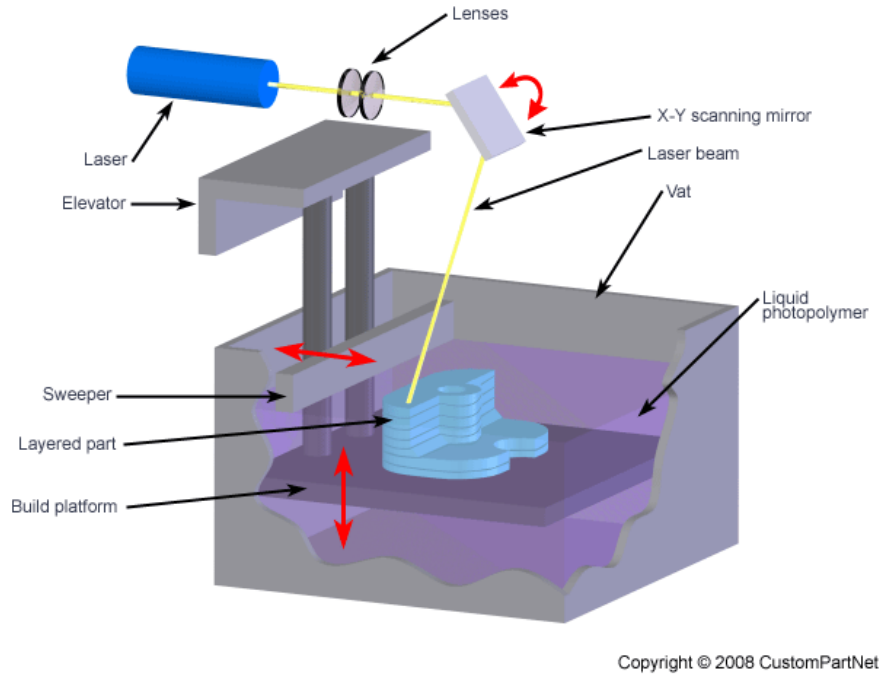

Figure 2.4: Schematic representation of the Stereolithography (SLA) additive manufacturing process (CustomPartNet, 2008*b*).

Extrusion-Based Bioprinting

Extrusion-based bioprinting is the most popular type of technology because it uses continuous deposition rather than droplet technology to deposit biomaterials layer by layer continually (Ozbolat and Hospodiuk, 2016). The biomaterial is extruded through a nozzle, either under pneumatic or mechanical pressure and placed in a predetermined structure. EBB is well regarded for its capacity to precisely extrude highly viscous material with the required accuracy for various applications (ranging from 0.03 to 60000$Pa \cdot s$) (Khoeini et al., 2021). However, He et al. (2016) was observed that the viscosity of the extruded material should be less than 100$Pa \cdot s$, and the optimal viscosity range is between 0.3 and 30$Pa \cdot s$ (He et al., 2016). Material with a viscosity of less than 0.3$Pa \cdot s$ is better suited for spreading than printing. In contrast, when the viscosity is greater than 30$Pa \cdot s$, substantial pressure is required to extrude the hydrogel from the nozzle, and the extrusion process becomes unstable.

EBB uses a deposition mechanism controlled by a computer to dispense biomaterial, resulting in the exact deposition of biomaterial enclosed in a cartridge. Due to the continuous deposition of biomaterial, this rapid production technique offers improved structural integrity (Khalil et al., 2005; Murphy and Atala, 2014). EBB can be categorised based on the extrusion force as pneumatically driven, piston-driven, and screw-driven, which can be an auger screw and PCP (see Figure 2.5).

Syringe pump-based extruders are the most popular option for EBB applications because of their simple operation and maintenance requirements. Even though this method yields adequate extrusion, several limitations remain challenging.

Pneumatic-driven extrusion uses regulated air pressure to discharge material (see (a) in Figure 2.5). While this technology is widely utilised in bioprinting applications, it has several drawbacks. One of the critical drawbacks is the low accuracy produced by the unstable pressure force caused by the cartridge's residual material capacity. Furthermore, the pressure control unit raises the system cost and requires additional safety precautions than mechanical-driven systems (Ozbolat et al., 2017).

Piston-driven extrusion uses mechanical force to dispense material through the nozzle (see (b) in Figure 2.5). In this method, high-viscous materials require high force and limit the material selection range. In addition, syringe cartridges restrict the dispensed biomaterial

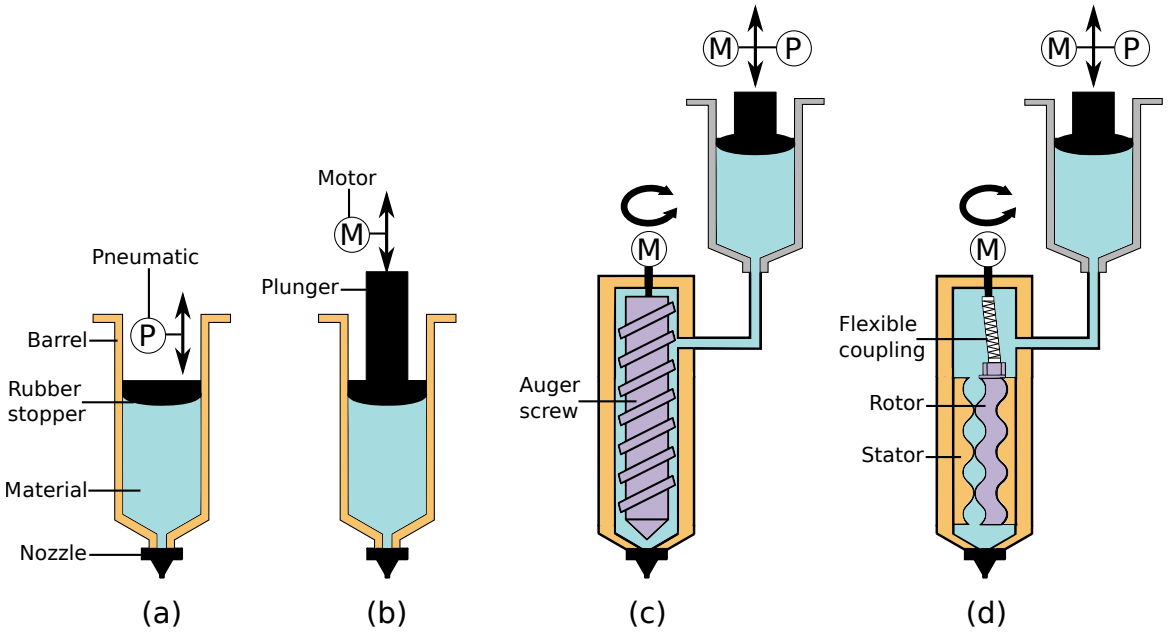

Figure 2.5: Extrusion-based bioprinting systems. (a) Pneumatic driven, (b) piston-driven, (c) auger screw-driven, and (d) progressive cavity pump.

volume (Fisch et al., 2020; Li et al., 2017; Pusch et al., 2018). Furthermore, piston-driven extrusion can also have low accuracy due to factors such as remaining material in the cartridge and shear thinning behaviours of the biomaterials. The constant cartridge volume can lead to inconsistencies in the amount of material dispensed because a non-Newtonian behaviour, where the viscosity of the material decreases under shear stress, can result in uneven extrusion rates and thus affect the accuracy of the process (Blaeser et al., 2016).

The review of auger screw and PCP approaches can be found in the following Section 2.3.

2.3 Positive Displacement Pumps Literature Review

Pumps can be divided into two groups according to adding energy to move liquid. These two classes are dynamic, and displacement pumps and the general classification of pumps can be seen in Figure 2.6. In dynamic pumps, the energy is continuously added to the fluid velocity, and they are not commonly used in the industry as metering or dispensing pumps. For this reason, the literature does not include dynamic pumps.

In displacement pumps, the energy is periodically added to the fluid velocity, providing a controllable pumping system. Displacement pumps are generally used in the industry for metering and dispensing purposes (Karassik et al., 2001). The standard dispensing pumps

are gear pumps, peristaltic pumps and screw pumps, including auger screw and progressing cavity pumps. Therefore, these pumps have the potential to be used as an extrusion system in bioprinting, and the following sections explain common dispensing pump technologies.

2.3.1 Gear Pump

Gear pumps transfer fluids by using the motion of spinning cogs or gears. The rotating element forms a liquid seal with the pump casing to create suction at the pump intake. The pump transfers fluid to the discharge by enclosing the fluid sucked into the pump within

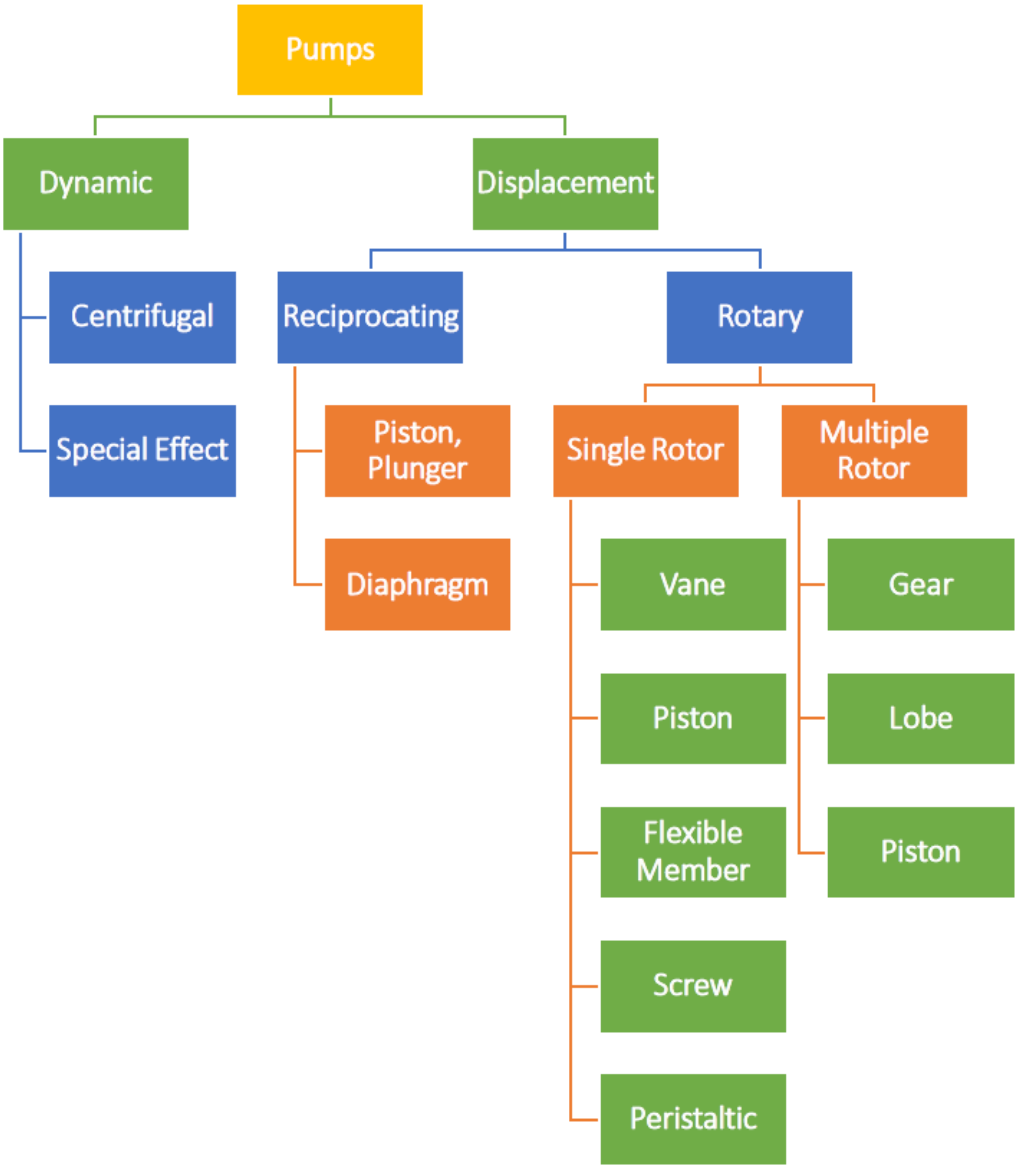

Figure 2.6: Classification of pumps. Adapted from Karassik et al. (2001).

the cavities of its spinning gears. Gear pumps can be divided into two groups, which are external and internal gear pumps (Karassik et al., 2001).

An external gear pump is comprised of two identical, interlocking gears that are supported by independent shafts. Typically, a motor powers one gear, and that power powers the other gear (the idler). In some circumstances, motors may be used to drive both shafts. Bearings on each side of the casing support the shafts (see Figure 2.7). The interlocking nature of the gears prevents any fluid from being transmitted back through the centre, between the gears. Due to the close fit between the gears and the casing, the pump can create suction at the input and stop fluid from flowing back from the discharge side.

The two interlocking gears in an internal gear pump operate on the same principle, but they are made of different sizes, with one moving inside the other. The larger gear (the rotor), which has teeth that protrude from the inside, is an internal gear. Within this larger gear, there is a smaller external gear (known as the idler) which is positioned off-centre. This idler is not driven directly, but rather, it's the rotor that is driven. The idler is designed to interlock with the rotor at one point for the gear teeth to engage. The idler is fixed in place by a pinion and bushing attached to the pump casing. The space left by the idler being mounted off-centre is filled by a fixed crescent-shaped spacer or partition that seals the intake and output ports.

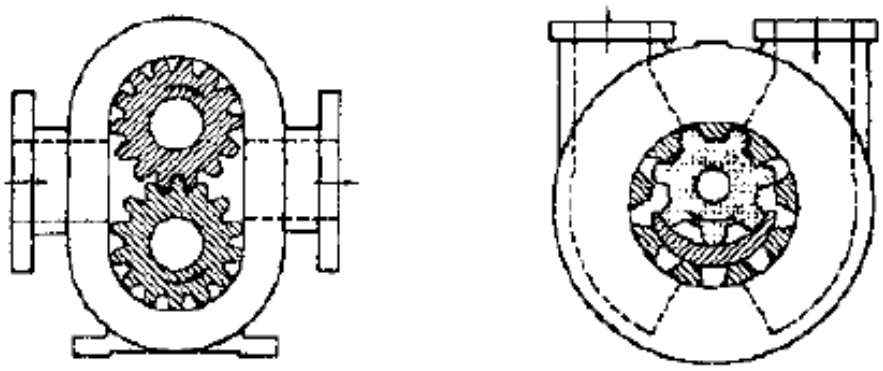

Figure 2.7: External (left) and internal (right) gear pumps to carry fluid (Karassik et al., 2001).

2.3.2 Peristaltic Pump

A peristaltic pump is a positive displacement pump commonly used in the dispensing and metering pump industry (Karassik et al., 2001). The main components of a peristaltic pump are a case, a rotor and an elastomeric tube (see Figure 2.8). The rotor compresses the tube into the casing, and liquid flows inside the sealed cavities by rotation. The fluid is carried in a flexible tube inside a spherical pump case. Although linear peristaltic pumps have also been created, the majority of peristaltic pumps operate through rotating motion. To compress the flexible tube as it rotates, the rotor contains several "wipers" or "rollers" attached to its outside circumference. Fluid is forced to flow through the tube because the compressed portion of the tube is sealed. More fluid is pulled into the tube when it opens to its initial state after the rollers pass.

A peristaltic pump's main drawback is pulsation, making it unsuitable for use as an extruder in bioprinting. Another drawback is the need for adjustments before each dispensing procedure. The restrictions in terms of frequency and speed are another drawback of this system. This implies that the highest flow rate you can achieve is severely constrained.

2.3.3 Auger Screw Pump

Auger screws have similar working principles as Archimedes‘ screw and provide a small clearance between the rotor and casing, dispensing performed. The flow rate is proportional

Figure 2.8: Peristaltic pump with a silicone tubing and two rollers (Karassik et al., 2001).

to the auger's velocity. Auger screws are often used to dispense fluids with high viscosity, and a pneumatic regulator is required to feed the screw.

When the auger pump operates, the inlet of the feed screw is always filled with material and pushed to the discharge point by a carefully controlled rotation. The rotation direction of the feed screw discretely determines how much material is discharged. Auger screw pump was mentioned as a good technology for high-viscosity biomaterials. However, low-viscosity materials can leak through the nozzle in auger screw-driven extrusion, which limits its use in bioprinting (Ozbolat and Hospodiuk, 2016).

2.3.4 Progressive Cavity Pump

PCP was invented by the French engineer René Moineau in 1930, and it can be referred to in the literature as progressing cavity pump, progressive cavity pump or Moineau pump (Moineau, 1930). PCPs have the ability to pump shear-sensitive materials because the design of PCP produces cavities to move fluid materials without deformation (see Figure 2.10). Therefore, it transfers fluid through the progress, a sequence of small, fixed shapes and discrete cavities. When these terms are searched on the Web of Science, there are 113

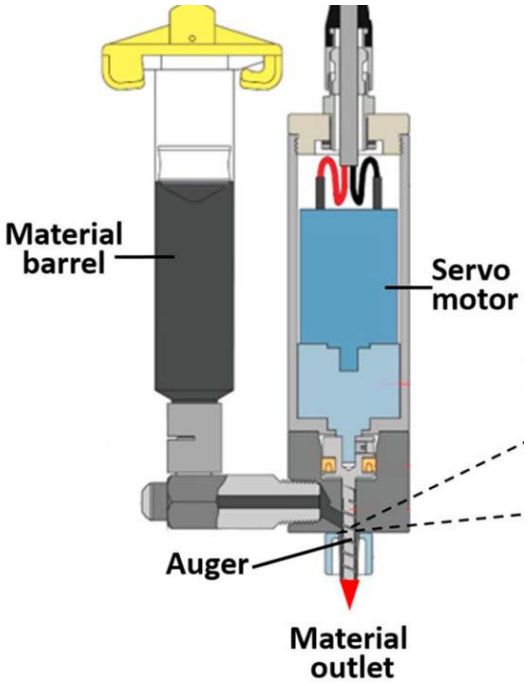

Figure 2.9: Dispensing pump with an air pressure driven material barrel and auger screw attachment (Li et al., 2017).

articles in total, and 58, 52 and 3 articles are found for progressing cavity pump, progressive cavity pump and Moineau pump, respectively. While many are related to high-speed and high-volume fluid pumping, only six articles related to AM (Shakor et al., 2019; Yao et al., 2015; Raval and Patel, 2022; Fisch et al., 2020; Canessa et al., 2017; Li et al., 2017). In addition, a noteworthy study, available outside the Web of Science, highlights the practical application of PCPs in 3D extrusion, providing insights into their utilisation (Wang et al., 2016).

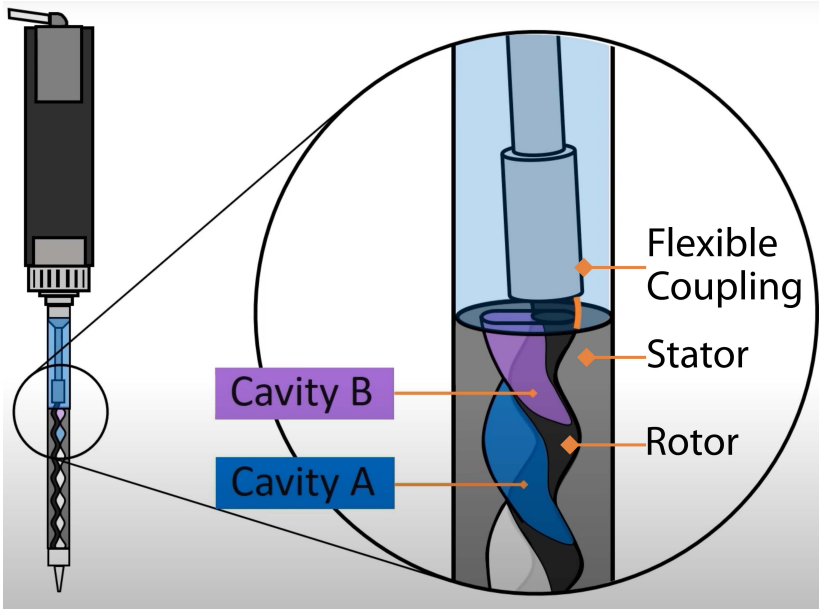

Figure 2.10: Progressive cavity pump on the left and a detailed view of the rotor, stator, flexible coupling and cavities on the right (Nordson, 2020).

Commercially available PCPs have received considerable attention in recent academic research due to their high accuracy in soft material dispensing (Gelber, 2015; Yao et al., 2015; Wang et al., 2016; Li et al., 2017). The PCP mechanism produces cavities to move the media without deformation; consequently, it transfers fluid through the progress, a sequence of small, fixed shapes and discrete cavities. PCPs have a great potential to provide better dispensing quality than pneumatic and piston-driven methods. Recent studies have shown that PCPs offer a valuable tool to improve the accuracy of EBB (Fisch et al., 2020; Wang et al., 2016; Yao et al., 2015). It is important to note that PCPs, while highly effective, are relatively expensive; the pump unit typically costs around £3000 and the control unit £2500 (ELPRO, 2023*a*,*b*).

Existing research recognises the critical role of the extrusion unit by comparing pressure-

driven and PCP-driven extrusion systems (Fisch et al., 2020). The research was conducted by printing a cube consisting of 26 lines at a length of 10.25 mm using a $410\mu m$ needle. The pressured-driven system achieved an overall accuracy of $12.4 \pm 4.3\%$ and a precision of $18.99 \pm 16.23\mu l$, and clogging was observed. On the other hand, the PCP achieved an overall accuracy of $0.3 \pm 0.2\%$ and a precision of $0.54 \pm 0.45\mu l$ without clogging. It has been noted that PCPs provide 41 times higher accuracy and 80 times higher precision than pneumatic extrusion, regardless of the biomaterials' rheological parameters (Fisch et al., 2020). It was also suggested that bioprinting applications benefit from a specifically designed PCP considering the current limitations of the large dead volume, high volume flow and cleaning difficulty. Several studies have reported similar future works for commercially available PCPs, including developing an open-source PCP to decrease costs and adapting the technology for multi-material 3D printing (Yao et al., 2015; Wang et al., 2016).

Recently, Yeh et al. (2020) studied the stator material hardness to develop a soft-matter PCP for high-viscosity fluids. Although the stator was successfully developed and tested, the scope of this research was relatively narrow to develop a PCP. Due to the exerted side loads on the stator wall, the existing PCP working mechanisms can only work with hard rubber stator materials (see Figure 2.11). Overall, Yeh et al. (2020) research focused only on the stator material, and the effect of the working mechanism on the compression of the stator was disregarded. However, it is clear that the extrusion accuracy is highly affected by the

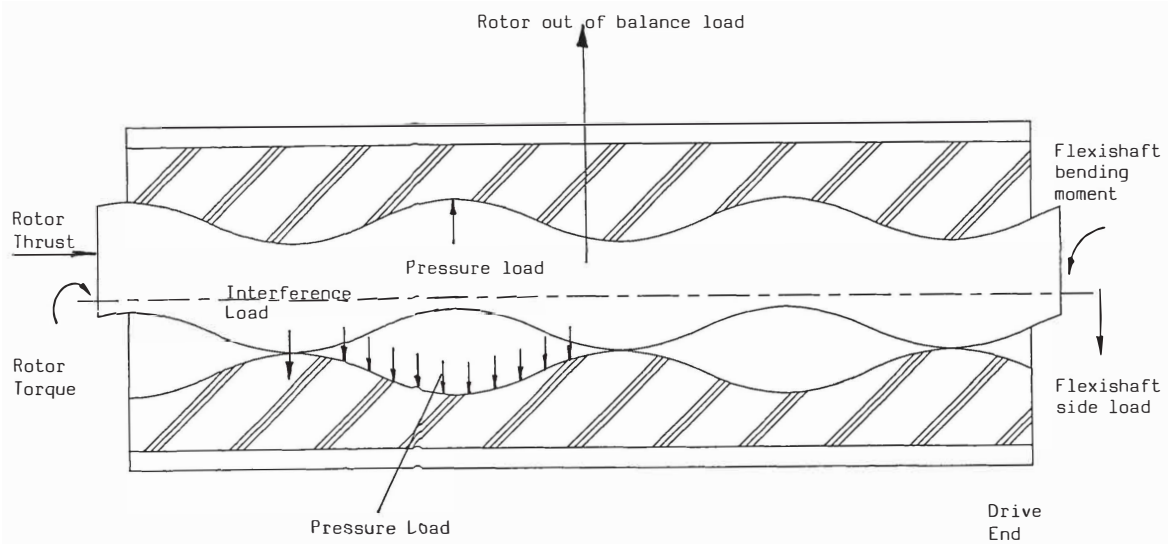

Figure 2.11: Loads on the stator (Belcher, 1991).

side loads exerted on the stator (Moineau, 1930). Consequently, it can be deduced that a novel PCP working mechanism which can eliminate the exerted side loads on the stator wall leads to an increase in the variety of materials that can be used for the stator. In addition, the extrusion accuracy of PCP increases due to an even motion of the rotor.

The previously described limitations have attracted the attention of dispensing industry. Viscotec company has recently developed the Puredyne kit b pump to meet the bioprinter user needs of single-use and precise dispensing for low to high-viscous material (see Figure 2.12) (ViscoTec Pumpen- u. Dosiertechnik GmbH, 2022). The puredyne pump extrudes material using air pressure to drive the wiper piston and control the flow with a PCP mechanism. However, what is not yet clear is the actual performance of the pump because it uses a pneumatic control unit which could make the pump non-volumetric. This view is supported in the Ojama (2022) research which found no significant difference between pneumatic and the puredyne extrusion units in terms of dimensional accuracy of the prints, and this is the only research in the literature (Ojama, 2022).

In conclusion, the need for an improved PCP for EBB is emphasised in a large portion of the present literature on printing with PCPs. While there has been recent progress in industry and academia, several questions about the role of the PCP working mechanism remain.

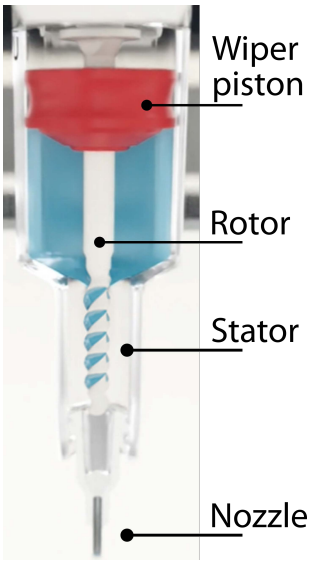

Figure 2.12: Schematic diagram of the Puredyne 3D printing system. Reproduced from (ViscoTec Pumpen- u. Dosiertechnik GmbH, 2022).

2.3.5 Progressive Cavity Pump (PCP) Design

In order to understand the design of Progressive Cavity Pumps (PCPs), this section explores the geometric principles underlying their operation. This section describes the PCP generation methods of PCP, specifically those based on hypocycloid, epicycloid, and hypo-epicycloid geometries and related literature. To provide available PCP geometries in the literature and their evaluation, the basics of these methods are defined in this section. The detailed hypocycloidal PCP generation method used in this research can be found in Chapter 6.

This section describes the PCP generation methods and related literature. The basics of hypocycloid, epicycloid and hypo-epicycloid based PCP geometry generation methods are defined in this section, and the detailed hypocycloidal PCP generation method can be found in Chapter 6.

The use of hypocycloid, epicycloid, and hypo-epicycloid geometries in PCP design results from their shared geometric properties, which are well-aligned with the operational requirements of progressive cavity pumps. These non-self-intersecting curves ensure continuous rotor and stator profiles, maintaining uniform pumped material flow and stability for efficient fluid transfer (Gravesen, 2008). Additionally, the consistent contact points between the rotor and stator enhance pump efficiency (Nguyen et al., 2014). These geometric advantages make these geometries ideal for designing PCPs for 3D extrusion.

A hypocycloid is a unique plane curve created by the trace of a fixed point on a tiny circle that rolls inside a bigger circle in geometry (see Figure 2.13). The hypocycloid resembles the cycloid made by rolling a circle down the line more as the radius of the larger circle increases.

The parametric equations for the curve can be obtained by either of the following equations, where r is the generator circle radius, and N is the number of lobes (R=Nr):

$$x(\theta) = r(N-1)\cos\theta + r\cos((N-1)\theta) \tag{2.1}$$

$$x(\theta) = r(N-1)\sin\theta - r\sin((N-1)\theta) \tag{2.2}$$

Epicycloids are planar curves created in geometry by following the route of a given point's

rotation around a fixed circle without slipping (see Figure 2.14).

The parametric equations for the curve can be obtained by either of the following equations, where r is the generator circle radius and the N is the number of lobes (R=Nr):

$$x(\theta) = r(N+1)\cos\theta - r\cos((N+1)\theta) \tag{2.3}$$

$$x(\theta) = r(N+1)\sin\theta - r\sin((N+1)\theta) \tag{2.4}$$

In the hypo-epicycloid geometry generation method, the generator circle follows a route both inside and around the base circle (see Figure 2.15). When the generator circle with radius r rolls inside the base circle with radius R, the stationary point on the generator circle draws a hypo-cycloid arc. When it rolls outside the base circle with radius R, the generator circle with radius r draws an epi-cycloid arc.

Gravesen (2008) discussed the geometry creation from the mathematicians' perspective and their findings show that hypocycloid geometry has some defects due to offsetting the base geometry and adding cusps (Gravesen, 2008). These defects occur between the cusps and extended hypocycloid intersection points. While the inventor of the PCP suggests both hypo

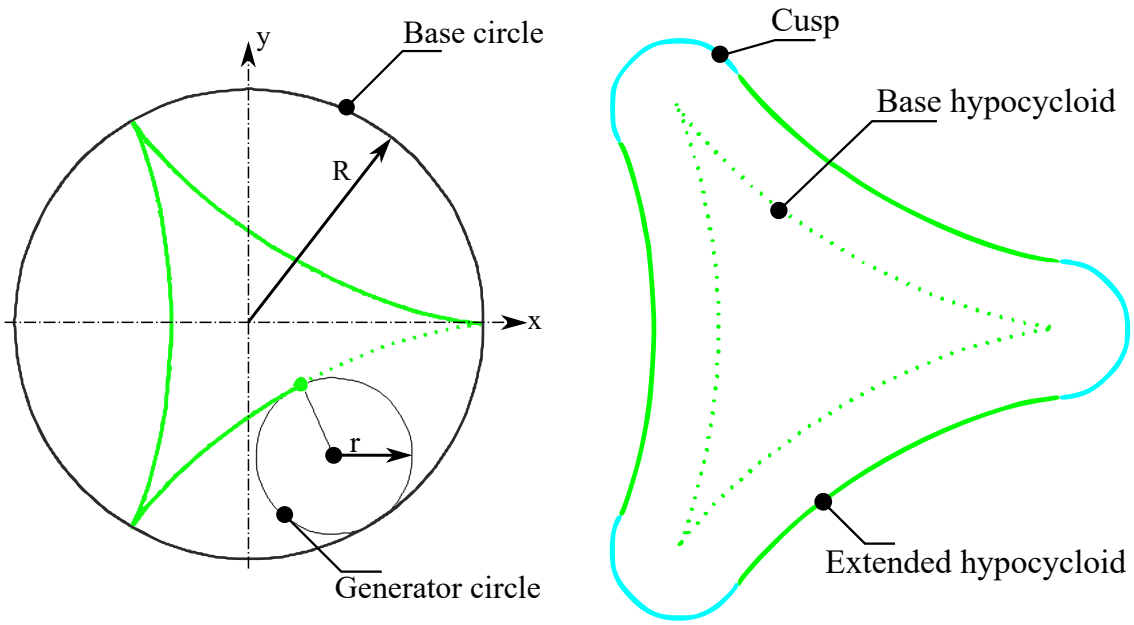

Figure 2.13: (a) Generation of a 3-lobe hypocycloid and (b) extended hypocycloid with cusps (Gravesen, 2008).

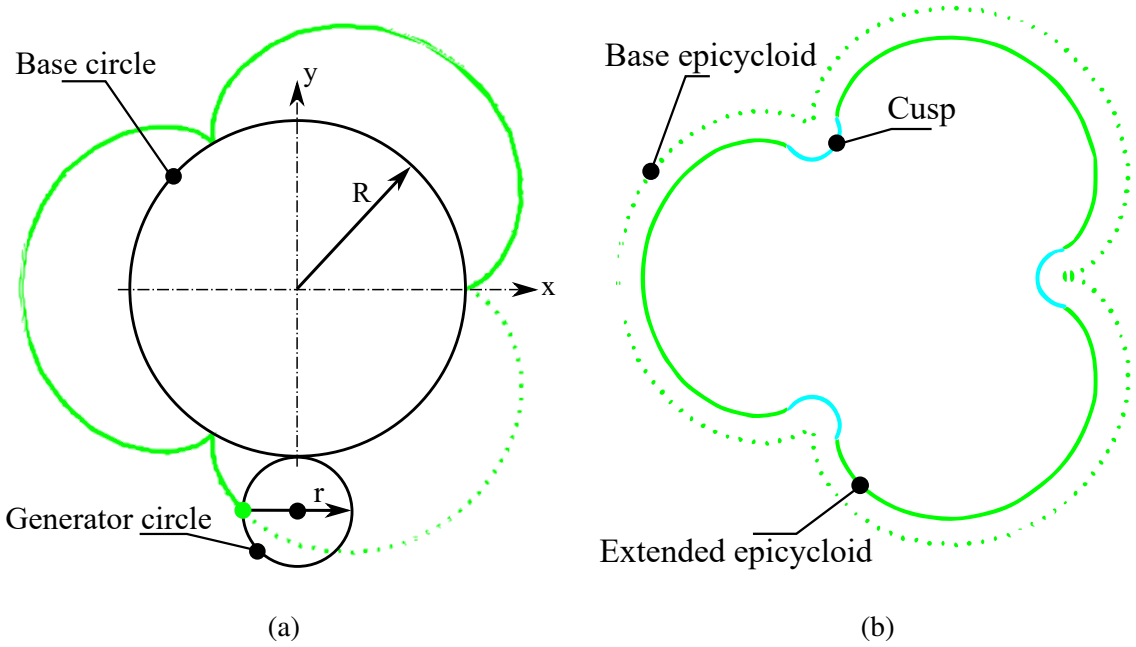

Figure 2.14: (a) Generation of a 3-lobe epicycloid and (b) extended epicycloid with cusps (Gravesen, 2008).

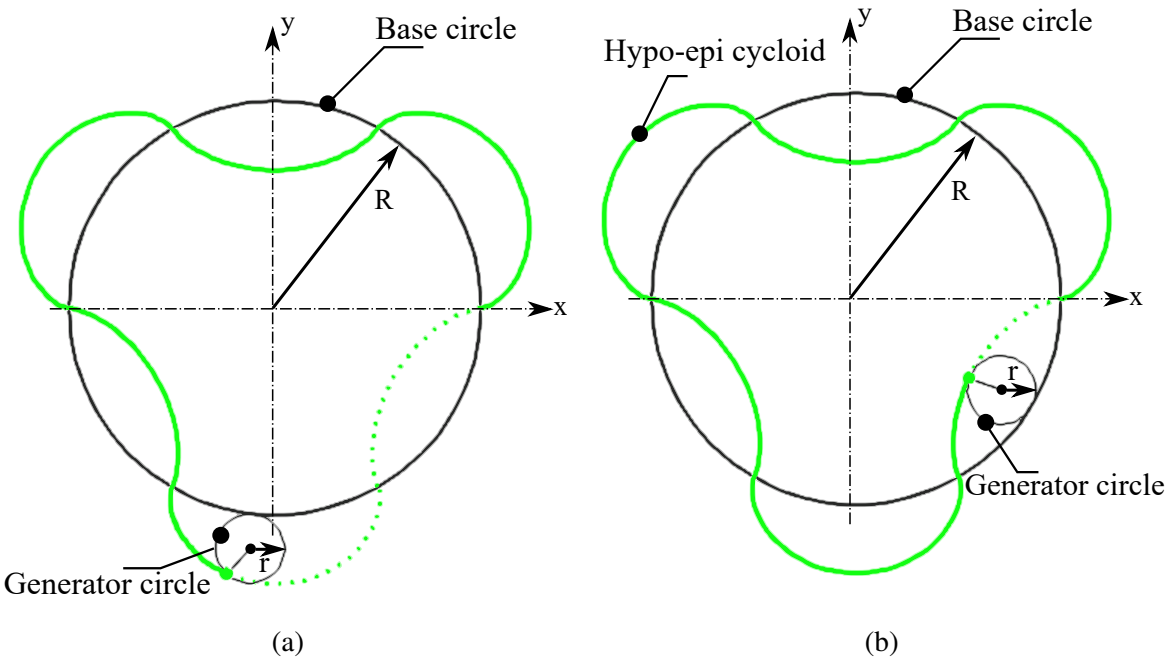

Figure 2.15: Generation of a 3-lobe hypo-epi cycloid. (a) The generator circle rotates outside of the base circle to create the epicycloid section. (b) The generator circle rotates inside of the base circle to create the hypocycloid section (Gravesen, 2008).

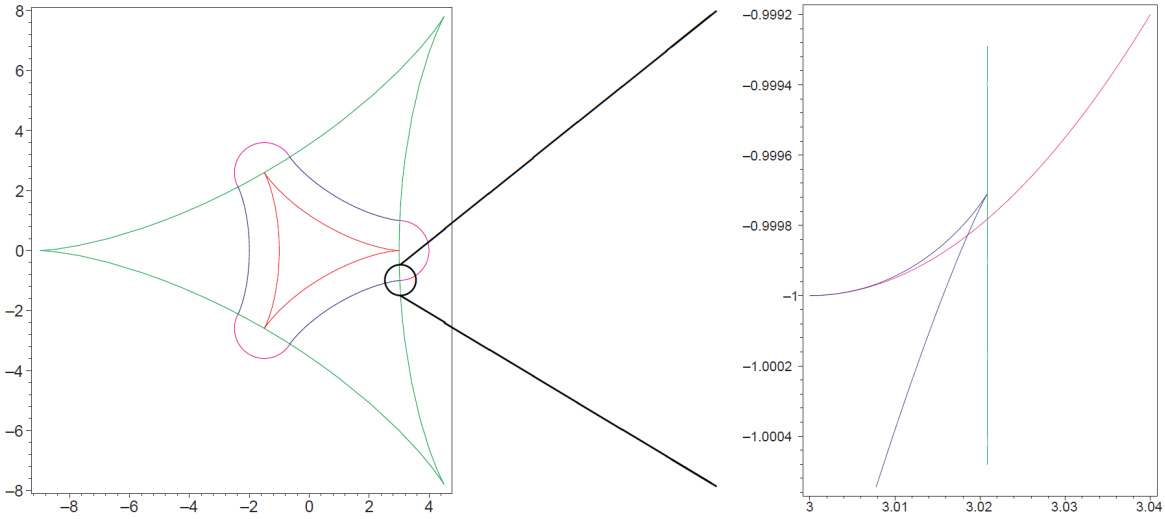

Figure 2.16: Left, Hypocycloid based PCP geometry with cusps; Right, focused the section where the hypocycloid offset changes to the half circle (Aage et al., 2006).

and epicycloids geometries, these defects may not be mentioned due to insufficient CAD facilities on those days. This assumption can be validated by considering the error scale because it is a millimetre scale for meter-sized pumps and a micron scale for centimetre-sized pumps (see Figure 2.16). As can be understood from the error scale, it does not significantly affect the precision and performance of the pump, and the elastomeric stator tolerates the error and enables a successful operation (Aage et al., 2006). In addition, the continuous curve in the creation of hypo-epicycloid geometry causes a difficult manufacturing process (Aage et al., 2006).

AM methods are promisingly used for intricate geometries, and the continuous curve problem can be overcome by using an AM technique. While the required tolerances for a dispensing pump is approximately 10 microns, AM technology has approx. 100-micron accuracy. However, AM's affordable and rapid manufacturing ability can provide more iteration possibilities and less costly manufacturing options. Consequently, AM can be used to obtain a working PCP by designing a wide variety of tolerances with 0.05mm intervals.

2.4 Literature Review Conclusion

This chapter reviewed current bioprinting technologies and an in-depth review of EBB. The experience and expectations of users from bioprinters are missing from the literature. It was concluded that the PCP development process could benefit from bioprinter user opinions.

Consequently, it was decided to conduct a user survey and user interview to learn more about the experiences and expectations of bioprinter users.

In terms of a PCP design, the following aspects can be drawn from the literature review:

- Commercial PCPs are costly due to the usage of off-the-shelf drive coupling and servo motors, which adds cost to the control unit. Therefore, the first aspect can be reducing the cost, which can be achieved by making the design simpler and using a stepper motor. The design simplification can be accomplished by eliminating the flexible coupling and reducing the number of components. In addition, the usage of a stepper motor enables an easy adaptation to readily available 3D printers.
- The design's scalability is another factor to consider. Scaling is limited because the design depends on commercial components. In bioprinting, the minimum dose and flow rate depend on the application, so a design that can be scaled could meet this requirement.
- Another aspect is the pump's sealing, which eliminates bubbles and increases precision. Eliminating assembly-required components facilitates the sealing function.
- Another consideration is the cell-friendly extrusion environment, which has been identified as the primary restriction of PCP in the literature. The bioprinting process necessitates using non-toxic materials, which can be achieved through a disposable extruder or an extruder that is easy to clean.

3

METHODS AND MATERIALS

3.1 Design and Development Methodology

PCPs have a long history; however, the first design's working mechanism and core components have almost never changed. Developing a new product requires extensive research on problem definition and many iterations of possible solutions. The use of the spiral development model allows the generation of various concepts quickly with the help of AM. Therefore, it was more likely to find an innovative solution to the current drawbacks of dispensing PCPs by obtaining insight from each concept. Consequently, a spiral development model was established in this research.

The spiral process was proposed by Boehm (1988) for software development. This leads to a faster product development cycle due to enabling quick prototyping features of software technologies. Ullman (2009) adapted the spiral process for mechanical product development. However, it was not widely used due to the slow manufacturing speed at that time. Recent developments in the field of AM have resulted in affordable machines and high-quality end products for experimental tests. Consequently, these advancements have led to a renewed interest in the spiral product development process. (Yahyaabadi et al., 2020; Pradel et al., 2019; Simontacchi et al., 2019)

In this research, a spiral development model was developed based on previous research, as seen in Figure 3.1 (Ullman, 2009; Ulrich and Eppinger, 2016). The model shows how a new PCP for EBB was made, but it can also be considered a general spiral model for the product development process.

The spiral development model can mainly be divided into three main phases: initials, concept development and product development (see Figure 3.1). As the general development model is described here, the term "product" is used. However, in this research, the product

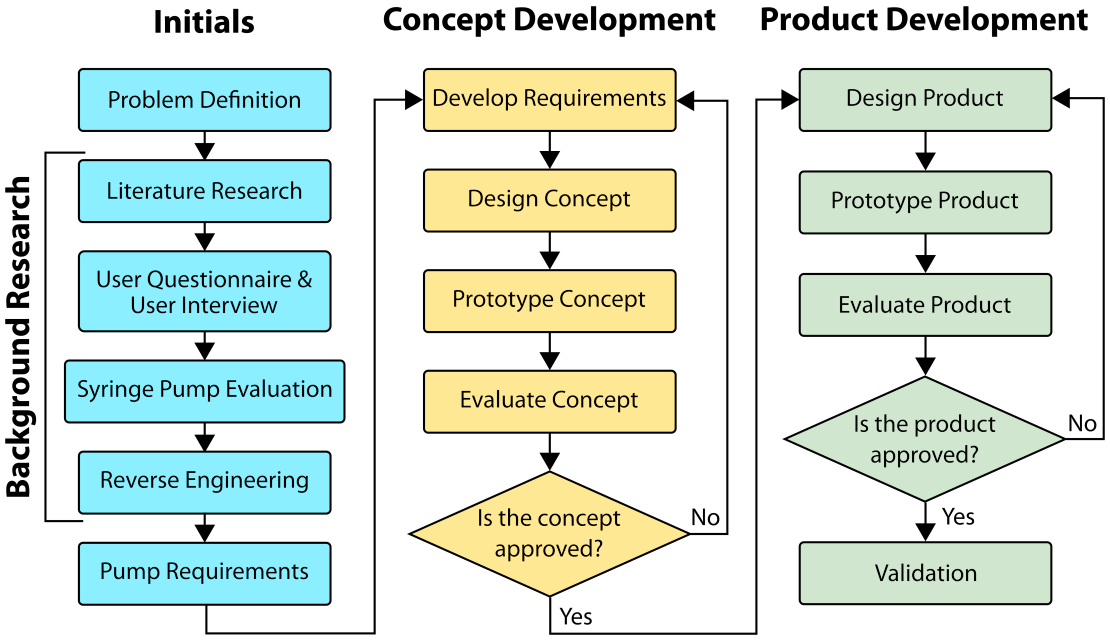

Figure 3.1: Spiral development model used for the research. Adapted from Ullman (1992) and Ulrich and Eppinger (2016).

is a PCP, and these terms are used interchangeably in the following sections.

The initials phase can also be considered background research to define current drawbacks and user needs. The motivation point of the research was the obvious need for a PCP for EBB applications due to the mentioned drawbacks in the literature, including the costly pump and control unit, cleaning difficulty and scalability of PCPs (Fisch et al., 2020; Wang et al., 2016; Yao et al., 2015). These drawbacks were mentioned in the background research (Section 1.1) and formed the basis of this research. In the development model, the mentioned drawbacks can be considered problem definitions, and literature research was conducted in the following step.

When the aim and objectives of this research were constructed (Section 1.2), assumptions were made based on a brief background research. Subsequently, the literature research, user questionnaires, user interviews, and syringe pump evaluation steps were conducted to validate these assumptions by following the objectives developed in Section 1.2. These steps are explained in detail in the following sections of this chapter. In the final step of the initials phase, the collected information was expressed as technical terms and specifications to produce pump requirements. These requirements were used to feed the concept development phase.

The concept development phase of the spiral model consists of many iterations until the approval of a concept that meets the pump requirements. In the first iteration, a conventional PCP concept was developed to gain a better understanding of the fundamentals of PCPs, including the working principle and essential features. In the subsequent iterations of the concept development phase, collected information from previous works was used to produce various concepts. These concepts were evaluated to produce a better PCP design by either changing the working mechanism or the cross-sectional geometry design of the rotor and stator. Detailed information on the prototype evaluation step is given in Section 3.1.3. The product development phase begins when a concept meets the defined pump requirements.

The product development phase of the spiral development model is similar to the concept development phase, consisting of several iterations until a satisfying product prototype is obtained. In this phase, product prototypes have been improved after each evaluation, and the validation step begins when a product prototype is approved. Detailed information about the validation step is given in Section 3.1.5.

It is important to note that the spiral development model can continue forever due to its iterative nature. For this reason, the project manager should decide when to move to the next stage to use the model efficiently.

3.1.1 Design for Additive Manufacturing

Design for Additive Manufacturing (DfAM) is an approach aimed at developing, refining, or altering the shape and function of a part to maximise the efficiency of its utilisation within additive manufacturing (AM) processes (Thompson et al., 2016). The design process for AM necessitates a thorough evaluation of numerous factors to ensure the optimal functionality and manufacturability of the designed part. These factors differ according to the design stage, and DfAM methodology encompasses these rules and restrictions (Yang and Zhao, 2015; Kumke et al., 2016; Pradel et al., 2018).

The use of this methodology is crucial due to the prevalent use of FFF for producing extrusion unit components. The capability of AM processes to deposit material anywhere in a component's cross-section allows for complex geometries to be fabricated without significant differences in time and cost compared to simpler forms. Careful integration of FFF manufacturing considerations remained crucial during each component's conceptualisation

and design phases.

The successful implementation of AM depends on its technological capabilities and a comprehensive understanding of its limitations and constraints. In this research, specific design constraints have been identified to ensure that components are optimised for AM and compatible with available equipment and established processes. The following design constraints have been established based on the capabilities and limitations of the FFF:

- **Build Volume Consideration:** The Ultimaker 3 FFF 3D printer, with dimensions of 200 mm in height, 216 mm in width, and 216 mm in depth, is available in the University laboratory (see Section 3.8.1). Components must be designed within this build volume.
- **Nozzle Diameter and Feature Design:** To ensure optimal print quality, design features must be dimensioned below the 0.4 mm diameter of the printing nozzle.
- **Curling Mitigation in PCP Gear Printing:** Prevent curling issues by designing features with less than a 45° overhang angle from the build plate or the preceding layer's surface and adjusting printing temperatures, especially when fabricating spiral-shaped PCP gears.

While adhering to design constraints is crucial, the establishment of design principles that guide the creation of components optimised for additive manufacturing is equally important. These principles encapsulate guidelines that enhance the manufacturability and the functional performance of the parts within the context of AM. The following design principles are derived from a careful consideration of factors related to additive manufacturing and the specific goals of this research:

- **Build Volume Optimisation:** Consider the available build volume of Ultimaker 3 FFF 3D printer to efficiently design components for printing.
- **Feature Size Optimisation:** Ensure that the designed features are adjusted to be smaller than the 0.4 mm nozzle diameter to ensure accurate printing.

- **Support Structure Minimisation:** Enhance efficiency and part quality by actively reducing the reliance on support structures during the design phase by applying the 45° overhang rule and part orientation.
- **Orientation for Mechanical Integrity:** Optimise part orientations according to anticipated loads and support requirements to ensure mechanical robustness.
- **Simplified Assembly:** Implement parts consolidation strategies where applicable to simplify assembly processes and reduce the overall component count.
- **Infill Strategy for Structural Integrity:** For components demanding solid structure, prioritise full wall thickness over 100 % infill options to maintain structural integrity. This principle is because a solid component was necessary for the rotor and the stator due to the potential gaps caused by movement during infill extrusion. Full wall thickness was prioritised to maintain structural integrity and avoid potential weak spots. This choice ensures the robustness of the overall structure by addressing gaps caused by infill extrusion movement. Using full wall thickness instead of infill facilitates consistent and even movement of the extrusion head during printing, resulting in enhanced part quality and dimensional accuracy.
- **Effective Curling Prevention:** Address curling challenges during printing, particularly for spiral-shaped PCP gears, by designing components with less than a 45° overhang angle.

3.1.2 Product Design Specification for a Progressive Cavity Pump

The Product Design Specification (PDS) is an important document that has been carefully created to guide the design and evaluation of PCP concepts. It helps to overcome the limitations of current extrusion-based bioprinting technology by providing a framework for design and evaluation. The PDS includes specific needs for a better PCP that are based on conclusive findings from a literature review (see Section 2.4). These findings identified four user needs for an improved PCP: low-cost, scalable, well-sealed and cell-friendly. These needs were then translated into measurable specifications to evaluate design concepts in future research phases. The PDS table was prepared based on the *Product Design and Development* book (Ulrich and Eppinger, 2016).

Table 3.1: Product Design Specification (PDS)

Need	Specification	Unit	Target Value
Low-cost	Reduction in pump cost	GBP	< 3000
	Reduction in the number of components	EA.	< 29
Scalable design	Scalable minimum dispensing amount	ml	0.001 to 0.06
	Scalable cartridge volume	ml	2.5 to 60
Pump Sealing	Reduction in the number of components	EA	< 29
Cell-friendly Design	Use of biocompatible materials	Binary	Yes
	Disposable or easy-to-clean pump design	Binary	Yes

In Table 3.1, you can find the PDS summary outlining the needs and specifications used to guide the design and assessment of the PCP concepts. These specifications are closely connected to the aim and objectives of the study and the literature review conclusion.

The PDS table was prepared using Viscotec's eco-PEN300 pump as a benchmark. The pump unit is typically priced around £3000 (ELPRO, 2023*b*). It comprises 29 distinct components (without fasteners), and the minimum dispensing amount it can handle is 0.001 ml (Preeflow, 2023*b*,*a*).

The low-cost PCP need was converted to specifications of reducing pump cost to less than £3000 and the number of components to less than 29. Component cost reduction is associated with commercial PCPs' dependence on off-the-shelf drive couplings and servo motors. Reducing the number of components determined to simplify the design, cost reductions, improved assembly efficiency and enhanced reliability for the extrusion system.

Specifications of the scalable minimum dispensing amount and cartridge volume were associated with the scalable design need. These specifications can be obtained by considering the parametric pump design and enabling various cartridge volumes. The minimum dispensing amount for the eco-PEN pump series varies from 0.001 to 0.06 ml; therefore, the target value was assigned accordingly (Preeflow, 2023*a*). In addition, the scalable cartridge volume specification was determined based on the most common syringe sizes used in bioprinting, which are between 2.5 and 60 ml (Pusch et al., 2018; Tashman et al., 2021).

The sealing issue is a key point in the PCP design because it decreases the printing accuracy. The one method to meet the need is to reduce the number of components, which reduces the assembly requirement and possible gap between components. Therefore, the target value is

set to less than 29, considering the distinct components number of eco-PEN300.

The cell-friendly design need can be met by using biocompatible materials when prototyping the concepts. In addition, the disposable or easy-to-clean PCP design approach can produce a cell-friendly printing environment. These specifications can be achieved depending on the designer's experience level. Therefore, the unit was indicated as "Binary" in Table 3.1, and the values can be "Yes" and "No".

3.1.3 Prototype Evaluations

Prototype evaluations are a critical phase in this research, stemming from the attributes defined in the PDS. This phase is divided into "Concept Prototype Evaluation" and "Product Prototype Evaluation" and defines how PDS was evaluated in the relevant phases of this research.

Concept Prototype Evaluation

The purpose of the development phase of the spiral model was to investigate a novel operating mechanism that satisfies EBB's product requirements. Initially, a prototype and evaluation of a standard PCP were conducted to gather knowledge regarding the working mechanism and basics of PCPs. Using the knowledge obtained from earlier concepts, subsequent PCP concepts were developed and evaluated.

The concept was evaluated by manipulating the rotor and stator to observe a satisfactory rotation and liquid transfer mechanism. The operation was performed either by hand or using a stepper motor. The extrusion capability was evaluated by filling the inlet of a PCP with petroleum jelly and observing the pump outlet. When a concept aligns with the criteria established in the PDS, it is deemed suitable for advancement to the next phase, the Product Prototype Evaluation.

Detailed information on the concept prototype evaluation is provided in Chapter 7.

Product Prototype Evaluation

The evaluation and selection of a working mechanism were carried out in the concept development phase, and the product development phase aimed to build a PCP-based extrusion

unit that meets the product requirements of EBB specified in the PDS. The extrusion unit consists of a PCP and feed pump, which is a syringe pump in this research. In the product prototype evaluation, the following features were evaluated:

- Design scalability
- Sealing performance of the PCP
- Power transfer from a motor to the rotor
- Adaptation to the existing 3D printers
- Easy to clean or disposable
- Easy modification for multi-material dispensing capability

Detailed information on the product prototype evaluation is provided in Chapter 8.

3.1.4 Syringe Pump Evaluation

The design and development of an innovative product require well-established background research and problem definition. Syringe pumps have commonly been used in the bio-printing method. However, most research has focused on the final product rather than the dispensing process itself. Therefore, the syringe pump validation was conducted with the in-house built large volume syringe pump (LVSP) and the PHD2000 pump using the experimental setups in Figure 3.2.

The syringe pump validation experiments examined the effect of syringe volume and plunger rubber compressibility on extrusion precision and accuracy. The experiment process parameters can be seen in Table 3.2. Syringe pumps were configured using these parameters. The experiment begins by filling the $5ml$ syringe with tap water and removing the air bubbles inside the syringe. Subsequently, the syringe was placed in the used pump to dispense the theoretical volume, and data were collected with a precision scale (Section 3.4.4) and a flow meter sensor (Section 3.4.3). Experiments were performed ten times for each pump and at $18^{\circ}C \pm 1$.

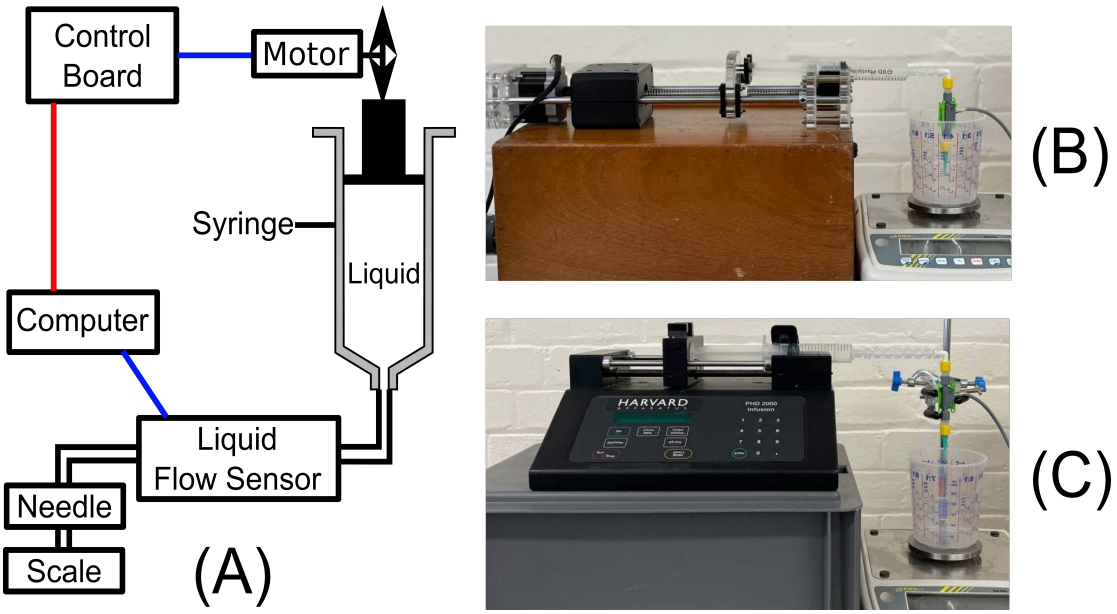

Figure 3.2: Diagram and demonstration of experimental setups. A) Experimental setup diagram for the LVSP and Harvard Apparatus PHD2000 Infusion syringe pumps. Blue and red lines show the connections and, the red line exists only in the LVSP. B) The LVSP with the sensor and weighing scale. C) The PHD 2000 with the sensor and weighing scale.

Table 3.2: Parameters that were used during the validation experiment for the syringe pumps.

Parameter	Value
Flow rate	0.5 ml/min
Theoretical extruded volume	0.5 ml
Needle diameter	0.41 mm

3.1.5 Extrusion Unit Validation

The approved PCP product was designed and prototyped to conduct validation experiments. The experiments were designed to benchmark the PCP against a commercial and an open-source syringe-based extruder. Evaluated features were the accuracy and precision of the PCP and 3D printing ability.

A flow sensor and a weighing scale were used to validate the accuracy and precision of the accepted PCP product prototype. In addition, 3D printing capability was evaluated using common 3D models, including a nose, an ear and a 3D benchy.

Detailed information on the PCP validation is provided in Chapter 8.

3.2 Design Software

Fusion 360 (Autodesk, US) cloud-based CAD software was used to design all components for this study. The Application Programming Interface (API) for Fusion 360 was written in Python. API was used to design PCP gears to accelerate the design and development process.

3.3 Data Analysis

Python programming language with pandas, matplotlib and seaborn libraries was used for data analysis. Seaborn was used to creating visualisations like figures and plots.

Excel (Microsoft, US) was used to calculate mathematical equations in the experimental part, including PCP design parameters, PCP torque requirements, and G-codes for extruded volume.

3.4 Electronics and Data Gathering Equipment

3.4.1 Control Board

Duet 2 Wi-Fi 32-bit control board (Duet, UK) was used to control the Makerbot Replicator 2x 3D printer and the stepper motors of the in-house constructed LVSP and prototyped PCPs (see Figure 3.3). RepRapFirmware 3.1.1 was installed to the control board as it was the Duet company (Duet, UK) recommendation. The control board is equipped with TMC2660 stepper drivers that allow up to 256 micro-stepping. Each stepper driver can handle 2.8A of motor current. The standard board can control two stepper motors, which were used to simultaneously power the developed syringe pump and PCP pump.

An integrated Wi-Fi module and PanelDue (Duet, UK), a full-colour graphic touch panel, were used to make the control board easily accessible. Consequently, the end-user may immediately control the system using PanelDue without installing additional software.

3.4.2 Stepper Motors

NEMA 17 and NEMA 23 stepper motors were used in the research and purchased from the motion control products company (UK). NEMA 17, FL42STH47-1684A-01, works with

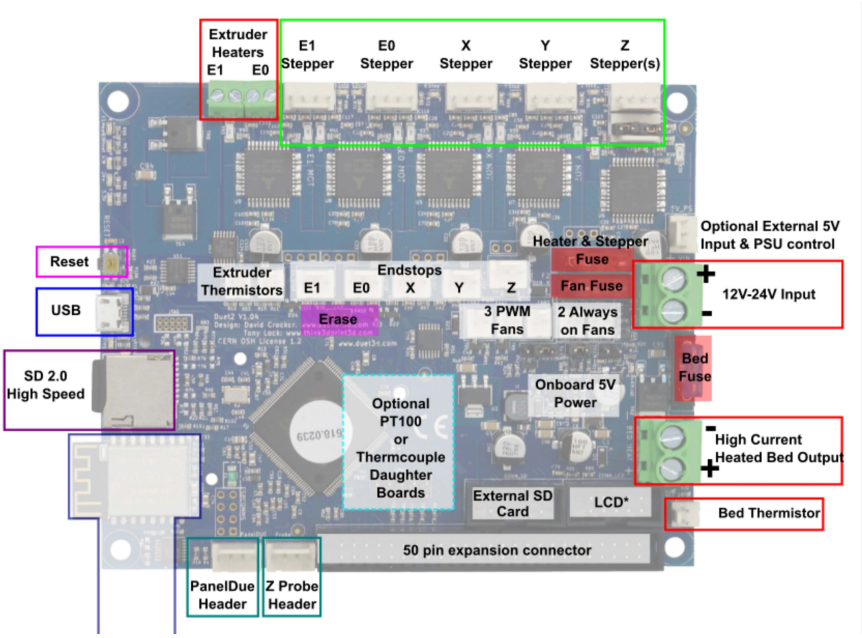

Figure 3.3: Schematic of the Duet 2 board (Duet3D, 2020).

3.2V and 1.68A, and the motor's holding torque is 0.44$N \cdot m$. NEMA 23, M57STH51-3008DC-S, works with 3.15V and 2.1A, and the motor's holding torque is 1$N \cdot m$.

3.4.3 *Flow Sensor*

SLF3S-0600F (Sensirion, Switzerland) liquid flow sensor was used in the flow rate measurement experiment. It can measure the flow rate with $\pm 5\%$ accuracy and repeatability (Sensirion, 2021).

The sensor was calibrated to water, isopropyl alcohol and acetone by the manufacturer. Therefore, the required calibration for glycerol was made by measuring the weight of extruded volume and comparing the sensor data.

3.4.4 *Weighing Scale*

PFB 200-3 (Kern, Germany) precision balance was used to measure the accuracy and precision of extrusion. It shows measurements with three decimal places and can measure with $\pm 0.001\%$ accuracy. The PFB 200-3 was chosen because it is small, light and portable. When weighing samples, the balance was placed on a lab table that was level to ensure accuracy.

3.4.5 Dimension Measuring

The accurate assessment of printed components is key for validating manufacturing quality and comparing dimensional accuracy between Fused Filament Fabrication (FFF) and Selective Laser Sintering (SLS) processes. The methodology for measuring component dimensions was as follows:

- **Instrumentation:** RS PRO digital metric calliper (RS Components, UK) was used to measure the dimensions of produced components to validate the manufacturing accuracy. It can measure up to $150mm$ with $\pm 0.01mm$ resolution.
- **Calibration:** The digital calliper was calibrated as per the guidelines of the manufacturer, setting the zero point to mitigate systematic errors.
- **Measurement:** Each component's dimensions were measured three times, and the calliper was applied gently to prevent deformation.
  - Length: Longest dimension between two distant points.
  - Maximum Diameter: Largest diameter, often perpendicular to the length axis.
- **Data:** Measurements, including uncertainties, were recorded for subsequent statistical analysis, comparing FFF and SLS components.

Measurements of FFF and SLS printed components were obtained using the established methodology. The results can be seen in Section 6.5, which presents a comprehensive evaluation of dimension accuracy.

3.5 Prototyping Materials

The purpose of this work is to design and development of a pump which is capable of handling complex fluids. The development of a pump is an iterative process and contains many prototyping cycles, resulting in many waste materials. Therefore, we selected biodegradable and recyclable materials whenever possible to decrease our research footprint.

3.5.1 Polylactic Acid (PLA)

Polylactic acid (PLA) is a biodegradable thermoplastic polyester. It was the main prototyping material in this research due to its low cost and easy printability by the fused filament fabrication (FFF) technique. PLA filament was used to prototype most PCP components in the concept and product development phases. This material offers a practical solution for developing prototypes that meet project budgets while delivering high-quality outcomes. This point is particularly noteworthy compared with other materials like ABS and PEEK, which might have better mechanical attributes but often come at a higher cost. This research aimed to find a middle ground between financial considerations and the demand for high-quality results by opting for PLA.

Moreover, PLA's exceptional ability to be printed using the FFF method made it an excellent choice, and this compatibility simplified the prototyping process during the concept development stage. In contrast, materials such as ABS and PEEK often presented intricate printing challenges while providing impressive mechanical strength and required higher printing temperatures. These complexities could introduce obstacles and hinder overall advancement. In addition, the easy and consistent printability of PLA contributed to the feasibility of the project timeline. Predictable performance decreased the risk of interruptions and enabled efficient progression through various stages of the research.

Furthermore, sustainability and environmentally responsible practices played a key role in selecting materials. The natural biodegradability of PLA fits well with the current focus on eco-friendly manufacturing methods. PLA has advantages over other materials, such as ABS, which could release harmful substances while being printed. This aspect highlights the research's commitment to addressing environmental concerns.

PLA filament with an average density of $1.24 g/cm^3$ and diameter of $2.85 \pm 0.10 mm$ was purchased from RS Components (UK) (details can be found in Appendix 2).

3.5.2 Polyamide 12 (PA 12)

Polyamide 12 (PA12) is widely used in the selective laser sintering (SLS) method in AM. Materialise (UK) company was selected to produce prototyping pump parts, and PA12 was selected due to its biocompatible feature among their material list. Manufactured parts used

in the PCP prototyping to compare the quality and performance of the FFF technique.

3.5.3 Poly(methyl methacrylate) (PMMA)

Polymethyl methacrylate (PMMA) was processed by laser cutting manufacturing method in prototyping due to its faster manufacturing time than AM.

PMMA, also known as acrylic or plexiglass, is supplied by Bay Plastics (UK) and processed in an LS6090 PRO Laser Cutter (HPC Laser, UK).

3.6 Validation Test Materials

3.6.1 Rationale

Hydrogel biomaterials used in the bioprinting application show non-newtonian and shear-thinning behaviours. Glycerol and Petroleum Jelly are the most available and the nearest alternatives to mimic its behaviours. These materials are low-cost and readily available for bioprinting experiments. Therefore, these two materials were used as initial test materials.

Nivea Creme is commonly used as a dispensing printer test material because of its shear-thinning and fast shear-recovery behaviour (Paxton et al., 2017). However, the syringe-filling process of the Nivea creme causes air-filled cavities and makes the extrusion process unstable. For this reason, petroleum jelly, which has shear-thinning behaviours, was selected, and it can be melted and filled in the syringe without air bubbles (Park and Song, 2010).

Glycerol was selected due to its similar viscosity to biomaterials used in bioprinting. Glycerol viscosity ranges from 0.6442 to $1.487 Pa \cdot s$ at the temperature ranges from 19.74 to 29.44 °C, and the suitable viscosity range for extrusion-based bioprinting is defined as the range from 0.3 to $30 Pa \cdot s$ (He et al., 2016; Ferreira et al., 2017).

Tap water was used to calibrate syringe pumps and to validate the large-volume syringe pump built in-house.

3.6.2 Glycerol

Pharmaceutical-grade glycerol (100%v/v) was purchased from Boots (UK). The experimental flow validation test was used as a dispensing fluid (Chapter 5).

3.6.3 Petroleum Jelly

Vaseline Original Petroleum Jelly was purchased from Boots (UK). It was used as a dispensing fluid in the extrusion validation test (Chapter 8).

3.6.4 Water

The PHD2000 (Harvard Apparatus, US) and an in-house built large-volume syringe pump (LVSP) were calibrated by weighing the amount of extruded tap water. It was used due to easy accessibility, and the calibration process does not require any safety requirements.

In addition to calibration, tap water was used to observe the sealing performance of generated concepts.

3.7 Syringes and Needles

In the research, $5ml$, $20ml$ and $60ml$ BD plastic syringes and $20ml$ and $50ml$ SAMCO glass syringes were used to compare the effect of cartridge volume on printing accuracy and precision.

The tapered plastic needles were selected with the internal diameter of $0,26, 0.41, 0.61$ and $0,84mm$ due to their common use in previous research (Pusch et al., 2018; Webb and Doyle, 2017; Fedorovich et al., 2012).

3.8 Material Processing Methods

This research proposes a proof of concept and prototype generation for a low-cost, novel PCP. Additive manufacturing is an accessible and fast option with the ability to fabricate parts with 100um accuracy. Therefore, most of this research used additive manufacturing technologies to produce prototypes.

PCPs have a rotor which rotates inside the stator part, and the manufacturing tolerance is a determining factor for the pump performance, including material leakage, backflow and viscosity range (Al-Safran et al., 2017; Canessa et al., 2017). FFF technology was the main manufacturing method, and SLS and SLA technologies were used for the comparison of the manufacturing accuracy of these technologies.

3.8.1 Fused Filament Fabrication (FFF)

The FFF technology was used to produce fast concept generation with the Ultimaker 3 using 0.4*mm* and 0.25*mm* print heads. While a 0.4*mm* print head can provide two times with the production speed, the 0.25*mm* print head produces better accuracy and surface quality. Therefore, PCP concepts were first produced with the 0.4*mm* print head. Compared to the printed prototype, the 0.25*mm* print head was selected due to better performance in terms of dimensional accuracy and surface quality.

3.8.2 Selective Laser Sintering (SLS)

The SLS additive manufacturing technology was used to manufacture prototype parts. The main reason behind the selection of this technology was to compare the part quality of FFF technology. SLS part production was outsourced by Materialise (UK) company. The prototype parts were fabricated using SLS additive manufacturing technology with PA 12 material. The selection of PA 12 allowed for a direct comparison of part quality against the FFF method. The purpose of using the SLS approach was to identify unique characteristics and understand the strengths of each methodology. The practical implementation of SLS part production was outsourced to Materialise (UK).

3.8.3 Laser Cutting

The LS6090 PRO laser cutting machine (HPC Laser, UK) was chosen to enable the precise fabrication of components which are suitable for laser cutting, and PMMA was employed as a material for this purpose. The decision was due to its significant advantage in quick processing compared to the more time-consuming additive manufacturing methods. This laser-cutting machine played a critical role in the prototyping phase, particularly in the prototyping of both the LVSP and PCP concept trials.

4

USER QUESTIONNAIRE AND USER INTERVIEW

This chapter was submitted as a part of an article to the CIRP Journal of Manufacturing Science and Technology, and it is under review with the title of "Conceptual design and development of a progressive cavity pump for extrusion-based additive manufacturing applications".

4.1 Introduction

The literature review described the advantages and limitations of bioprinting methods. There was not enough literature review regarding the bioprinter user experience, and one of the key elements in the product development method can be the gathering of user requirements. Therefore, a user questionnaire and interview were conducted to obtain insight into bioprinter capabilities and user expectations. The expectation from this study was to feed the product development process to obtain a better extrusion unit.

4.2 Survey Methodology

This section outlines the survey methodology employed in this study, including participant invitations and demographics.

4.2.1 Participant Invitations

To ensure comprehensive and representative research, we invited individuals to participate in our survey using the following key components:

- **Selection Criteria:** Participants were invited based on their active involvement in bioprinting research and their status as bioprinter users. This criterion was essential to ensure that the respondents possessed relevant knowledge and practical experience.
- **Institutional Diversity:** We aimed to include individuals from a wide range of academic and research institutions, including universities and research centres. This approach ensured a diversity of perspectives.
- **Invitation Channels:** Invitations were extended through a combination of email requests and verbal communication. Email invitations were sent to eligible participants, and in some cases, verbal invitations were also extended to ensure a broad reach and engagement with potential participants.

4.2.2 Demographics of Participants

It is crucial to understand the demographics of survey participants to put the survey results in context and identify potential biases. The following demographic information was collected:

- **Number of Participants:** A total of 20 participants responded to the survey, representing 16 different academic institutions. This diverse group of respondents contributed to a comprehensive understanding of bioprinter user experiences.
- **Institutional Affiliations:** Participants from a variety of academic and research institutions enhanced the degree of experiences and insights.
- **Academic Roles:** Participants held various positions, including 4 Professors, 9 with a PhD, and 7 PhD students.
- **Geographic Diversity:** Participants were located in various regions, contributing to the international nature of the study. These regions include the following countries:
  - United Kingdom: 4 participants
  - United States: 8 participants
  - South Korea: 1 participant
  - Germany: 1 participant

- Italy: 4 participants
- Slovenia: 1 participant
- Turkey: 1 participant

4.2.3 Survey Platform

The user questionnaire was distributed via the online survey platform provided by Jisc (UK), ensuring a secure and user-friendly environment for data collection (Jisc, n.d.). Efficient data gathering and analysis were made possible by the online survey format.

4.2.4 Interviews

User interviews were conducted through a combination of face-to-face meetings and virtual interviews using the Skype (U.S.) application (Microsoft, n.d.).

4.3 Results

4.3.1 User Questionnaire

In the user questionnaire, ten questions were asked to define the bioprinter's capabilities, machine features and user expectations from a bioprinter regarding material printing ability. Out of the 20 participants, only 18 answered the first seven questions since two were not using a bioprinter. The questions were as follows:

1. Which company's bioprinter do you use?
2. What materials do you commonly print?
3. How long does it take to prepare the bioprinter for printing?
4. How do you rate the bioprinter's complexity of use?
   (a) Machine use
   (b) Software use
   (c) Sterilization process

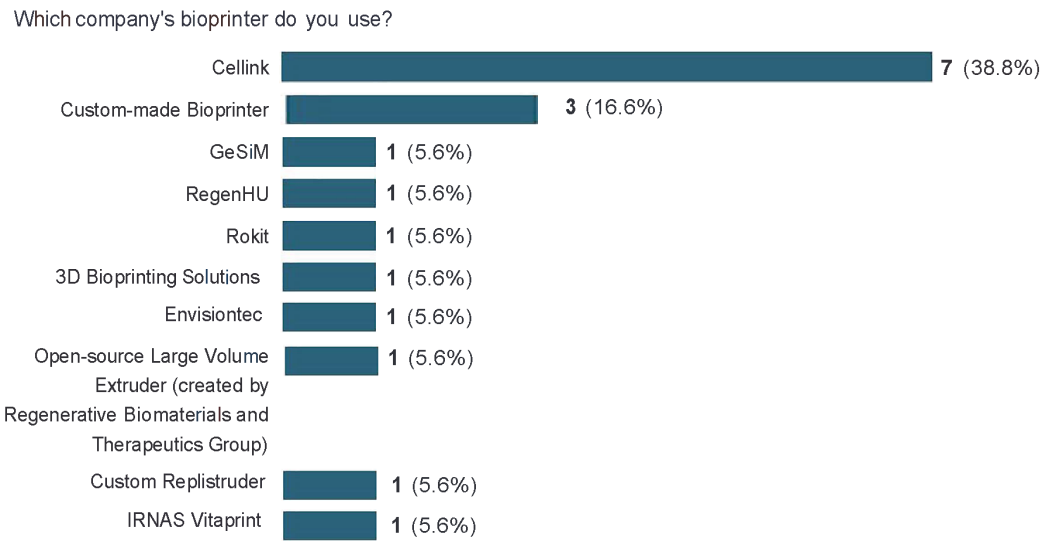

Figure 4.1: Bioprinters used by the participants.

5. How do you rate the customization practicality of the bioprinter for future use? (E.g. changing print head of adding new apparatus.)
6. Which of the following liquids are printable with the bioprinter
7. What is the software you normally use to drive the bioprinter?
8. Could you please rate the importance of extrusion features?
   (a) Hydrogel extrusion
   (b) Filament extrusion
   (c) Pellet extrusion
   (d) Multi-material extrusion
9. Could you please rate the importance of following features?
   (a) UV light for cross-linking
   (b) Print head temperature control
   (c) Print bed temperature control
   (d) Enclosed and controllable printing environment
10. How many materials do you need to print simultaneously in a process?

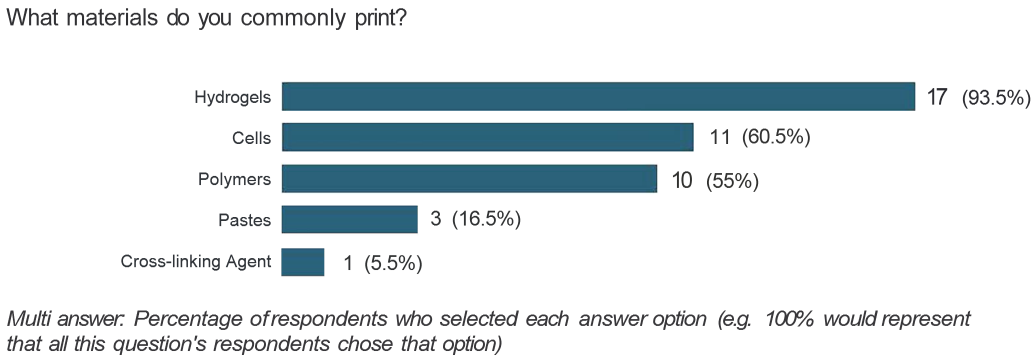

Figure 4.2: Materials used by the participants in bioprinting.

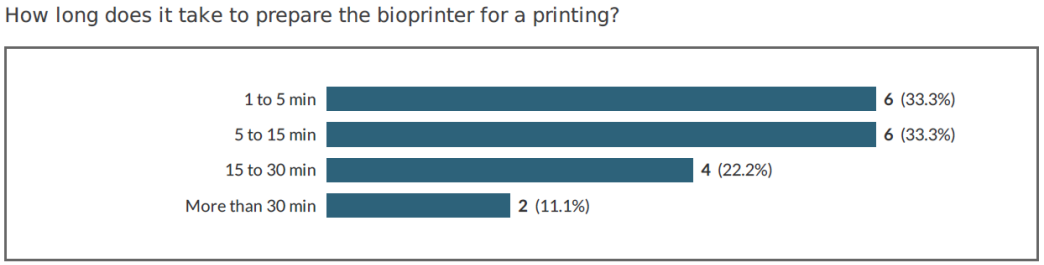

Figure 4.3: Preparation time of a bioprinter.

The first question aimed to learn which company has the most costumer and the prevalence of custom-made bioprinters. As seen from Figure 4.1, the Cellink (USA) company is the most popular among the commercial bioprinter companies, and 25% of the users own an open-source or custom-made bioprinters.

In Figure4.2, the results show the usage prevalence of biomaterials in bioprinting applications. Multiple answers were allowed from participants, and it can be seen that hydrogels and cells are the most common biomaterials. In addition, it can be seen from the figure that different materials are used in bioprinting, including silicones, cross-linking agent, pastes, cements, glass nanoparticles and ceramics.

Figure 4.3 displays the results of the time required to prepare a bioprinter, and it can be seen that up to five minutes and 5 to ten minutes range constitutes the 66.6% of the users.

The questions of machine use complexity level were asked for machine use, software use and sterilization process. As can be seen from Figure 4.4, the distribution is in the range of easy to an acceptable levels for all three questions. What is interesting about the results is that the users find the sterilization process more difficult than machine use and software use.

The results of the question about the difficulty level of bioprinter customisation are presented

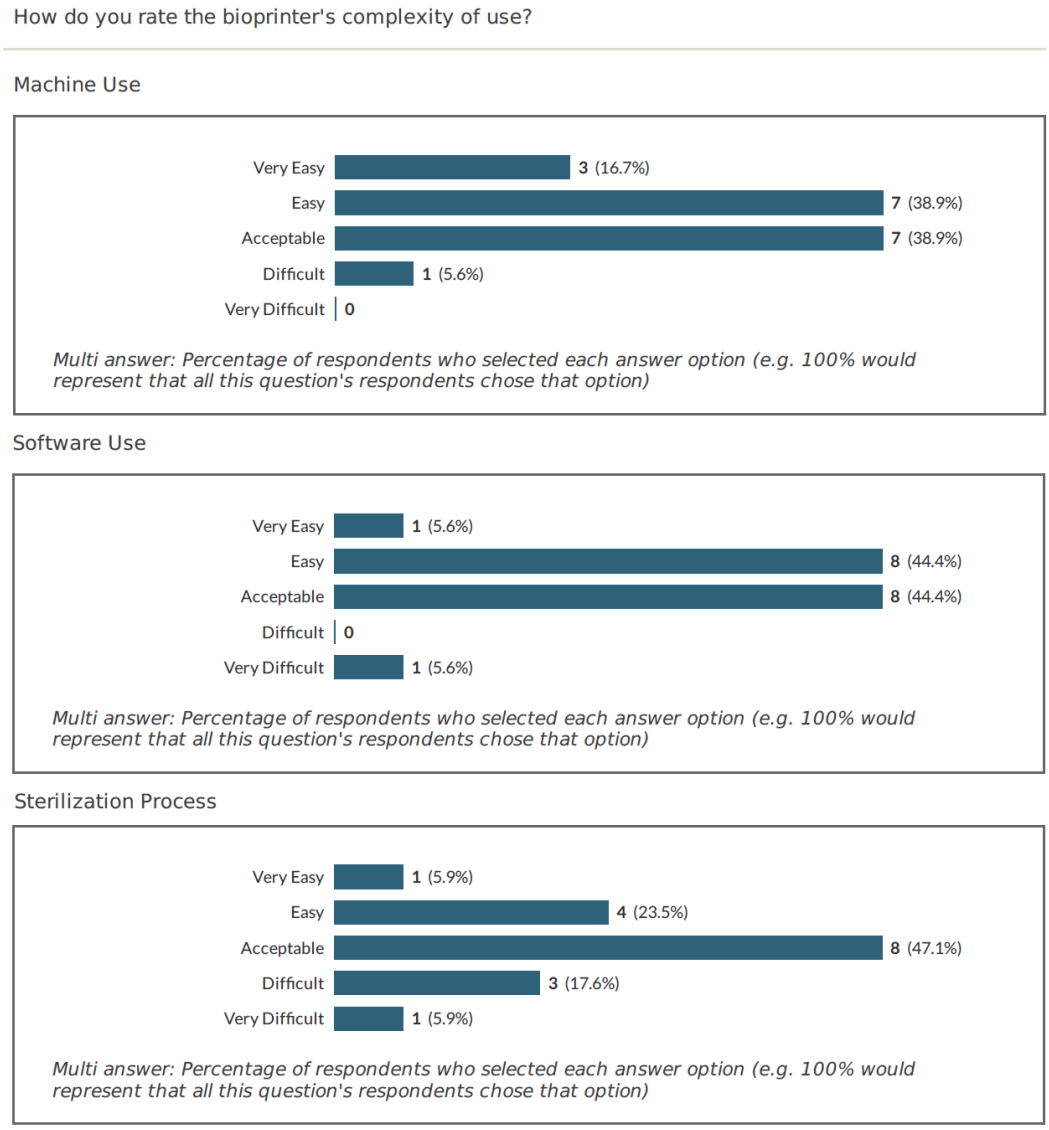

Figure 4.4: Complexity level of the machine use, software use and sterilization process.

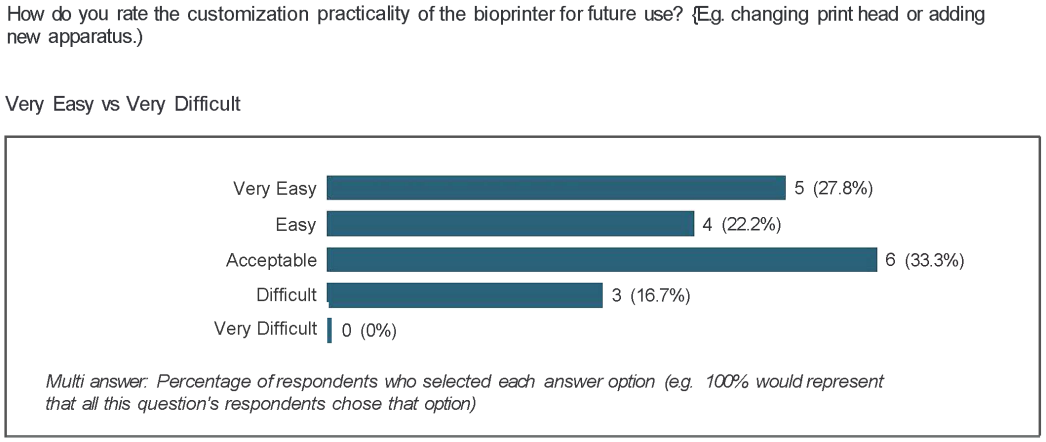

Figure 4.5: Difficulty level of customization practicality of a bioprinter for future use.

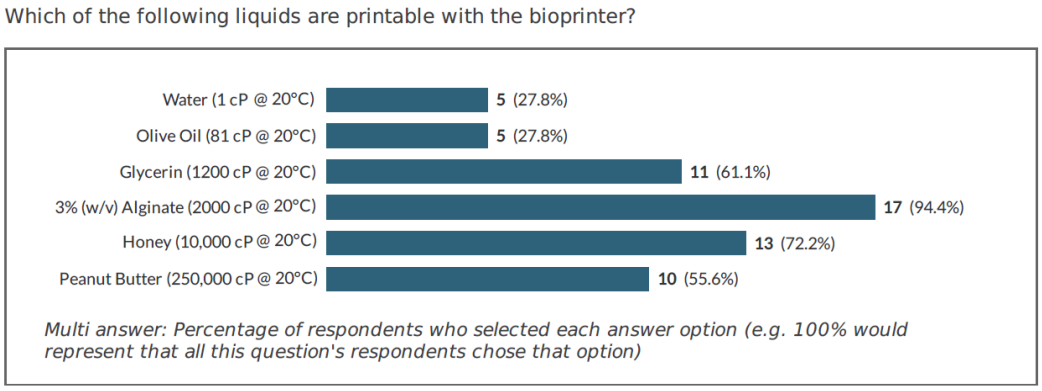

Figure 4.6: Evaluation of extruding materials of different viscosities.

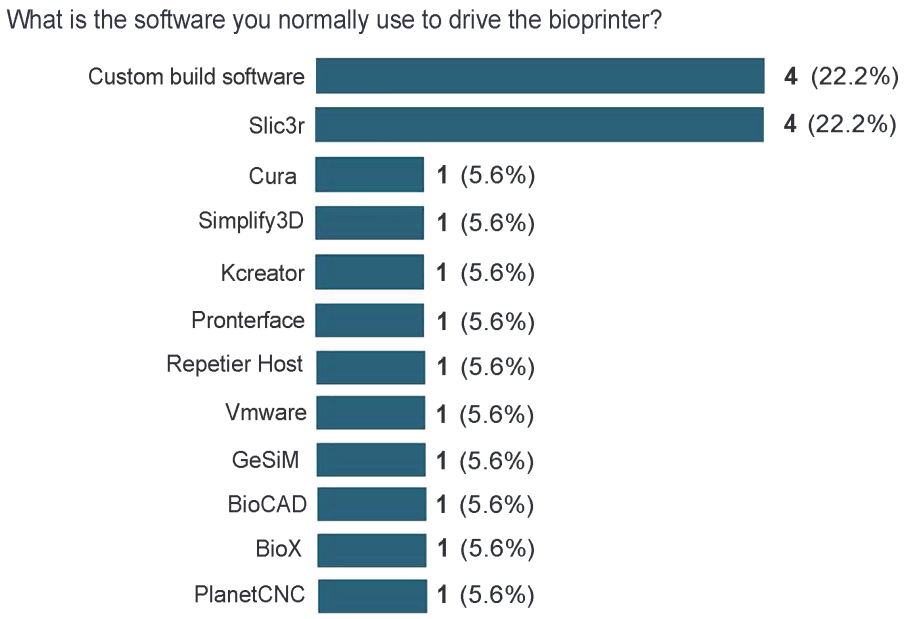

Figure 4.7: Software used by the participants.

in Figure 4.5. While nine participants found the customisation very easy or easy, six and three considered it medium and highly difficult, respectively.

Figure 4.6 provides the results of printability consideration of bioprinter users, and multiple answers were allowed from participants. As can be seen from the bar chart results that the alginate with the viscosity of $2Pa \cdot s$ at $20 \deg C$ has the best printability. The most surprising aspect of the results is the printability consideration of the peanut butter (viscosity of $250Pa \cdot s$) because it contradicts the literature review conclusion. In particular, it was observed in the literature that the extruding material's viscosity should be less than $100Pa \cdot s$, and the optimal viscosity range is between 0.3 and $30Pa \cdot s$ (He et al., 2016).

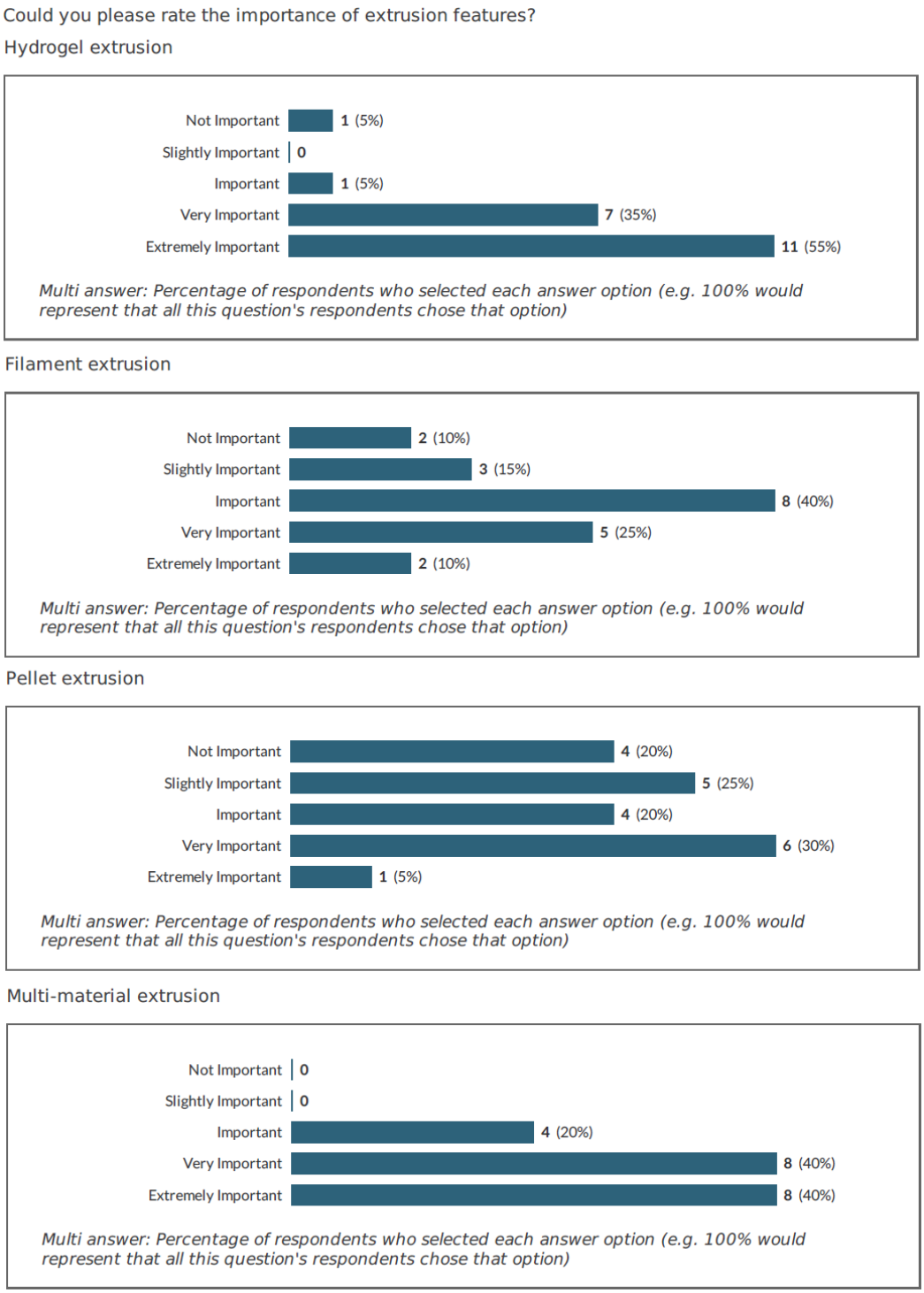

Figure 4.8: Importance level of the type of material extrusion.

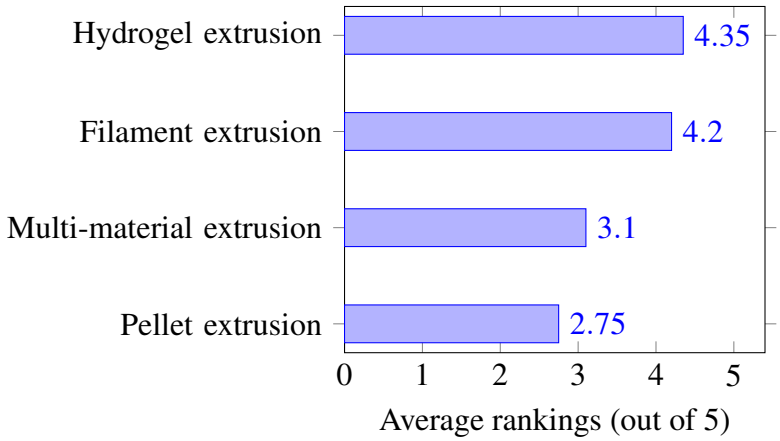

Figure 4.9: The chart displays the rankings for the following features: hydrogel extrusion, filament extrusion, multi-material extrusion and pellet extrusion. The rankings are on a scale of 1 to 5, with higher values indicating greater importance.

Figure 4.7 shows the results of the open question of which software is used by the participants. The question was aimed at learning the distribution of commercial and open-source software usage.

The questions of importance level of extrusion features were asked for the hydrogel, filament, pellet and multi-material extrusions. The results can be seen in Figure 4.8 and Figure 4.9 shows the average importance rankings of features. In the figure, the most important extrusion feature can be seen as the hydrogel extrusion. Similarly, multi-material extrusion can be considered as an important requirement for bioprinter users. However, filament and pellet extrusion features were attributed to medium-level importance.

Figure 4.10 presents the results of the importance level of the following features; UV light for cross-linking, print head temperature control and enclosed and controllable printing environment, and the average importance rankings of features can be seen in Figure 4.11. In terms of UV light feature importance, it can be concluded that 50% more users found it important. It could be because of the cell usage of these users, and UV light is required for cleaning purposes. The results of the importance level of the other three features show that these features are crucial for a bioprinter.

The last question aimed to obtain the needs of how many materials are required in a single bioprinting process. As can be seen from Figure 4.12, eleven and nine participants need one to two materials and three to four materials in a single print, respectively. It is clear that almost 50% of the bioprinter users require more than two materials.

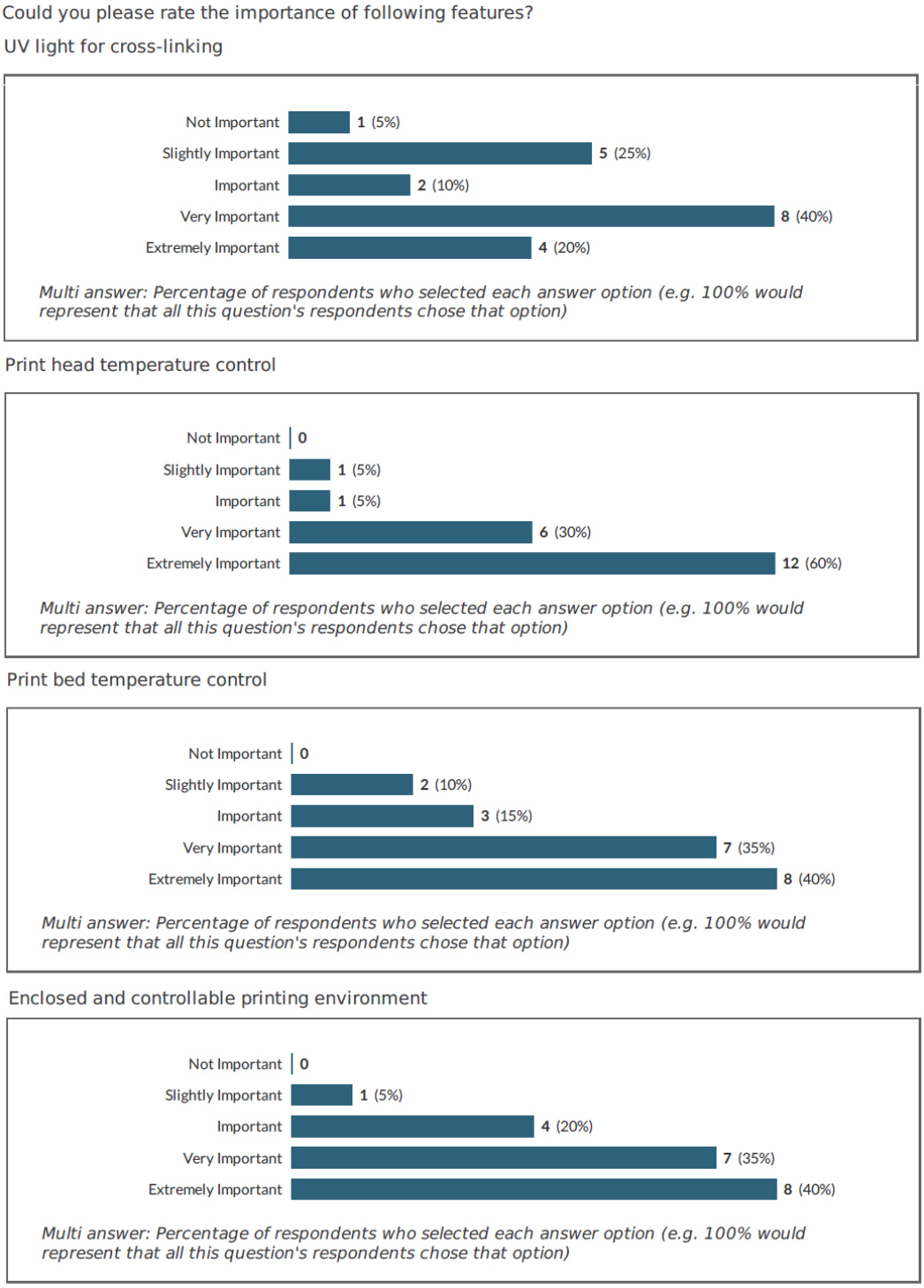

Figure 4.10: Importance level of the bioprinter features.

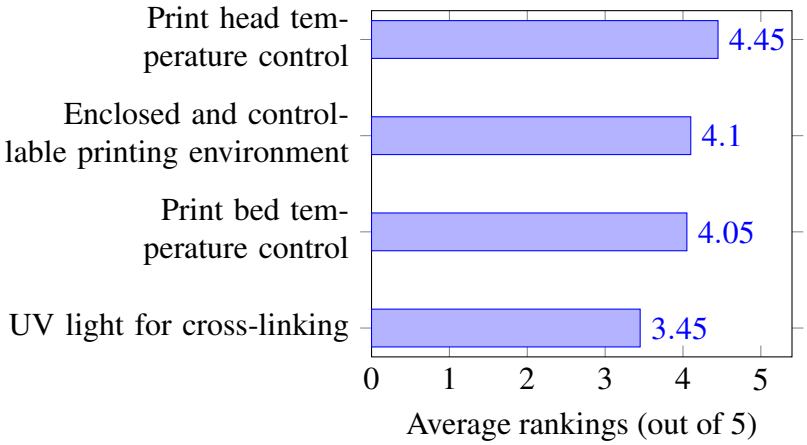

Figure 4.11: The chart displays the rankings for the following features: print head temperature control, enclosed and controllable printing environment, print bed temperature control, and UV light for cross-linking. The rankings are on a scale of 1 to 5, with higher values indicating greater importance.

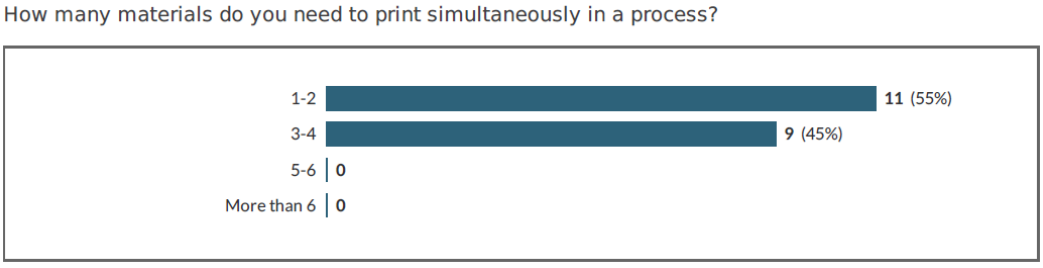

Figure 4.12: Number of multi-materials needed in a printing process.

4.3.2 User Interview

User interviews were conducted with five bioprinter users from two different universities. The same questionnaire and the question about problems they face when using a bioprinter were asked to identify the types of problems. Four of the participants were from the United Kingdom, and one participant was from Slovenia.

In the first interview, there was an opportunity to observe the bioprinting process. The most important finding in the observation was the leakage from the plastic syringes before and after the bioprinting process. The leakage before the process happened after the syringe filling operation. The user waited around two minutes to stop leaking from the syringe needle. It can be concluded that it is an important problem because printing is not a continuous process and requires movement without print. While the solution to the problem is the retraction in FFF, it is not a straightforward solution in bioprinting due to the usage of various materials having different flow properties. Therefore, the solution to the problem requires adjustment for each print; however, it is time-consuming and causes a lot of biomaterial waste. In order to provide a clearer understanding of user interviews, we include direct excerpts from participant experiences and concerns. One interviewee stated that "leakage is a significant issue as it wastes expensive biomaterials and valuable time". These quotes emphasize the seriousness of the leakage issue. Similarly, this problem was mentioned by Banović and Vihar (2018), and details can be found in the literature (see Chapter 2).

In the following interviews, participants mentioned the same problem described in the previous paragraph. In addition, there were three notable requirements mentioned by participants; 1) easy-to-clean extrusion unit and environment, 2) large-volume bioprinting, and 3) low-cost extrusion unit.

Easy-to-clean is an obvious requirement for bioprinting due to the usage of cells. It can be divided into bioprinter printing chamber cleaning and extrusion unit cleaning. The focus of this research is the extrusion unit, and it will be the main consideration. The most common approach to make the printing process clean is to use a disposable syringe driven by pneumatic or mechanical forces. However, they have less accuracy and precision than advanced extrusion units (i.e. progressive cavity pump), as mentioned in the literature (Fisch et al., 2020). Consequently, the requirement for easy-to-clean or disposable features can be

inferred as a novel PCP design objective.

Large-volume bioprinting was mentioned by two participants, while others found it unnecessary, which was due to their research areas. In syringe pump-based large-volume bioprinting, two main limitations can be described for direct and indirect extrusions. In the direct extrusion, the syringe is placed onto the gantry. Consequently, the greater the volume, the greater the weight on the 3D printer gantry, which causes low accuracy or slow speed. To explain, the fast movement and stopping cause a vibration of the printer and decrease the accuracy; therefore, there is an inverse relationship between the accuracy and the speed. In the indirect extrusion, the syringe is not placed onto the gantry, and the connection between the needle and syringe is provided with a tube. Consequently, the printing process produces a large volume of waste material, and the usage of the tube increases the required torque to push the material due to the pressure drop.

The last and obvious expectation from the participants was the low-cost extrusion unit. In the words of one participant, "Affordability is important, especially in an academic setting where budgets can be tight". The PCP is the most common approach in the literature after the syringe-based extrusion units. However, it is a costly unit, and this prevents its widespread use (Wang et al., 2016). Therefore, PCP technology can highly benefit from a novel approach of decreasing the cost or developing a disposable pump.

4.4 Discussion

In the user questionnaire, bioprinter user experience was collected through ten questions. The most important questions were considered as the material extrusion and bioprinter features, as can be seen in Figure 4.8 and Figure 4.10. In order to provide more clear representation of these results, Figure 4.13 is produced.

The first four results show the importance of printing materials for bioprinter users, and the last four results show the importance level of machine features for bioprinter users. The figure shows that the most significant demand is for hydrogel extrusion compared to the filament and pellet extrusion. Therefore, it can be concluded that the PCP development process will benefit from a liquid flow characterisation of a syringe-based extrusion unit.

Multi-material extrusion is seen as a required feature for bioprinter users. Concerning this

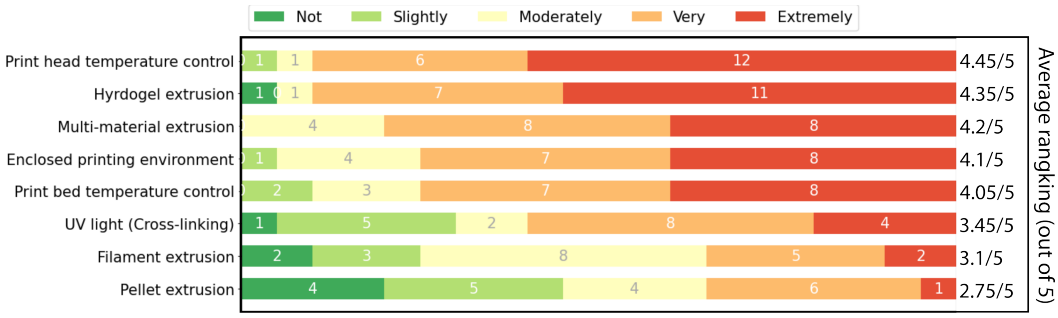

Figure 4.13: Importance level of bioprinter features.

result, the question of "how many materials are needed for a process" was asked. The results revealed that nine participants indicated three to four materials, and eleven participants found one to two materials enough (see Figure 4.12). Consequently, the aspect of multi-material printing capability will be a consideration point in the PCP design.

It is apparent from the results of the last four questions that all features are essential for users. The only significant difference is the high importance of the print head temperature control. The feature of the print head temperature control was the most relevant and significant results to use in the design stage. However, it can also be considered as an further work due to time-constraint of the project. Besides, The fact that the heating feature can be added later will be useful to consider at the design stage.

4.5 Conclusion

The purpose of the current study was to determine the bioprinter user experience and requirements to feed the product development process to obtain a better extrusion unit.

Together these results provide important insights into user needs in terms of expected material extrusion and bioprinter features. The most important conclusion can be drawn from the user questionnaire is that bioprinter users expect an extruder that can print multiple hydrogel materials in a temperature-controlled environment. In addition, The user interview revealed that the syringe-based extruders were insufficient in terms of easy-to-clean extrusion unit, large-volume bioprinting and low-cost extrusion unit, and there was a leaking problem.

Several design aspects were determined by deducing from the results. Before moving into design and development stage, the limitations of syringe-based extruder units requires a further investigation. For this reason, the performance evaluation of syringe pumps was

considered as a necessary need, and it was decided to conduct a study on this subject. This study can be found in the following Chapter 5.

5

SYRINGE PUMP EVALUATION

This chapter was presented at AMC TURKEY 2021 (TURKEY) conference and published in the Journal of Additive Manufacturing Technologies as a selected paper with the title of "Effect of process parameters of the positive displacement pump for extrusion based bioprinting application.".

5.1 Introduction

EBB attracts great attention due to its ability to extrude high viscous material (range from 0.3 and 30$Pa \cdot s$) with necessary precision for various applications (He et al., 2016). In the EBB applications, syringe pump-based extruders are the main choice due to their uncomplicated usage and easy-to-clean attributes. While this method provides acceptable extrusion, several disadvantages remain challenging, such as material leakage from the nozzle, extrusion precision and cartridge volume restriction.

In the bioprinting literature, a relatively small body of research is concerned with the controllability of the flow and the effect of extrusion parameters on printability. One study suggests that the compressibility of the plunger rubber of a plastic syringe has a negative effect on extrusion accuracy in terms of start and stop accuracy, which results in delayed extrusion start and material leakage after stopping the extrusion (Banović and Vihar, 2018; Pusch et al., 2018). However, fluid flow behaviour still requires more attention to understand other effects stemming from the extrusion unit, such as the effect of compressed volume in the syringe.

While tissue engineering researchers use the EBB, the same syringe pump-based extrusion method is used in various research areas, including the direct-ink-writing (DIW) of ceramic pastes, 3D food printing, micro dispensing of conductive inks and adhesive dispensing (Li,

2019; Karyappa and Hashimoto, 2019; Abas et al., 2021; Chen and Kai, 2004). Therefore, more detailed research on the controllability of the flow can be found in the related research areas.

The effect of compressed volume can be understood from the research comparing syringe-based pumps with other methods, including needle valve and progressive cavity pump (PCP). This kind of comparison can be seen in recent articles from the DIW and bioprinting research areas (Li et al., 2017; Fisch et al., 2020). A recent study compares the performance of a pneumatic syringe-based pump and a PCP (Fisch et al., 2020). It can be clearly understood from the Figure 5.1 that the usage of PCP increases the precision and accuracy of the printed object due to the constant compressed volume at the outlet of the pump (Fisch et al., 2020).

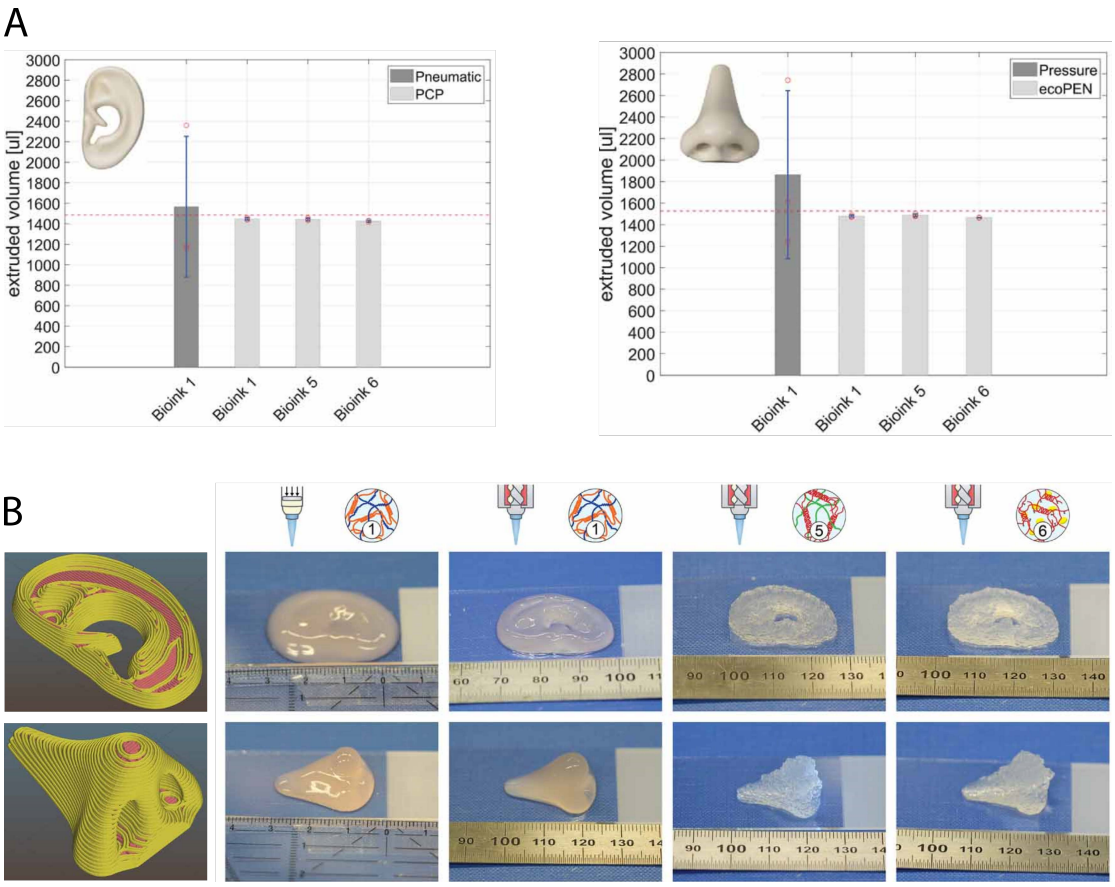

Figure 5.1: (A)Extruded ear and nose volume using the pneumatic system and the PCP (three different bioinks were used). (B) Illustrations of the sliced and printed ears and noses with a ruler Fisch et al. (2020).

This Chapter presents the construction of a large-volume syringe pump (LVSP), the examination of the plunger rubber compressibility of a plastic syringe, and the influence of the

amount of compressed volume inside the syringe on extrusion accuracy.

5.2 Methodology

5.2.1 Experimental Setup

The LSVP was used in the extrusion quality test to assess the effect of volume on extrusion because the PHD2000 could not handle the 60ml syringe. Therefore, two experimental setups were set up with the LVSP and the PHD2000 pumps (see Figure5.2). Experiments measuring extruded volume were carried out to validate the LSVP's accuracy and precision compared to the PHD 2000. Subsequently, the LVPS was used to evaluate the effect of extruded material volume on printing accuracy.

Figure 5.2 provides a schematic overview of the experimental setups (A) and actual setup photos (B). Duet 2 control board was used to drive the in-house developed pump by sending G-codes via a computer. Sensirion flow rate sensor was used to measure the flow rate, and the dispensed volume was measured with PFB 200-3 (Kern, Germany) weighing scale. The details of the sensor, the scale and the control board can be found in Chapter3.

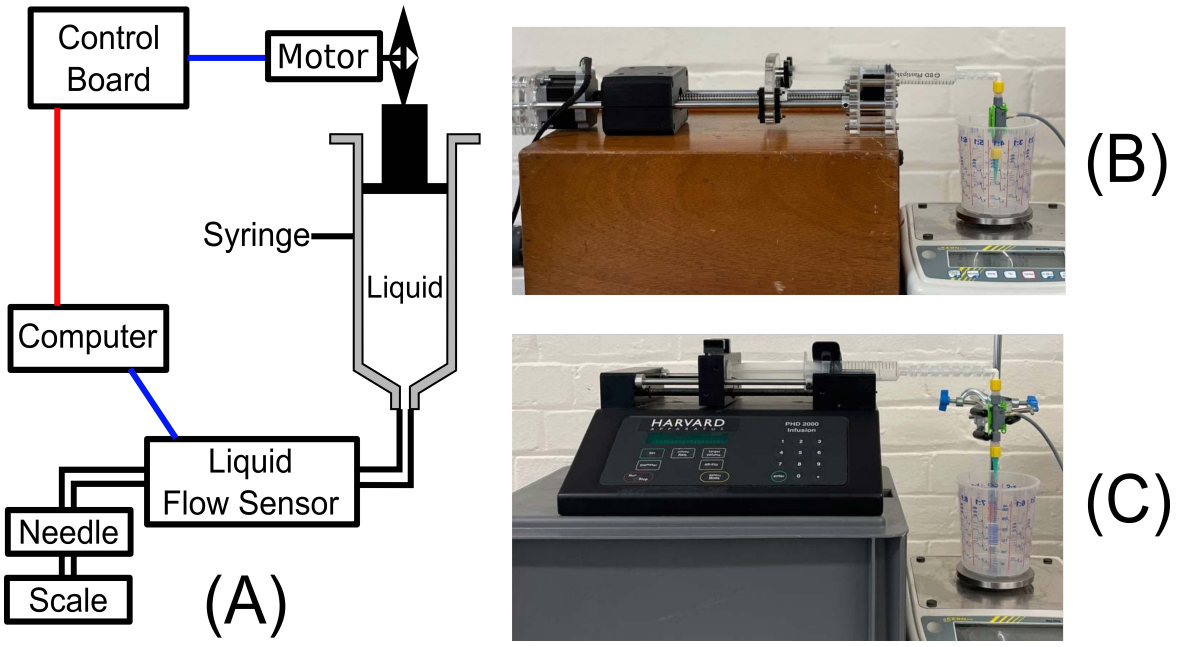

Figure 5.2: Diagram and demonstration of experimental setups. A) Experimental setup diagram for the LVSP and Harvard Apparatus PHD2000 Infusion syringe pumps. Blue and red lines show the connections, and the red line exists only in the LVSP. B) The LVSP with the sensor and weighing scale. C) The PHD 2000 with the sensor and weighing scale.

5.2.2 Validation of the LVSP

The experiment process parameters can be seen in Table 5.1. Syringe pumps were configured using these parameters. The experiment begins with filling the $5ml$ syringe with water and removing the air bubbles kept inside the syringe. Subsequently, the syringe was placed in the used pump, and the theoretical volume was extruded and then measured with the precision scale. Experiments were conducted ten times for each pump and at $18°C \pm 1$.

Table 5.1: The experimental parameters of the LVSP validation.

Parameter	Value
Flow Rate	$0.5ml/min$
Theoretical Extruded Volume	$0.5ml$
Needle Diameter	$0.41mm$
5 ml Plastic Syringe Diameter	$12.06mm$

5.2.3 The Effect of Plunger Rubber Compressibility of a Plastic Syringe on Extrusion Accuracy

The effect of plunger rubber compressibility on extrusion was investigated using the LVSP experimental setup. The experiment process parameters can be seen in Table 5.2.

Table 5.2: The experiment parameters of the effect of plunger rubber compressibility of a plastic syringe on extrusion.

Parameter	Value
Flow Rate	$500\mu l/min$
Theoretical Extruded Volume	$500\mu l$
Needle Diameter	$0.41mm$
Syringes	$60ml$ Plastic Syringe and $50ml$ Glass Syringe

The experiment begins with filling the used syringe with $20ml$ glycerol and removing air bubbles kept inside the syringe. Subsequently, the used syringe was placed in the pump, and the theoretical volume was extruded and then measured with the precision scale. Experiments were conducted three times for each pump and at $18°C \pm 1$. Subsequently, average values were calculated and multiplied by the calibration value (2.47) by fitting the sensor reading with the theoretical flow rate.

5.2.4 The Effect of Filled Syringe Volume on Extrusion Accuracy

This experimental plan was designed to show the effect of compressed volume inside the syringe and its effect on the flow rate. The LVSP experimental setup was used, and the process parameters of the experiment can be seen in Table 3.

The same experimental procedure as the previous section was applied, and $50ml, 40ml, 30mland20ml$ filled syringes were used. All experiments were conducted three times, and average values were calculated and multiplied by the calibration value (2.47) by fitting the sensor reading with the theoretical flow rate. The experiment was carried out at $18°C \pm 1$.

5.3 Results and Discussion

5.3.1 Design of the LVSP

This research aimed to develop an extrusion unit with a PCP. PCPs require a controllable material feeding unit, which could either be a pneumatic or a positive displacement pump. To decrease the cost and make the extrusion unit easy to use, the option of a positive displacement pump was selected to feed the PCP. Therefore, an LVSP was designed and developed, as seen in Figure5.3. The pump was designed to feed the PCP via silicone tubing, which also increases the volume of printing materials.

The design consists of laser cut, 3D printed and off-the-shelf components, and details can be seen in see Table 5.3. Figure 5.3 does not contain fasteners in order to make Figure understandable.

A NEMA 23 stepper motor powers the pump, and the power is transferred via a threaded rod. Linear bearings are placed in the carriage pusher, and the bearing stoppers hold the bearings in place to prevent wobbling. The syringe holder was designed to hold various syringes from $5ml$ to $60ml$, and the syringe fixer requires adjustment according to the selected syringe diameter. The 3D printed parts were designed to print without support, and a design with a less than 45° overhang angle rule was followed.

Laser-cut components were cut from a $5mm$ acrylic, and before the cutting operation, a test part was cut to evaluate the laser spot diameter. Subsequently, the design of the components was adjusted to obtain the required accuracy of the holes.

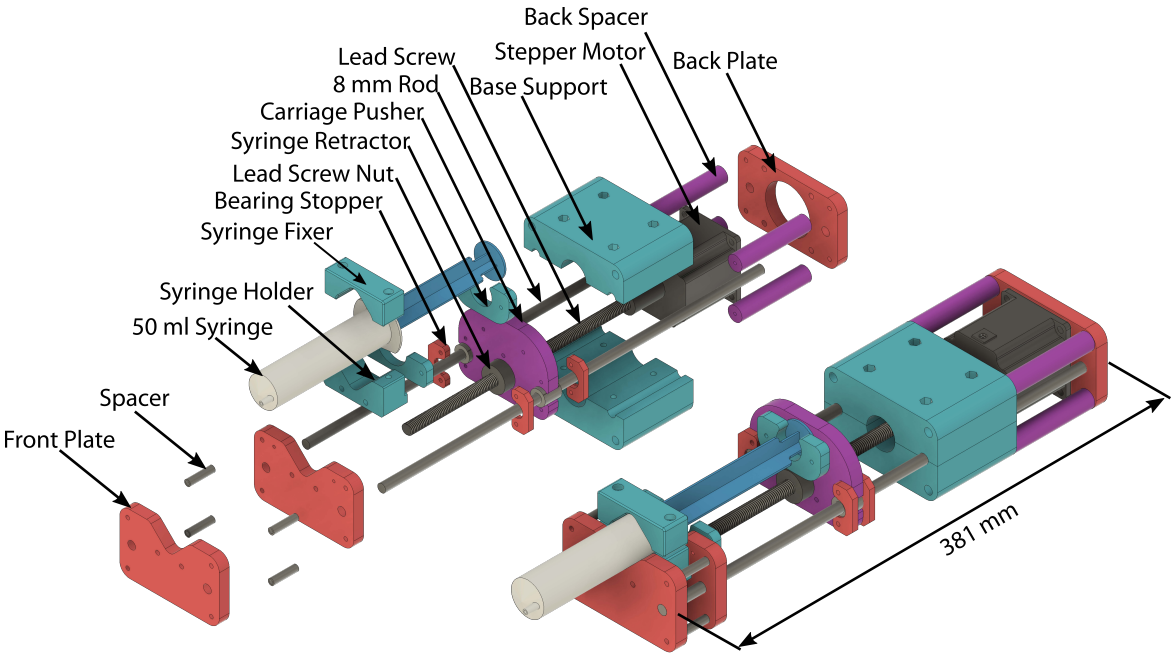

Figure 5.3: Large volume syringe pump design. Exploded view on the left and assembled view on the right.

5.3.2 *Validation of the LVSP*

The purpose of this experiment was to validate the LVSP. The comparison of accuracy, precision and repeatability of the PHD2000 and LVSP pumps are shown in Figure 5.4.

The average measured value for the PHD2000 pump is 0.4845*ml* with a standard deviation of 0.005212. While the theoretical extruded volume was calculated as 0.5*ml* according to the parameters given in Section 2, measured values are below the theoretical value. Similar results were observed for the LVSP as the average measured value of 0.4862*ml* with a standard deviation of 0.005281.

Results show that the LVSP can perform just as well as the PHD200 pump, and both pumps can provide repeatable extrusion with precision and accuracy. Therefore, there is no inconvenience in using the LVSP for the following experiments.

5.3.3 *The Effect of Plunger Rubber Compressibility of a Plastic Syringe on Extrusion Accuracy*

The correlation between rubber compressibility and extrusion accuracy was tested in this experiment. Figure 3 shows the result of the flow rate measurement for the plastic and glass

Table 5.3: Parts list of the LVSP components.

	Part Name	Product Code	Type	Qty	Cost (£)	Supplier
1	Front Plate	-	Laser Cut	2	5.50	-
2	Carriage Pusher	-	Laser Cut	1	2.75	-
3	Back Plate	-	Laser Cut	1	2.75	-
4	Syringe Holder	-	3D Printed	1	0.83	-
5	Syringe Fixer	-	3D Printed	1	0.80	-
6	Bearing Stopper	-	3D Printed	4	0.62	-
7	Syringe Retractor	-	3D Printed	1	0.12	-
8	Base Support	-	3D Printed	2	4.66	-
9	Back Spacer	-	3D Printed	4	1.96	-
10	Spacer	HPS-6-30-BR-NI	-	4	9.08	Accu
11	Lead Screw Nut	HPN-M8-A2	-	2	4.40	RS Components
12	Lead Screw	280-408	-	1	7.22	RS Components
13	8 mm Rod	786-6015	-	1	6.75	RS Components
14	Linear Bearings	172-1276	-	2	27.26	RS Components
			Total		£74.70	

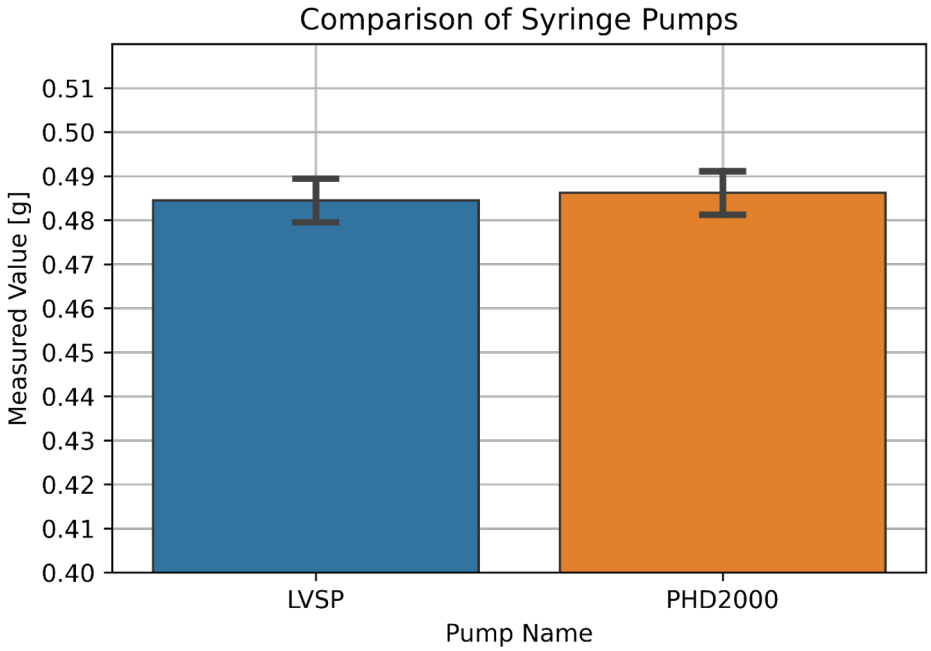

Figure 5.4: The weight measurement of the LSVP and PHD2000 pump.

syringes with the same process parameters.

The flow rate was set to $500\mu l/min$ and $500\mu l$ glycerol extruded. The sensor readings multiplied by 2.47 to fit the graph with the flow rate and a sensor reading below $5\mu l/min$ of

measured value disregarded according to the sensor accuracy data sheet (Sensirion, 2021).

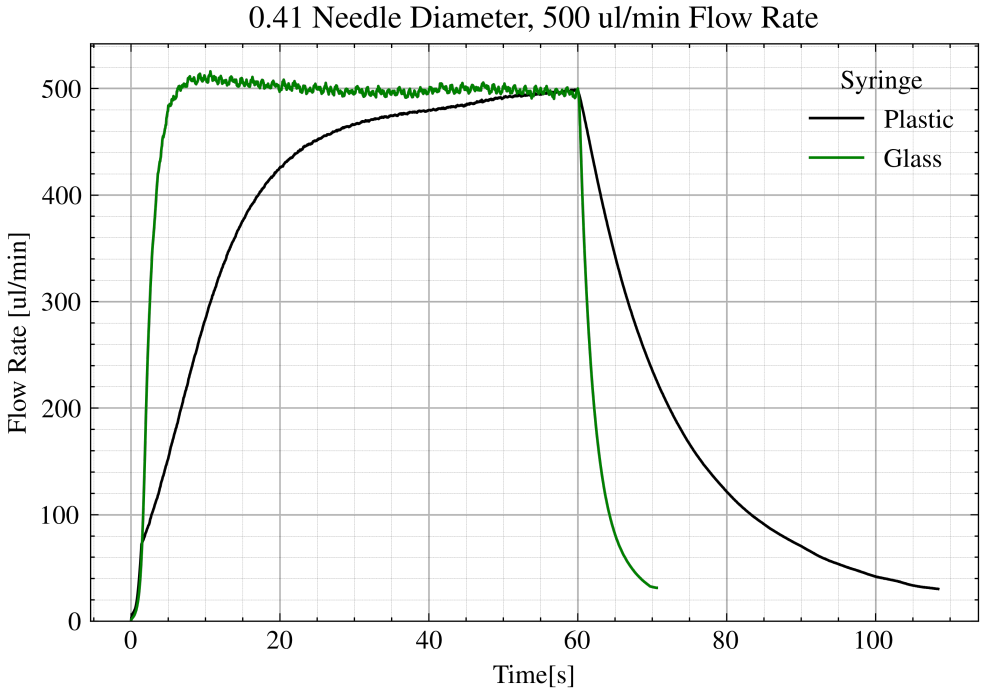

Figure 5.5: The flow rate measurement of the plastic and glass syringes to see the effect of plunger rubber compressibility.

As Figure 5.5 shows, there is a significant difference between the two syringes in terms of the required time to reach the desired flow rate and to complete extrusion. The required time to reach the desired flow rate was measured as $60s \pm 0.5$ and $7s \pm 0.5$ for plastic and glass syringes, respectively. Similar behaviour was observed during the completion of extrusion as $48s \pm 0.5$ and $11s \pm 0.5$ for plastic and glass syringes, respectively.

This result confirms the effect of rubber compressibility on the flow rate claimed by the recent research on developing an extruder for the bioprinting application (Banović and Vihar, 2018).

5.3.4 The Effect of Compressed Syringe Volume on Extrusion Accuracy

This experiment aims to show the effect of compressed syringe volume on extrusion quality. The result of the flow rate measurement for the glass syringe filled with $50ml$, $40ml$, $30ml$ and $20ml$ are shown in Figure 5.6.

Data filtering methods were not used when plotting the graph to see the compressed syringe volume's effect clearly. The flow rate was set to $500\mu l/min$ and $250\mu l$ glycerol extruded.

The sensor readings multiplied by 2.47 to fit the graph with the flow rate and a sensor reading below $5\%\mu l/min$ of measured value disregarded according to the sensor accuracy data sheet (Sensirion, 2021). Therefore, the graph was plotted with the sensor readings above the $10.1\mu l/min$ flow rate.

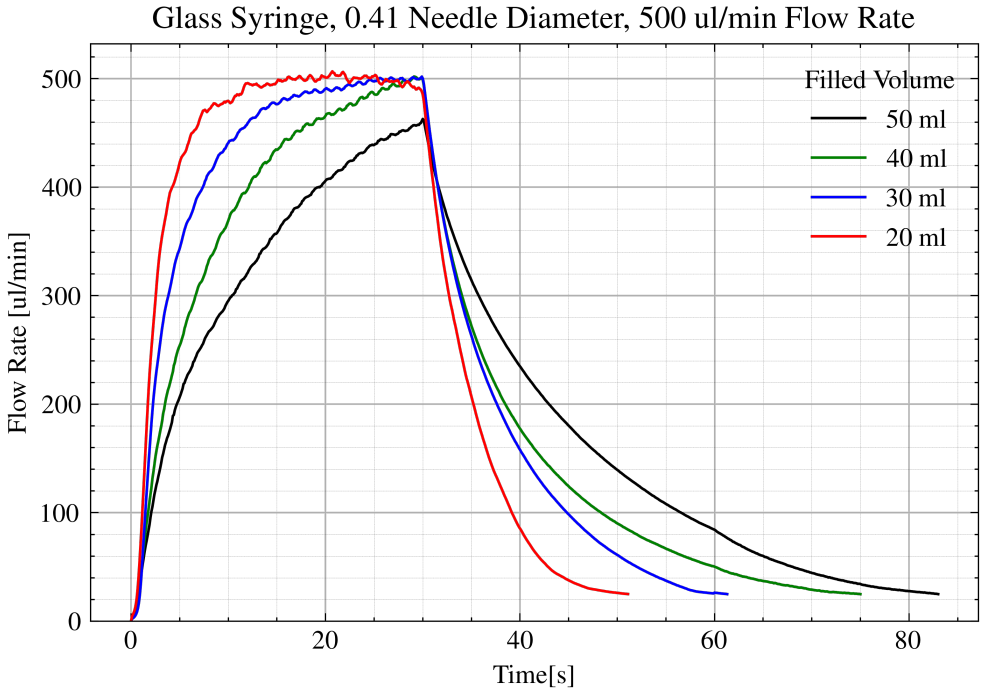

Figure 5.6: The flow rate measurement of the glass syringe to compare the starting and stopping time dependency on filled volume. Measurements were taken for 50 ml, 40 ml, 30 ml and 20 ml filled volumes with a $0.41mm$ needle diameter at $500\mu l/min$.

As seen in Figure 5.6, the time required to reach the desired flow rate and complete extrusion differs significantly depending on the compressed syringe volume. While the 20 ml filled volume extrusion reached the desired flow rate in $17s \pm 0.5$, the extrusion of $50ml$ filled volume could not reach the desired flow rate, and it stayed below $40\mu l/min$. The required time to reach desired flow rate for 30 ml was $25s$ and $29s \pm 0.5$ for $40ml$. Similarly, the completion of the extrusion process was measured as $51, 61, 75$ and 83 seconds ± 0.5 for $20, 30, 40and50$ ml filled volumes, respectively.

These results suggest a strong correlation between the compressed syringe volume and the flow rate. It also explains why the shutter valve-based extruder and the PCP perform better than syringe based extruder in terms of time required to reach the desired flow rate and to complete the extrusion process (Li et al., 2017). This better extrusion quality can be

attributed to the valve closing mechanism in the shutter valve and fixed compressed volume at the outlet in the PCP.

Bioprinting technique generally uses $1ml$ to $10ml$ syringe volume for extrusion. While the result shows the considerable effect of large volumes on compressibility, a similar effect can be observed in small volumes with less delayed time at the beginning and the end of the extrusion. This inaccuracy and a possible solution were mentioned in the introduction section; in the research, the PCP performed better than the syringe pump regarding the extrusion accuracy and precision in the bioprinting application (Fisch et al., 2020).

These results help to explain why the PCP performs better than the syringe pump by showing the effect of compressed volume. The PCP pump has recently been used in the additive manufacturing area, and it produces promising results. However, the cleaning difficulties, scalability of the pump and high cost can be considered the main drawbacks of this technology (Fisch et al., 2020; Wang et al., 2016). Therefore, it is clear that adapting PCP technology for the bioprinting application with a low-cost and easy-to-clean attribute can help move this technology forward.

5.4 Conclusion

The main aim of this chapter was to examine the effect of plunger rubber compressibility on a plastic syringe and the effect of compressed syringe volume on extrusion accuracy. The LVSP was developed and validated to perform the experiments with 50 ml glass and 60 ml plastic syringes.

The start and stop accuracy comparison of a plastic and glass syringe was presented. This study shows the strong negative relationship between the effects of the plunger rubber compressibility of a plastic syringe on extrusion accuracy. Therefore, the result confirmed the suggestion of the previous research (Banović and Vihar, 2018). The research has also shown a negative relationship between the amount of compressed volume and the extrusion accuracy.

By taking these findings into account, the EBB can benefit from a better extrusion pump, and a PCP is the strongest candidate according to the previous research and literature review (see Chapter 2) (Li et al., 2017; Fisch et al., 2020; Wang et al., 2016). Future studies

on developing a PCP for the bioprinting application are recommended to improve extrusion accuracy. This pump needs to be simple to operate, easy to clean or disposable, and uncomplicated to modify for application with various bioprinting materials.

The following chapter will describe the necessary background information for designing, prototyping, and implementing a novel PCP.

6

DESIGN, PROTOTYPING AND IMPLEMENTATION OF A PCP

This chapter was submitted as a part of an article to the CIRP Journal of Manufacturing Science and Technology, and it is under review with the title of "Conceptual design and development of a progressive cavity pump for extrusion-based additive manufacturing applications".

6.1 Introduction

In Chapter 5, an investigation was conducted on the limits of the syringe pump to build a new PCP. In this chapter, the fundamental stages of the product development process of PCPs are explored, with a particular focus on design, prototyping, and implementation. The theoretical modelling of PCPs is explored in this chapter, based on historical work by Rene Moineau and more recent research by Nguyen (Moineau, 1930; Nguyen et al., 2014). The chapter introduces parametric modelling, including an API for Fusion 360 CAD software to generate PCP components. Furthermore, this chapter investigates the optimisation of FFF parameters for PCP prototyping, and it highlights the comparison between FFF and SLS prototypes in terms of dimensional accuracy.

The PCP design was first described in the thesis of Rene Moineau with the title of "A new capsulism." (Moineau, 1930). PCPs cross-section generation, the pump capacity calculation and manufacturing methods were described in Moineau's research, and his cross-section generation method can be seen in Figure 6.1. Subsequently, the 3D vector approach to generate an extended hypocycloid was presented Nguyen et al. (2014), and it is widely used for the PCP cross-section generation method. This method is explained in detail in the following sections, and a parametric modelling tool for fast iteration of the rotor and stator

of PCP is presented.

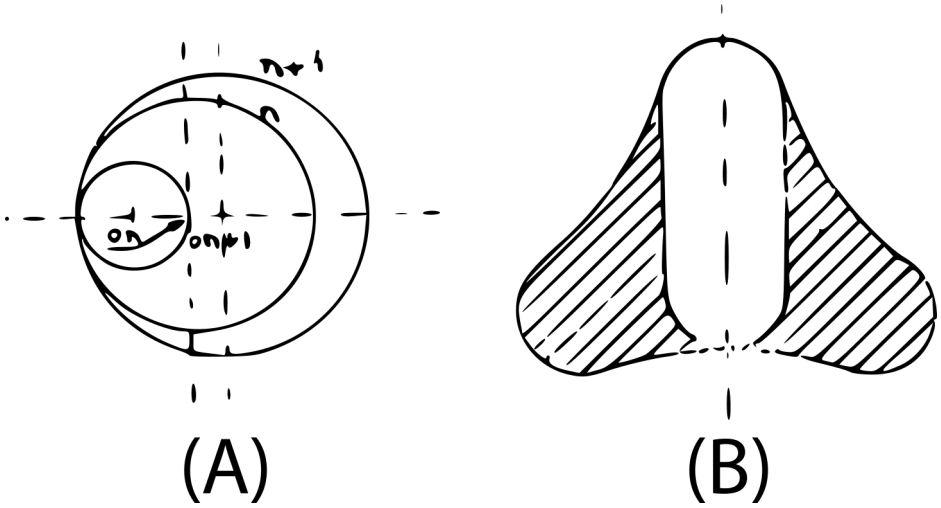

Figure 6.1: Drawing of 2-lobe and 3-lobe PCP cross-section from the work of Moineau. Figure A shows three circles used to generate the hypocycloidal path of the rotor and stator, and B shows the rotor (clear) and stator (shaded) of a 3:2 PCP (Moineau, 1930).

The literature research described the cross-section generation methods of PCPs (Section 2.3.5): hypocycloid, epicycloid and hypo-epicycloid. This Chapter describes the theoretical modelling of PCPs based on the study of Moineau (1930) and Nguyen et al. (2014). Consequently, the parametric modelling of PCPs is proposed using Python programming language to produce an application programming interface (API) for Fusion 360 CAD software. Subsequently, FFF and SLS additive manufacturing methods to prototype rotor and stator were compared and discussed in terms of manufacturing tolerance and cost.

This research used AM technologies to develop a novel PCP concept because AM enables rapid prototyping, resulting in quick concept trials to find the best possible solutions to the problem. FFF is one of the low-cost and easy-to-access AM methods; however, it requires fine-tuning to obtain functional prototypes for experimentation. Therefore, experiments were conducted to find the best FFF machine setting for functional PCP prototypes regarding dimensional accuracy and object integrity.

In the literature, a rotor was defined as a rotating gear, and a stator was defined as a fixed gear. Note that in this study, rotor and inner gear and stator and outer gear are used interchangeably.

6.2 Theoretical Modelling of PCPs

The most common cross-section generation method is obtained using hypocycloid theory and the 3D vector approach (Moineau, 1930; Nguyen et al., 2014). This method was selected in this research; therefore, the hypocycloid theory, the 3D vector approach and the modified hypocycloid equations are described in this Section.

6.2.1 Hypocycloid Theory

The cross-section geometry of inner and outer gears is generated by extending a hypocycloid shape. Hypocycloid is a special plane curve created by the trace of a fixed point on a small circle rotating in a larger circle (Weisstein, 2003). A certain ratio exists between the smaller and larger circle radius to obtain a hypocycloid. If we describe the radius of the smaller circle as r and the radius of the larger circle as $R = Nr$, the ratio N should be an integer to obtain a closed hypocycloid and it also defines the number of PCP lobe (see Figure 6.2).

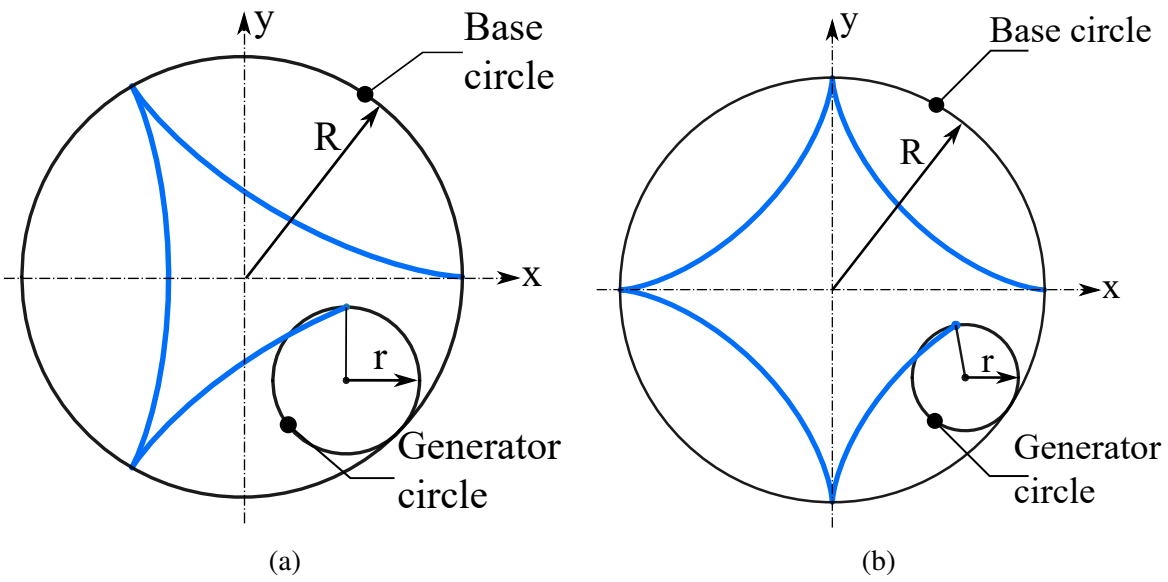

Figure 6.2: The generation of (a) 3-lobe and (b) 4-lobe hypocycloids.

The parametric equations for a hypocycloid curve can be given as follows:

$$x(\theta) = r(N-1)\cos\theta + r\cos[(N-1)\theta] \tag{6.1}$$

$$y(\theta) = r(N-1)\sin\theta - r\sin[(N-1)\theta] \tag{6.2}$$

where $x(\theta)$ is the coordinate of x at (θ) angle, r is the radius of smaller circle, and N is the

number of lobe.

6.2.2 3D Vector Theory

The 3D vector approach is a method used to generate the cross-section geometry of inner gears and outer gears from a hypocycloid (Nguyen et al., 2014). This approach calculates the position vector, tangent vector and normal vector to obtain an extended modified hypocycloid (see Figure6.3). In a rectangular coordinate (x,y,z) system, one point can be determined by a position vector P(x,y,z) (see Figure6.3). The position vector $\vec{r}(s)$ is defined by its magnitude (the length of the line from origin O to point P) and direction (from origin O to point P). The arc length from the O and P is defined as (s).

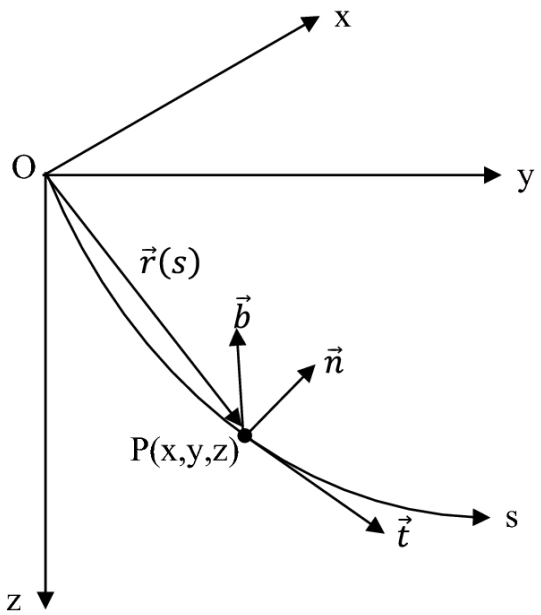

Figure 6.3: A three dimensional space curve (Nguyen, 2020).

The position vector in a 3D space of a curve can be given as (see Equation 6.3):

$$\vec{r}(s) = x(s)\vec{i} + y(s)\vec{j} + z(s)\vec{k} \tag{6.3}$$

where $\vec{r}(s)$ is the position vector, $x(s)\vec{i}, y(s)\vec{j}, z(s)\vec{k}$ are the x, y and z coordinates in 3D space.

The tangent vector is the first derivative of the position vector, which is expressed as:

$$\vec{T}(s) = \vec{r'}(s) = \frac{dx(s)}{ds}\vec{i} + \frac{dy(s)}{ds}\vec{j} + \frac{dz(s)}{ds}\vec{k} \tag{6.4}$$

where $\vec{T}(s)$ is the tangent vector.

The unit tangent vector is expressed as:

$$\vec{t}(s) = \frac{\vec{T}(s)}{||\vec{T}(s)||} \tag{6.5}$$

where $||\vec{T}(s)||$ is the magnitude of the unit tangent vector $\vec{T}(s)$.

The first derivative of the unit tangent vector with respect to (s) gives the curvature vector, which measures the speed of the curve changing direction at a certain point and is given by:

$$\vec{K} = \vec{t'} = \vec{r''} = \frac{d^2x}{ds^2}\vec{i} + \frac{d^2y}{ds^2}\vec{j} + \frac{d^2z}{ds^2}\vec{k} \tag{6.6}$$

where $\vec{K}$ is the curvature vector.

This leads to the following expression for the magnitude of the curvature vector:

$$|\vec{K}| = \sqrt{\left(\frac{d^2x}{ds^2}\right)^2\vec{i} + \left(\frac{d^2y}{ds^2}\right)^2\vec{j} + \left(\frac{d^2z}{ds^2}\right)^2\vec{k}} \tag{6.7}$$

where $|\vec{K}|$ is the magnitude of the curvature vector.

Consequently, the perpendicular unit normal vector to the tangent vector can be described as:

$$\vec{n}(s) = \frac{\vec{K}}{|\vec{K}|} \tag{6.8}$$

where $\vec{n}(s)$ is the unit normal vector.

The generation of a modified hypocycloid to produce a PCP cross-section will be obtained by using equations of the tangent vector (6.5) and the unit normal vector (6.9) in the following Section.

6.2.3 Modified Hypocycloid

The PCP consists of the stator and the rotor components. The stator always has one more lobe (N) than the rotor to produce enclosed cavities for pumping action. The design of a 4-lobe cross-section can be seen in Figure 6.4. In this design, hypocycloid is generated by using Eq. 6.1 and Eq. 6.2 where θ changes from 0 to 360° and the position vector $\vec{r}(\theta)$ consists of x and y components in 2D space.

By applying the 3D vector approach to the position vector in 2D space, the tangent vector,

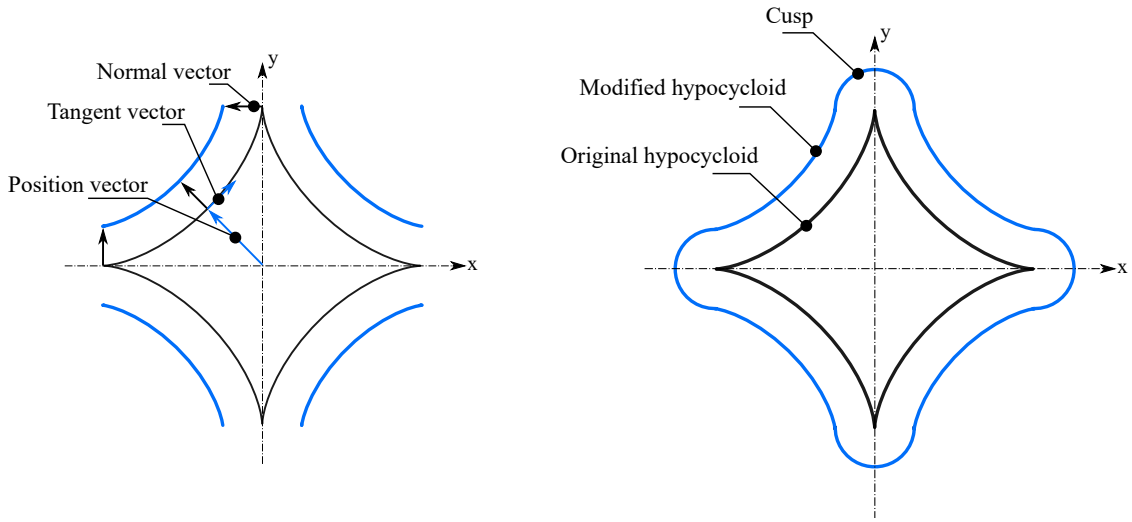

(a) Generation of extended hypocycloid by 3D vector approach

(b) Original hypocycloid and modified hypocycloid (extended hypocycloid with cusps)

Figure 6.4: The generation of the 4-lobe PCP gear cross-section.

which is the first derivative of the $\vec{r}(\theta)$ is as follows:

$$\vec{T}(\theta) = \vec{r'}(\theta) = x'(\theta)\vec{i} + y'(\theta)\vec{j} \tag{6.9}$$

where

$$x'(\theta) = \frac{dx}{d\theta} = -r(N-1)[sin\theta + sin((N-1)\theta)] \tag{6.10}$$

$$y'(\theta) = \frac{dy}{d\theta} = r(N-1)[cos\theta - cos((N-1)\theta)] \tag{6.11}$$

The unit tangent vector of any point on the hypocycloid can be given as:

$$\vec{t} = -\frac{[sin\theta + sin((N-1)\theta)]}{\sqrt{2}\sqrt{1-cosN\theta}}\vec{i} + \frac{[cos\theta - cos((N-1)\theta)]}{\sqrt{2}\sqrt{1-cosN\theta}}\vec{j} \tag{6.12}$$

The unit normal vector, which is described in Eq.6.8, can be expressed as:

$$\vec{n} = \frac{[cos\theta - cos((N-1)\theta)]}{\sqrt{2}\sqrt{1-cosN\theta}}\vec{i} + \frac{[sin\theta + sin((N-1)\theta)]}{\sqrt{2}\sqrt{1-cosN\theta}}\vec{j} \tag{6.13}$$

The generation of PCP cross-section consists of modified hypocycloid and cusps, as seen in Figure 6.4. Cusps are semi-circles to connect modified hypocycloid arches. These semi-circles with diameter "d" are added at the corners of the original hypocycloid.

To generate a modified hypocycloid, the original hypocycloid is extended by multiplying the x and y components of the unit normal vector with the radius of a cusp, $d/2$. Then, the

following parametric equations of the modified hypocycloid can be given:

$$x_n = x + \Delta x = r[(N-1)cos\theta + cos((N-1)\theta)] + \frac{[cos\theta - cos((N-1)\theta)]}{\sqrt{2}\sqrt{1-cosN\theta}}\frac{d}{2} \quad (6.14)$$

$$y_n = y + \Delta y = r[(N-1)sin\theta - sin((N-1)\theta)] + \frac{[sin\theta + sin((N-1)\theta)]}{\sqrt{2}\sqrt{1-cosN\theta}}\frac{d}{2} \quad (6.15)$$

These two parametric equations (Eq.6.14 and Eq.6.15) are used to create a modified hypocycloid. By adding cusps at each corner of the original hypocycloid, we obtain a PCP cross-section (see Figure 6.4b).

Figure 6.5 shows the arrangements of three different PCP rotor and stator lobes with zero tolerance between a rotor and stator. PCPs can be designed as clearance fit or interference fit. Interference fit PCPs consist of a rigid rotor and elastic stator, and clearance fit PCPs consist of a rigid rotor and stator. The interference and clearance fit design affect the accuracy, precision and pressure performance of PCPs, and the fit tolerance varies from $-0.5mm$ to $0.5mm$ (Gamboa et al., 2003; Nguyen et al., 2021). The final parametric equations to design the cross-section of modified hypocycloid-based PCP gears can be given by arranging 6.14 and 6.15 and adding the tolerance parameter "w":

$$x_n = x + \Delta x = r[(N-1)cos\theta + cos((N-1)\theta)] + \frac{[cos\theta - cos((N-1)\theta)]}{\sqrt{2}\sqrt{1-cosN\theta}}(\frac{d}{2} + \frac{w}{2}) \quad (6.16)$$

$$y_n = y + \Delta y = r[(N-1)sin\theta - sin((N-1)\theta)] + \frac{[sin\theta + sin((N-1)\theta)]}{\sqrt{2}\sqrt{1-cosN\theta}}(\frac{d}{2} + \frac{w}{2}) \quad (6.17)$$

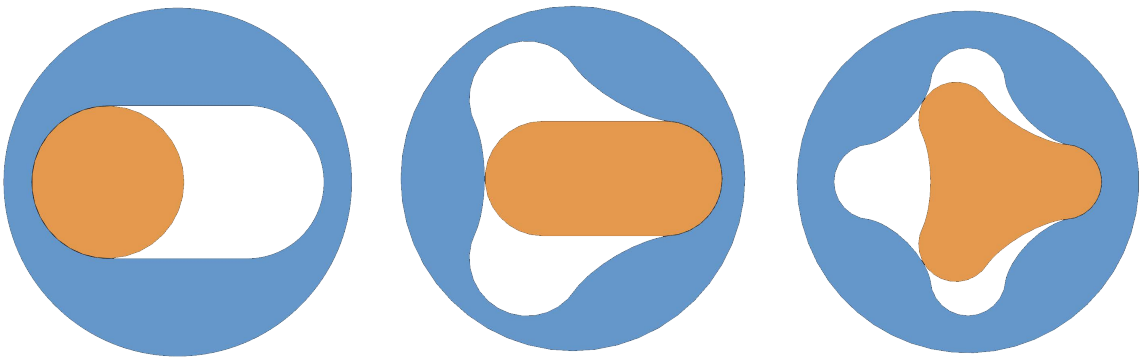

(a) 2:1 Lobe PCP (b) 3:2 Lobe PCP (c) 4:3 Lobe PCP

Figure 6.5: Cross sections of PCPs with various arrangements. A) The rotor and stator cross-section of the most common 2-1 lobe PCP arrangement. B) The 3-2 lobe PCP rotor and stator cross-section, and C) The 4-3 lobe PCP rotor and stator cross-section.

6.2.4 PCP Design Parameters

The design of the PCP differs for the 2:1 lobe arrangement and multi-lobe arrangements (more than 2:1). The main difference is the generation of the 1-lobe rotor component, which requires producing a helix by shifting its rotation axis as much as the eccentricity (e) (see Figure 6.6).

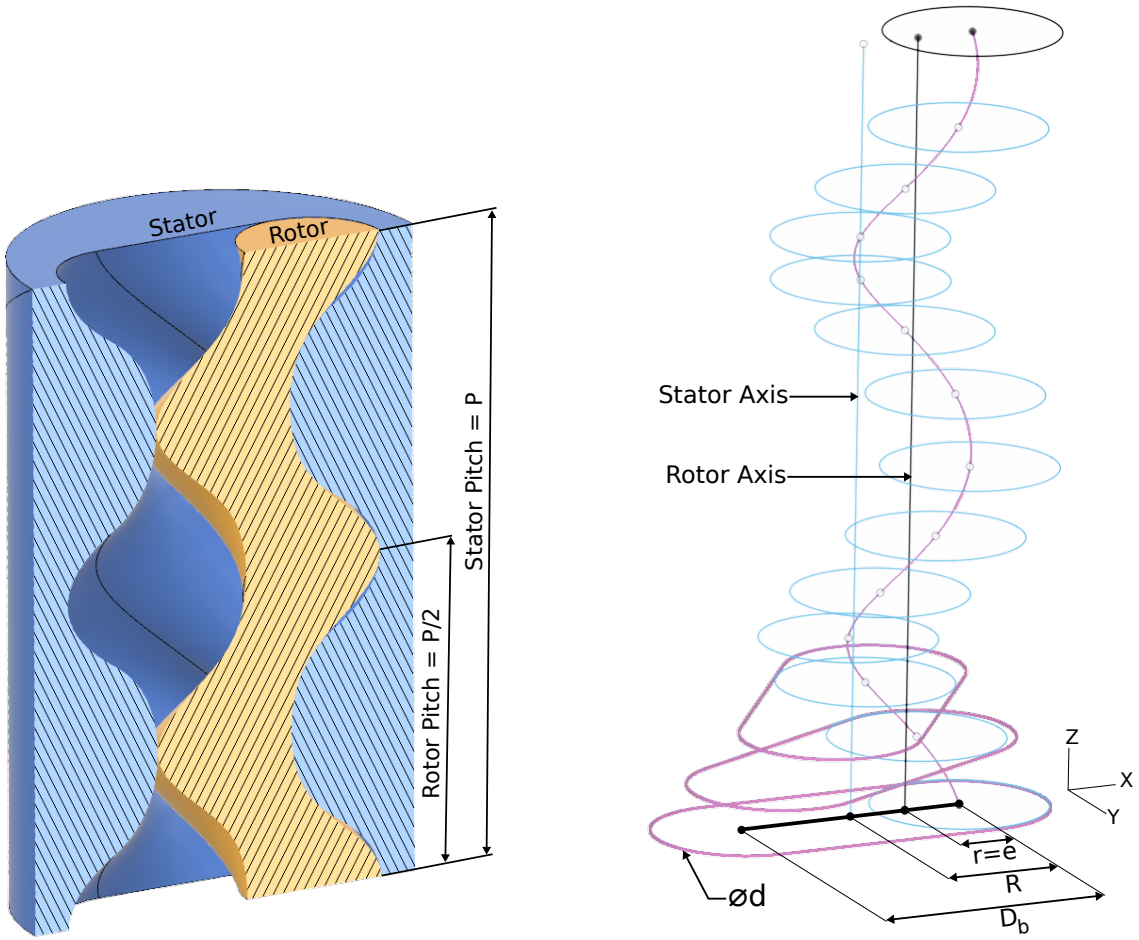

(a) (b)

Figure 6.6: The generation and parameters of 2:1 PCP.

The eccentricity is defined as the difference between the rotor and stator axis, which equals the generator radius "r". As described in the hypocycloid theory section, there is a relationship between the generator circle r and base circle R as $R = Nr$. If the 4:3 lobe PCP is considered, the 4-lobe stator will have a $4r$ radius, and the 3-lobe rotor will have a $3r$ radius which gives the r difference. This difference is defined as eccentricity, which is the radius of the circular path of the rotor when it rotates inside the stator.

The length of a 360° rotation of the stator lobe is defined as a stator pitch (P_s), as shown in Figure 6.6. The relationship between rotor pitch (P_r) and stator pitch length is given as:

$$P_s = \frac{N}{N-1} P_r \tag{6.18}$$

6.2.5 Theoretical Flow Area and Volumetric Flow Rate of PCPs

PCPs consist of N lobe modified hypocycloid stator and $N-1$ lobe modified hypocycloid rotor. The flow area for any given PCP can be calculated by subtracting $N-1$ lobe modified hypocycloid from N lobe one. Therefore, the theoretical flow area of a PCP can be calculated as follows (Nguyen et al., 2014):

$$A_F = A_N - A_{N-1} = 2\pi e^2(N-2) + 4de \tag{6.19}$$

where A_F is the flow area, A_N and A_{N-1} are the area of N and N-1 lobe profiles.

Equation 6.19 gives the flow area of a PCP without any clearance or interference between a rotor and a stator. If we take the tolerance factor "w" into consideration, the flow area equation becomes as:

$$A_F = A_N - A_{N-1} = 2\pi e^2(N-2) + 4de + 8(N-1)ew + \pi(wd + w^2) \tag{6.20}$$

The total fluid volume a PCP can discharge as the rotor turns one cycle is defined as theoretical pump factor (F_p), which can be given as:

$$F_p = (N-1)A_F P_s \tag{6.21}$$

The theoretical volumetric flow rate (Q_{theo}) of a PCP as the rotor turns with a rotational speed of V can be expressed as:

$$Q_{theo} = F_p V = (N-1)A_F P_s V = [2\pi e^2(N-2) + 4de](N-1)P_s V \tag{6.22}$$

The minimum dispensing amount for stepper motors can be calculated based on equation 6.19 and parameters of a stepper motor, which can be given as:

$$\text{Minimum dispensing} = A_F \frac{(N-1)P_s}{360/\text{Step angel}} \tag{6.23}$$

6.3 Parametric Modelling

Computer-aided design (CAD) is the use of computer software to assist designers in various steps of the design and development process, including the design, optimisation and simulation steps. (Sarcar et al., 2008) Parametric modelling is a CAD technique used to produce parts and assemblies by generating a relationship between the dimensional and positional parameters of design entities. Parametric modelling allows rapid changes in the design process, and this feature makes it a useful technique in the spiral development model (Shih, 2013).

The spiral development model was used in designing and developing an innovative PCP, and this process requires a large number of design iterations. Therefore, the parametric modelling technique was applied to the design of the two key components of PCPs, namely a rotor (i.e. inner gear) and a stator (i.e. outer gear). Fusion 360 CAD software supports parametric modelling and allows programming an API for parts design. In the following Section, the produced API was explained in detail.

6.3.1 Application Programming Interface for PCPs Design

The programming environment of Fusion 360 enables a generation of API using the Python programming language. The base API was developed with an object-oriented programming paradigm (OOP) which can be find in Autodesk website to use inside the Fusion 360 (Autodesk, 2018). The base API can only produce a hypo-epicycloid-based PCP rotor and stator, however the hypocycloid-based PCP cross-section is used in this research. Therefore, the objects of the base API was used to accelerate the development process, and modified and advanced to generate 3D hypocycloid-based PCP gear components. Modifications and advancements included adding the tolerance parameter to the interface and the entire geometrical equations to generate 3D rotor and stator components.

The design of PCPs was described in the Section 6.2 with parametric hypocycloid equations and design parameters. The base API was modified using these equations, and the tolerance parameter was added to the code and design interface.

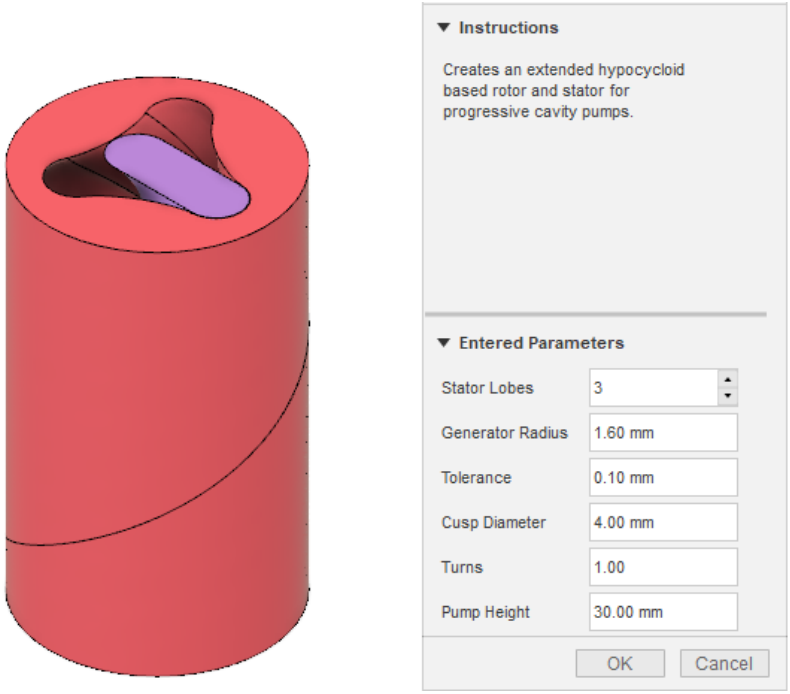

Figure 6.7: Figure shows the API interface (on the right) and 3 lobe stator and 2 lobe rotor (on the left).

In Figure 6.7, the API generated 3-2 lobe PCP can be seen on the left where the purple 2-lobe rotor is inside and the pink 3-lobe stator outside. On the right of the figure, the API interface can be seen, which enables input of required parameters for a PCP rotor and stator generation. The first parameter of stator lobes defines both rotor and stator parameters, as the code was written based on an N-lobe outer gear and an N-1 inner gear. The minimum value of the stator lobes was limited to two to prevent API errors. The generator radius parameter was described in the previous Section as "r". It defines the circle radius of a one-lobe PCP gear that rotates inside a base circle shown in Figure 6.2. The tolerance parameter can be either positive or negative, and it determines the fit types: the clearance fit or the interference fit. The tolerance parameter was added to the base code. This modification makes the API more useful in generating PCP gears with various tolerances for either the prototyping or the final production. The cusp diameter is the diameter of semi-circles added to corners of the original hypocycloid (as seen in Figure 6.4). The pump height and turns parameters define the pitch and pump height of the generated PCP gears. For example, if the turns value is one, the pitch and the pump height are the same, and if the turns value is two, the pitch is half of the pump height.

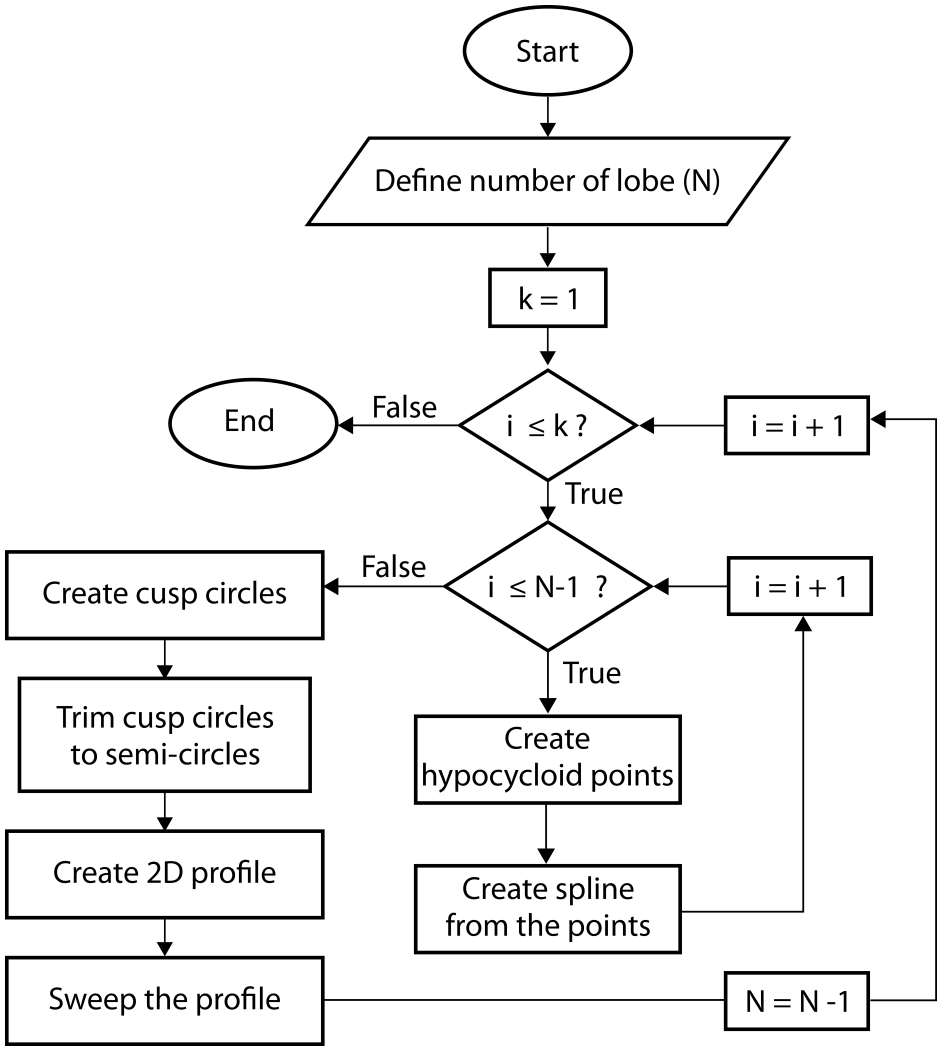

Figure 6.8: Flow chart of the developed API for PCP gears. The parameter *k* is the minimum limit of iterations, and *i* is the temporary variable used to store the integer value of the current position in the range of the for loop.

The API is programmed to generate a series of operations step by step, and the flowchart can be seen in Figure 6.8 (c). Firstly, Python libraries, required parameters and objects were defined, and a 2-dimensional sketch was created. Operations begin with the definition of the number of lobes and input parameters. The parameter *k* is the minimum limit of iterations, and *i* is the temporary variable used to store the integer value of the current position in the range of the for loop. Subsequently, the modified hypocycloid equations for the x and y co-ordinates generate eighty points which were defined at the beginning as a $defaultPointNum$ (see Appendix 1). These points produce splines of the modified hypocycloid. However, if the number of stator lobes parameter was selected as two, the API generates a single point for the 1-lobe gear and two straight lines for the 2-lobe gear. After splines of the modified

hypocycloid were generated, circles were added to produce cusps. This was performed by adding the trim operation to make the semi-circles from the added circles. The trim operation requires a specific point to execute the trimming. These specific points are located at the corners of the original hypocycloid and were calculated using the original hypocycloid equations. By following these sequences of operations, a cross-section of an N-lobe PCP gear can be obtained, and the next step is to produce a feature of PCP gear using this sketch.

The feature of PCP gear was produced using the *Sweep* function, which requires a sketch profile, the number of turns (*Turns* parameter) and a straight path defined as pump height. As a result, a solid feature of an N-lobe PCP gear is formed, and a for loop was used to generate an N-1 lobe PCP gear by following the same steps.

The complete Python code can be found in Appendix 1.

6.4 FFF Parameter Optimisation

The design equations and methods of the inner and outer gears of PCPs were discussed in the previous sections. Before moving to the concept generation phase of the research, FFF parameters were compared and discussed because the concept generation phase requires physical prototyping.

Inner gear and outer gear components were selected in the parameter optimisation process. Designs were exported as a stereolithography (STL) file format and sliced in the Cura software to generate a G-code file (see Figure 6.9. Subsequently, the Ultimaker 3 FFF printer processed the generated G-code file to produce a physical model using a PLA filament.

Designs were printed as a solid object using maximum wall thickness rather than making the infill parameter %100 because the infill process requires uneven movements over the part, and this decreases the overall part quality. The line width is set to the same size as the nozzle diameter to prevent under-extrusion and to obtain fully filled physical models. This also simplifies the quality comparison. The wall thickness and line width settings were kept the same for all printing processes, and the build plate temperature was set to $60°C$. All other parameters were selected as default in the Cura except the comparison parameters, as seen in Table6.1.

The optimum parameter selection was a crucial part of the product development process due

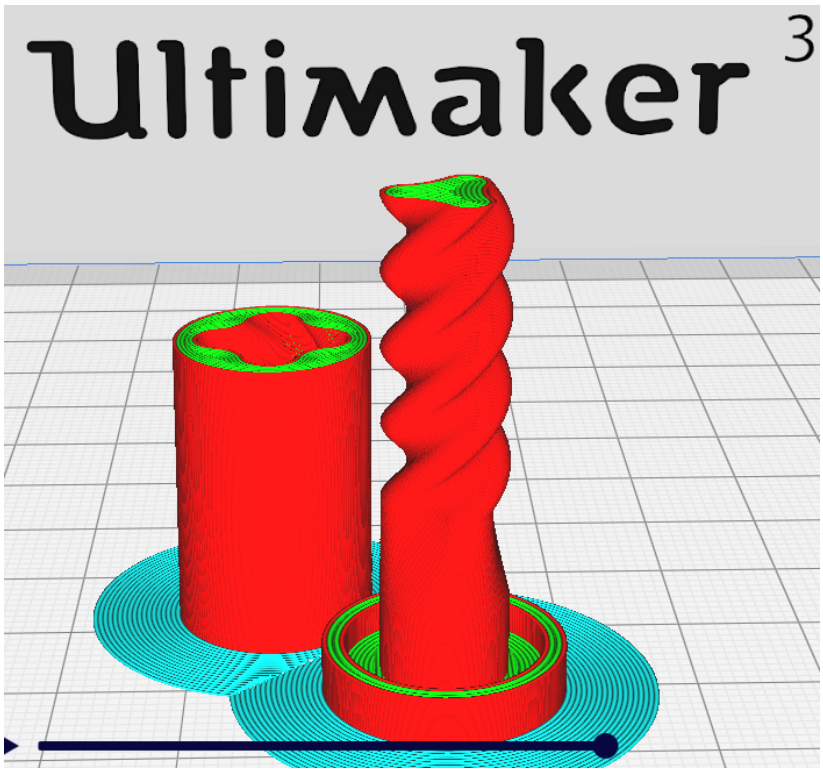

Figure 6.9: Cura interface showing a sliced 3-lobe rotor (on the right and a 4-lobe stator (on the left).

to the involvement of an excessive amount of physical prototyping. To decrease the amount of waste material, the FFF process should be optimised to obtain usable and defect-free physical prototypes. The most important parameters in the FFF printing process are nozzle diameter, layer height, printing temperature and printing speed (Buj-Corral et al., 2021). These parameters were compared by observing the printing process and the printed physical object quality. The parameters to be evaluated were divided into three groups to compare the effects of a single parameter (see Table6.1).

In the first four trials, printing speed was kept medium at $50mm/s$, and $5°C$ nozzle head temperature intervals were selected to compare printing quality. The first trial at $200°C$ was the best result, and it was slightly more durable than the $195°C$ trial.

In the second group, the effect of printing speed was compared by using $15mm/s$ intervals at $200°C$. The inner gear and outer gear of PCP are spiral-shaped objects, and the extruded material at the edges is not fully supported. For this reason, if the material were not fully cooled or printed at high temperatures, it would cause a curly edge and affect the overall printed object shape quality.

Table 6.1: Comparison of FFF parameters and results.

	Nozzle Diameter	Layer Height	Printing Temperature	Printing Speed	Result
1	0.4mm	0.15mm	210$^{\circ}C$	55mm/s	3 (Stringing)
2	0.4mm	0.15mm	205$^{\circ}C$	55mm/s	4 (Curling)
3	0.4mm	0.15mm	200$^{\circ}C$	55mm/s	5
4	0.4mm	0.15mm	195$^{\circ}C$	55mm/s	2 (Layer Separation)
5	0.4mm	0.15mm	190$^{\circ}C$	55mm/s	2 (Grinding Filament)
6	0.4mm	0.15mm	200$^{\circ}C$	65mm/s	3 (Curling)
7	0.4mm	0.15mm	200$^{\circ}C$	55mm/s	5
8	0.4mm	0.15mm	200$^{\circ}C$	45mm/s	4 (Slower)
9	0.4mm	0.15mm	200$^{\circ}C$	35mm/s	4 (Slower)
10	0.4mm	0.15mm	200$^{\circ}C$	25mm/s	4 (Stringing)
11	0.4mm	0.1mm	210$^{\circ}C$	55mm/s	3 (Stringing)
12	0.4mm	0.1mm	205$^{\circ}C$	55mm/s	3 (Curling)
13	0.4mm	0.1mm	200$^{\circ}C$	55mm/s	4 (Curling)
14	0.4mm	0.1mm	195$^{\circ}C$	55mm/s	5
15	0.4mm	0.15mm	190$^{\circ}C$	55mm/s	2 (Layer Separation)
16	0.4mm	0.1mm	195$^{\circ}C$	65mm/s	3 (Nozzle clogging)
17	0.4mm	0.1mm	195$^{\circ}C$	55mm/s	3 (Curling)
18	0.4mm	0.1mm	195$^{\circ}C$	45mm/s	5
19	0.4mm	0.1mm	195$^{\circ}C$	35mm/s	3 (Curling)
20	0.4mm	0.1mm	195$^{\circ}C$	25mm/s	3 (Layer Separation)

Result scale: Excellent: 5, Good: 4, Fair: 3, Poor: 2, Very poor: 1

The same process was followed in evaluating 0.1mm layer height for 0.4mm nozzle. The 0.1mm layer height caused a nozzle clogging at 190$^{\circ}C$. When the printed object size decreased, the 0.4mm nozzle could not meet the required printing quality because it limits the number of lines printed on a single layer.

In summary, the best parameters for 0.15 layer height found as 55mm/s printing speed at 200$^{\circ}C$. In addition, when the layer height was decreased to 0.1mm, the best parameters observed as 45mm/s at 195$^{\circ}C$

6.5 Evaluation of FFF and SLS Prototypes

The optimisation of printing parameters was discussed in the previous Section by comparing the physical printed object quality. In this Section, FFF and SLS printed objects are compared in terms of dimensional accuracy to select the most suitable AM method for prototyping. All parts were printed with maximum wall thickness to obtain 100% dense rotors

and stators.

The main components of PCPs are the rotor and stator, which enable fluid dispensing by rotation. In the experiment, these components were printed using FFF and SLS processes. The rotor was printed in one size, and the stator was printed with a tolerance of $0.1mm$ intervals in four sizes. The tolerance was given to the external diameter and the cusp of the stator lobe. The measurements were taken for the length and the maximum diameter of 3D printed components.

Figure 6.10: FFF printed 3-lobe rotors and 4-lobe stators for dimensional measurement.

The FFF process is an easily accessible and low-cost manufacturing method, and the FFF printing quality is gradually increasing nowadays due to the involvement of industry, hobbyists and academia. In-house lab facilities enable access to an Ultimaker 3 FFF machine and various filaments. However, PLA filament was selected because it is biodegradable, easy to print and low-cost. These features make it the most suitable material for this research; details can be found in Section3.5.1. Figure 6.10 shows the printed parts together.

Laser-sintered PA 12 was selected for comparison because it is commonly used in various applications, from functional prototypes to end-use parts. In addition, this material is biocompatible and food-safe and has a water-tightness feature. Therefore, it is an appropriate candidate for the PCP prototype. This is because bioprinting applications require cell-friendly components, and the sealing of PCPs is the primary consideration. SLS printed samples can be seen in Figure 6.11.

Table 6.2 shows all measurement results, and the bar chart results of length and diameter

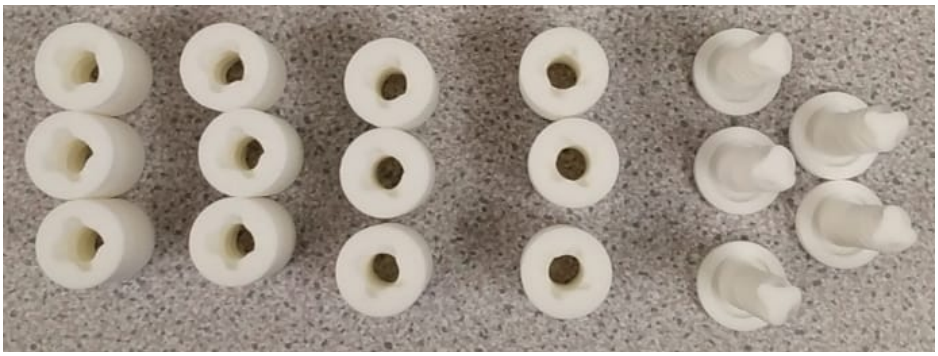

Figure 6.11: SLS printed 3-lobe rotors and 4-lobe stators for dimensional measurement.

errors can be seen in Figure 6.12 and Figure 6.13. The components were printed as three copies. The rotor measurements can be seen in the Table's first six rows; the first three are FFF rotors, and the remaining are the SLS ones. The most interesting measurement result of the entire experiment was the rotor measurement. This is because the mean error for the length was observed as 0.0066*mm* for FFF rotors and 0.19*mm* for SLS rotors. A similar but less significant difference was calculated in the diameter to mean error of 0.0467*mm* for FFF rotors and 0.0566*mm*.

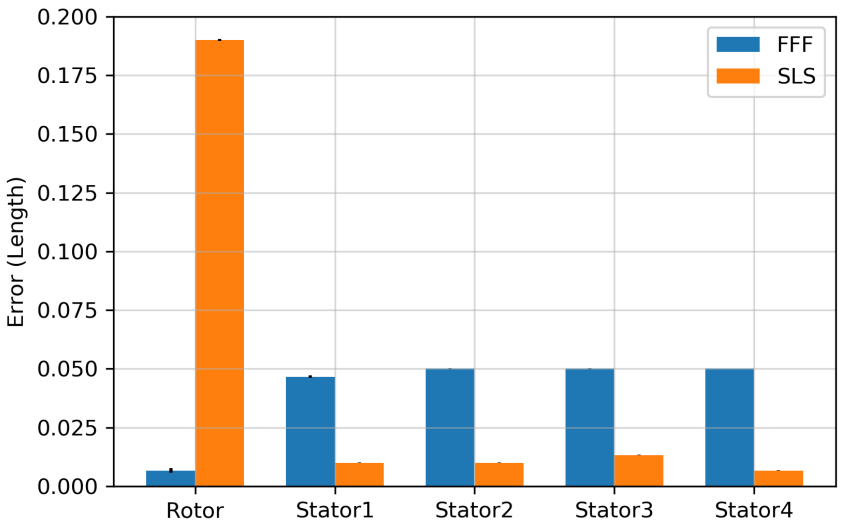

Figure 6.12: Error of the measured length compared to theoretical length, and black lines show the error variance.

In the measurement of SLS stators, the remaining printed parts had very similar results as the mean length of 30.0091*mm* with 0.0079*mm* standard deviation. While FFF stators showed more errors than SLS stators, they were in the acceptable range. FFF stators had a mean

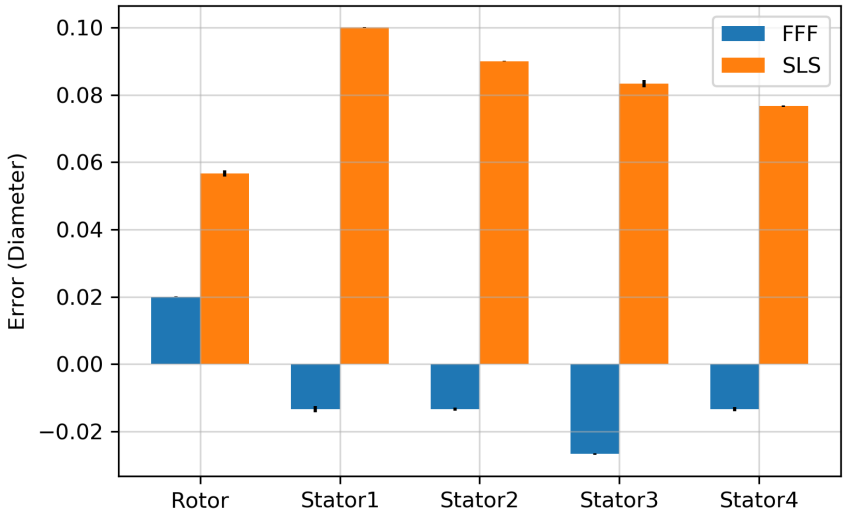

Figure 6.13: Error of the measured diameter compared to theoretical diameter, and black lines show the error variance.

length of 30.0533*mm* with 0.0227*mm* standard deviation.

The measurement of stator diameters showed a significant error difference between the FFF and SLS technology. The first set of stators was printed with $+0.2mm$ tolerance. The mean error of the FFF set was measured as $-0.0133mm$, and the SLS set was $0.1mm$. The remaining sets had similar results, $-0.0133mm$, $-0.0266mm$ and $-0.0133mm$ for the second, third and fourth sets of FFF, and for the SLS sets, $0.090mm$, $0.0833mm$ and $0.0766mm$ respectively.

This study set out to assess the manufacturing quality of SLS and FFF printers. The aim was to select the most suitable prototyping method for the prototype development phase of this research. The result shows that FFF performed better than SLS in printing the X and Y direction, especially for the stator. However, SLS printing in the Z direction showed better accuracy than the FFF method. When the product cost was compared, the rotor and stator set for SLS were 11.916 and 0.49 for FFF.

6.6 Conclusion

The aim of this study was to develop a novel low-cost PCP for extrusion-based bioprinting applications. This Chapter has examined the theoretical and parametric modelling of PCPs,

Table 6.2: Quality comparison of FFF and SLS printed parts.

	Name	Theoretical Length (*mm*)	Measured Length (*mm*)	Error (*mm*)	Theoretical Diameter (*mm*)	Measured Diameter (*mm*)	Error (*mm*)
1	FFF Rotor	51.2	51.17	-0.03	20	20.02	+0.02
2	FFF Rotor	51.2	51.22	+0.02	20	20.03	+0.03
3	FFF Rotor	51.2	51.23	+0.03	20	20.01	+0.01
4	SLS Rotor	51.2	51.37	+0.17	20	20.03	+0.03
5	SLS Rotor	51.2	51.41	+0.21	20	20.09	+0.09
6	SLS Rotor	51.2	51.39	+0.19	20	20.05	+0.05
7	FFF Stator 1	30	30.05	+0.05	19.2	19.22	+0.02
8	FFF Stator 1	30	30.02	+0.02	19.2	19.18	-0.02
9	FFF Stator 1	30	30.07	+0.07	19.2	19.16	-0.04
10	SLS Stator 1	30	30.01	+0.01	19.2	19.29	+0.09
11	SLS Stator 1	30	30.02	+0.02	19.2	19.31	+0.11
12	SLS Stator 1	30	30	0	19.2	19.3	+0.1
13	FFF Stator 2	30	30.04	+0.04	19.1	19.11	+0.01
14	FFF Stator 2	30	30.06	+0.06	19.1	19.07	-0.03
15	FFF Stator 2	30	30.05	+0.05	19.1	19.08	-0.02
16	SLS Stator 2	30	30	0	19.1	19.2	+0.1
17	SLS Stator 2	30	30.01	+0.01	19.1	19.18	+0.08
18	SLS Stator 2	30	30.02	+0.02	19.1	19.19	+0.09
19	FFF Stator 3	30	30.08	+0.05	19	18.97	-0.03
20	FFF Stator 3	30	30.06	+0.05	19	18.96	-0.04
21	FFF Stator 3	30	30.03	+0.05	19	18.99	-0.01
22	SLS Stator 3	30	30.01	+0.01	19	19.12	+0.12
23	SLS Stator 3	30	30.01	+0.01	19	19.07	+0.07
24	SLS Stator 3	30	30.02	+0.02	19	19.06	+0.06
25	FFF Stator 4	30	30.02	+0.05	18.9	18.89	-0.01
26	FFF Stator 4	30	30.09	+0.05	18.9	18.86	-0.04
27	FFF Stator 4	30	30.07	+0.05	18.9	18.91	+0.01
28	SLS Stator 4	30	30.02	+0.02	18.9	18.96	+0.06
29	SLS Stator 4	30	30	0	18.9	18.99	+0.09
30	SLS Stator 4	30	30	0	18.9	18.98	+0.08

and low-cost prototyping methods.

In the theoretical modelling section, the modified hypocycloid production method is presented, and the tolerance factor was added to the work of Nguyen et al. (2014). Subsequently, the produced extended hypocycloid equation was used to develop a parametric modelling API for the rotor and stator components of PCPs. The API development study has been one of the first attempts to thoroughly examine the parametric modelling of PCPs.

The API was produced to increase prototyping speed, and it can be practically used in future PCP design research.

The study of FFF process parameter optimisation was conducted to obtain the best parameters for PCP prototyping. Subsequently, FFF and SLS manufacturing technologies were compared to select the most suitable methods for prototyping in terms of accuracy cost and accessibility. Consequently, the FFF method was chosen as a prototyping method for this research because there was not a considerable part quality difference between FFF and SLS, and the FFF method has cost and accessibility advantages.

In the following Chapter 7, the concept development phase of the spiral development model will be studied.

7

PCP Concept Development

This chapter was submitted as a part of an article to the CIRP Journal of Manufacturing Science and Technology, and it is under review with the title of "Conceptual design and development of a progressive cavity pump for extrusion-based additive manufacturing applications".

7.1 Introduction

Recent academic research has paid considerable attention to commercially available PCPs because of their excellent accuracy in dispensing soft materials (Gelber, 2015; Yao et al., 2015; Wang et al., 2016; Li et al., 2017). Compared to piston-driven and pneumatic methods, PCPs have a great potential to deliver better dispensing quality. Recent research has shown that PCPs can help improve EBB accuracy (Fisch et al., 2020; Wang et al., 2016; Yao et al., 2015). Several future developments for the PCP technology have been noted in the literature, including creating an open-source PCP to reduce costs and adapting the technology for multi-material 3D printing (Yao et al., 2015; Wang et al., 2016). Additionally, EBB applications take advantage of a specifically adapted PCP, taking into account the existing limitations of the large dead volume, high volume flow, and cleaning difficulty (Fisch et al., 2020).

In conclusion, the need for a better PCP for EBB is addressed in the present literature. While there has been recent progress in industry and academia, there are still some unanswered questions regarding the working mechanism of PCPs.

The aim of this study was to develop a low-cost, scalable, easy-to-clean extrusion system based on the PCP principle to overcome the mentioned limitations. The key research question of this study was whether or not there is a better unknown PCP mechanism for EBB. Therefore, a spiral development model was proposed to explore the PCP working mechanism with the help of AM. An application programming interface (API) was developed

for Fusion 360 CAD software to enable rapid design iterations. Subsequently, user requirements were determined through literature research, a user questionnaire, user interviews and redesigning of a conventional PCP. Finally, three PCP concepts were designed, prototyped and evaluated to meet the EBB requirements.

7.2 Methodology

7.2.1 Redesigned conventional PCP evaluation

In the redesigning phase of the spiral development model, a conventional PCP was designed using a 2:1 lobes arrangement and double universal joint. In-house FFF prototyping was used to obtain all components except fasteners.

The redesigned prototype was evaluated to obtain necessary information about the limitations and fundamentals of PCPs. The design's coupling, gears and sealing performance were analysed to find an innovative solution. In addition, the part quality and accuracy of the FFF machine prototype were evaluated for the dispensing evaluation phase.

7.2.2 Concept prototyping

The Ultimaker 3 was used to print designed concepts, and the printing parameters are as follows:

- Nozzle diameter: $0.4mm$
- Layer height: $0.15mm$
- Printing temperature : $200°C$
- Printing speed: $50mm/s$

Poly-lactic acid (PLA) filament was used to produce most PCP components in the concept prototyping. It was the primary prototyping material in this research due to its biodegradable feature, low cost, and easy printability by the fused filament fabrication (FFF) technique.

PLA filament with an average density of $1.24g/cm^3$ and diameter of $2.85 \pm 0.10mm$ was purchased from RS Components (UK).

7.2.3 Concept prototype evaluation

In the concept development phase of the spiral development model, the aim was to explore a novel working mechanism that meets the product requirements of EBB. PCP concepts were designed and prototyped using collected information from the redesigning phase and in line with the knowledge gained from the previous concepts.

The concept evaluation was performed by manipulating the rotor and stator to observe a satisfactory rotation mechanism and liquid transfer. The manipulation was carried out manually or with a stepper motor. The extrusion ability was tested by filling the inlet of PCPs with petroleum jelly, and the outlet was observed for extrusion. In addition, tap water was used to observe pump leakage and sealing performance. The detailed evaluation methodology and product design specifications can be found in Chapter 3.

7.3 Results and Discussion

7.3.1 Redesigning a conventional PCP for additive manufacturing

The main components of PCPs can be divided into gears and coupling. Gears are the rotor and stator, and coupling transfers power from the motor to the rotor. Various gears arrangements, including 2:1, 3:2, and 4:3 lobes, and the 2:1 lobes are the most common in dispensing pumps. Therefore, the 2:1 lobes arrangement was selected for redesigning, and the main components of this arrangement can be seen in Figure 7.1.

PCPs used in dispensing industry have elastomeric stators to provide an interference fit between gears and clearance fit pumps used in high-speed pumping. While the interference fit design is a common approach, the clearance fit design was chosen due to the available FFF prototyping method. Petroleum jelly was used to evaluate the dispensing action because the clearance between the rotor and stator can be filled by fluid flow.

Two types of commonly used couplings in PCPs are double universal joint or flexible coupling for power transmission from the motor to the rotor. Commercial PCPs use flexible coupling; however, the double universal joint mechanism was selected because it is easy to prototype and test.

The design consists of four components (1) the upper case to hold the bearing, (2) the stator designed as the main case, which includes the inlet and outlet, (3) the double universal

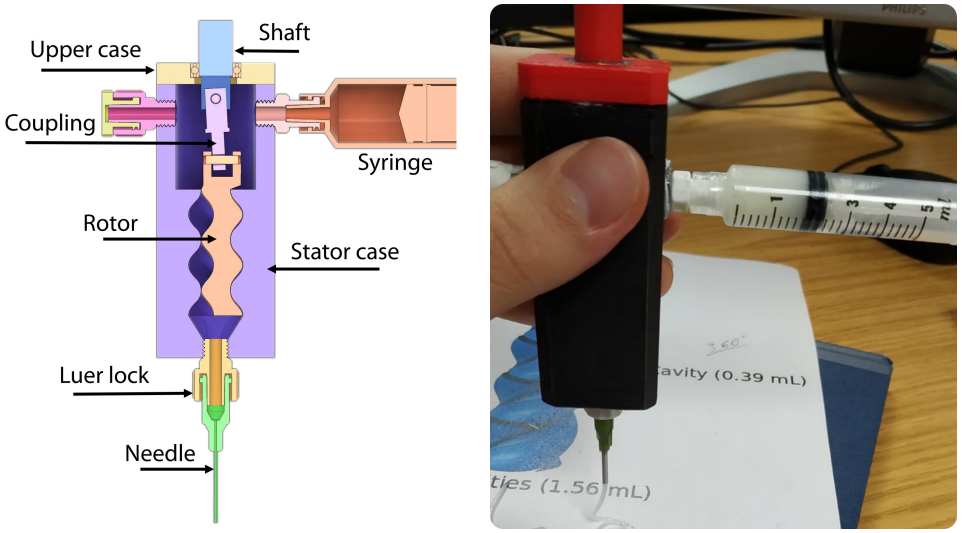

Figure 7.1: The redesigned prototype of a conventional 2:1 lobe PCP.

joint and (4) the rotor. The main design parameters are 1.5*mm* generator radius, 7*mm* cusp diameter, 30*mm* stator pitch, 1.25 revolution and 0.2*mm* clearance between gears.

The upper case holds the bearing, and the actuated end of the double universal joint was fitted into the bearing to enable balanced rotation. This design causes material leakage during the inlet filling operation and print retraction. The shielded bearing was used for the observation, which was an expected result. Therefore, leakage can be defined as the primary consideration point in the PCP design.

The inlet volume was observed as a limitation due to the high height compared to the pump length. While the PCP design works, inlet volume can be considered a dead volume for a small amount of material dispensing. The coupling length limits the inlet volume, and this also limits the scalable PCP design. Therefore, coupling can be considered one of the most critical components in the PCP design.

The double universal joint was used to enable horizontal movement of the rotor caused by the eccentricity of the pump. However, vertical movement of the coupling was observed due to the decreasing length of the coupling during horizontal movement, as can be seen in Figure 7.2. In addition, this jerky movement causes side loads to be exerted onto the stator during the rotor rotation and limits the stator material selection. This issue can be carefully evaluated for high-precision dispensing, and it can cause pulsation due to non-uniform clearance or interference between gears. While this problem can be solved using a

telescopic universal joint to enable vertical movement, it restricts the scalable PCP design and increases the cost. Therefore, finding a solution for power transmission between the motor and rotor can be defined as one of the objectives in the concept generation phase.

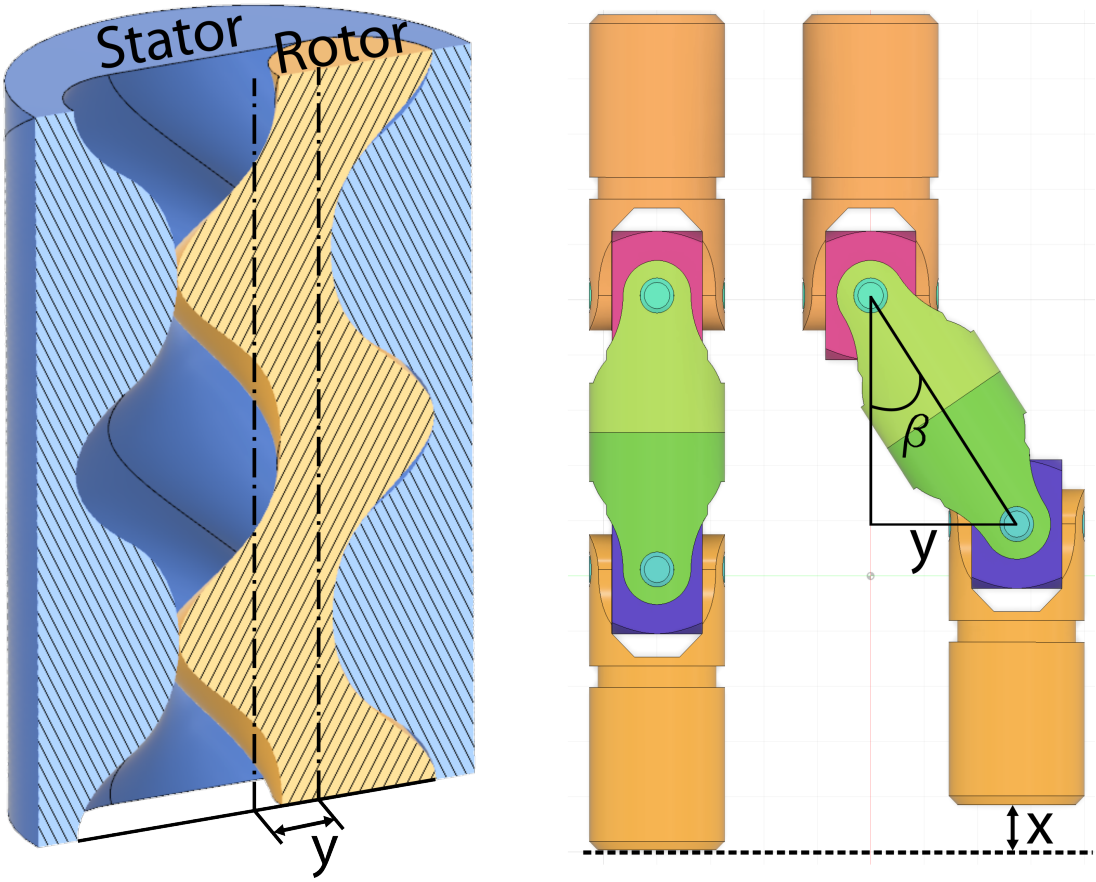

Figure 7.2: Explanation of the standard double universal joint's vertical misalignment caused by horizontal movement. The figure shows the 3D section view of the rotor and stator on the left and the straight and misaligned joint on the right. The angle β represents the angle between two angular connection points of the joint, y represents the horizontal movement due to the eccentric movement of the rotor inside the stator, and x represents the vertical misalignment of the joint.

Gears tolerance ($0.2mm$) enabled easy rotation, and the 2:1 lobes arrangement worked as expected. The stator, inlet and outlet sections were designed as a single component to simplify the PCP design.

Luer lock connectors were used in the design for easy syringe and needle installation, and they worked as expected. Therefore, they will be used in the concept generation phase as they are standard connectors in the biomedical and dispensing industry.

7.3.2 PCP requirements

The main limitation in EBB technology can be defined as start and stop printing accuracy problems. In other words, when the user initiates the print, it does not begin immediately, and when the print finishes, the liquid continues to leak. There are two main reasons for this problem. The first one is the material-related reason which stems from the rheological properties of biomaterials, including non-Newtonian behaviours, yield stress and viscosity. The second one is the extrusion unit-related reason which is the volume of pressurised material. This pressure causes a low printing accuracy and generates a back-flow inside the pump. Therefore, a requirement can be defined as minimising the outlet volume and clearance between the gears.

We can describe two different motions in the working principle of PCPs, which are rotational and transitional. In commercial PCPs, the rotor carries these two motion types, and flexible coupling provides power transmission from a motor to the rotor. The reason to use a flexible coupling is the uneccentric motion of the rotor. We can define two problems of using a flexible coupling: the exerted force on the stator's side walls and the axial movement from the stator inlet to the outlet. These problems cause flow pulsation and low dispensing accuracy.

7.3.3 Concept 1: Outer gear actuated PCP

The working mechanism of a PCP was selected as a focusing point in the first concept development. After intensive research, an alternative working mechanism was discovered by changing rotary gears from the inner gear to the outer gear (see Figure7.3).

The PCP was designed with hypocycloid geometry as conventional PCPs. This solution enables the scalable design of a PCP, and scaling can solve the mentioned limitations of conventional PCPs.

The outer gear actuated PCP design consists of 2:1 lobes of outer and inner rotating elements, which are a stator and rotor in conventional PCP. Internal rotor inserted into housings in both ends clearance for axial movement. The external rotor motion was aligned using six PolyTetraFluoroEthylene (PTFE) O-rings, which provided sealing. The design was produced using the API with the following parameters; 2mm generator radius, 0.2mm tolerance, 10mm cusp diameter, 1.25 rotation and 30mm pump height.

Gears have a specific rotation ratio: the inner gear rotates two times the outer gear. In this design, the outer gear is driven by the NEMA17 stepper motor, and the inner gear motion was expected to be automatic due to axis restriction. However, this could not be achieved due to the rotation ratio between gears; therefore, the design did not work as expected. In the concept evaluation, required rotation was observed in a few attempts, but generally, it was not satisfactory.

The PCP alignment was designed horizontally to prevent the cell settling and nozzle clogging in the bioprinting process due to the gravitation. Luer-lock adapters worked as intended, and they enabled easy syringe connection.

Additively manufactured gears were designed as chamfer edges to enable the fit between the motor gear and outer gear. The trial of using PTFE o-rings to align and seal the PCP was partially successful. Required axial alignment and rotation were provided; however, the sealing required high compression, and this caused a high torque requirement. When the compression was increased, the required torque increased due to friction load between PTFE o-rings. Therefore, the selection of PTFE o-rings did not meet the sealing requirement, and the solution can be to use a sealed bearing and rotary shaft seal.

In summary, the rotation ratio between gears should be considered carefully, and there can

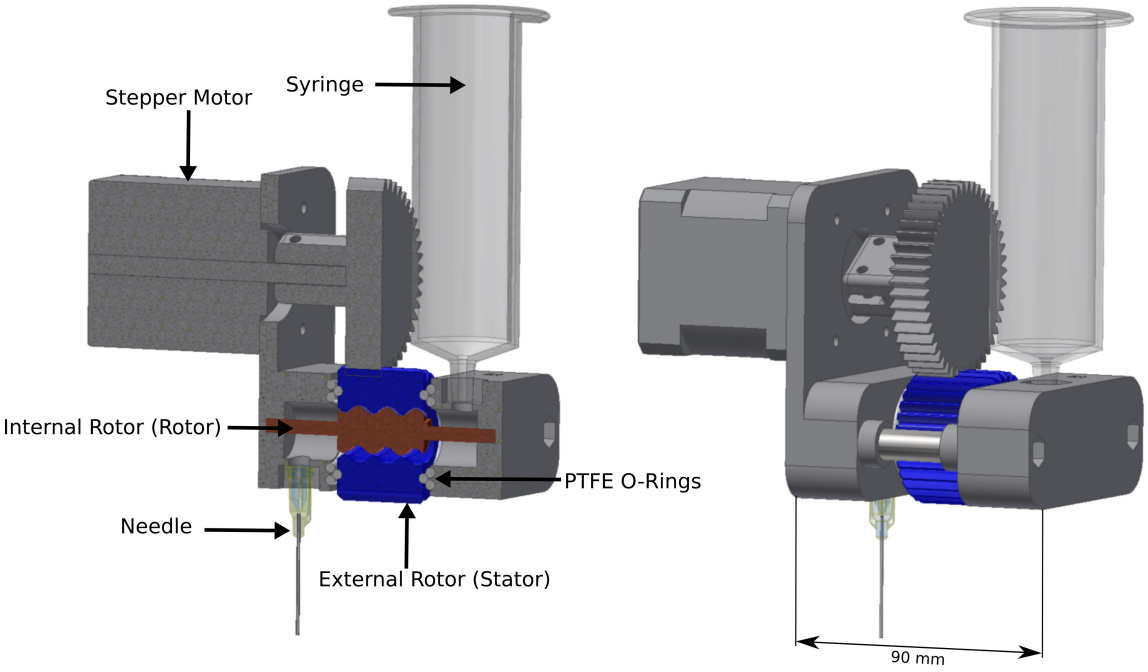

Figure 7.3: Design and explanation of the outer gear actuated PCP.

be two solutions. First, using simultaneous driven gears to provide a fixed rotation ratio. Second, changing the actuated gear from outer to inner and increasing the number of lobes increases the contact point between gears. The conceptual phase continued with these two concept designs to solve these problems.

7.3.4 Concept 2: Synchronised actuated PCP

The synchronised actuated PCP design has a similar mechanism as the previous prototype; however, in this design, the inner gear was actuated with the outer one by transmitting power using spur gears (see Figure7.4).

In the design, a 2:1 lobes arrangement was selected, and spur gears were used to provide synchronised rotation of the inner and outer gears with a specific ratio. The ratio is two times the inner gear rotation for one outer gear rotation. Gears were 3D printed with 1 MOD and 20 deg pressure angle design parameters. One of the 30 teeth gears was connected to the motor shaft to drive the other 30 teeth gear, and this rotation was transmitted to the outer gear via 25 teeth and 50 teeth gears. Therefore, the ratio of two inner to one outer rotations was obtained for the PCP prototype.

The inlet housing was designed to act as a bushing for outer gear housing, and two washers were used to seal the PCP pump. The bushing type of housing was designed to provide easy assembly of the PCP prototype. Luer-lock adaptors were used to connect a syringe and a needle for easy assembly. The design was produced using the API with the following parameters; 2*mm* generator radius, 0.2*mm* tolerance, 10*mm* cusp diameter, 2 rotation and 50*mm* pump height.

In the prototype evaluation, a NEMA17 stepper motor was used to drive the PCP, and successful rotation was obtained. Subsequently, the petroleum jelly was filled to the inlet volume for the material dispensing test, and the PCP was able to dispense the material through an 18 gauge needle. However, the subsequent trials caused the failure of the inner gear due to the missing rotational ratio of the drive gears. This issue can be solved by using precision-manufactured drive gears, inner gear and outer gear; however, this increases the cost of the PCP.

In summary, two main limitations can be concluded from the synchronised PCP prototype. First, the high cost of precision manufacturing, and second, the complicated assembly of

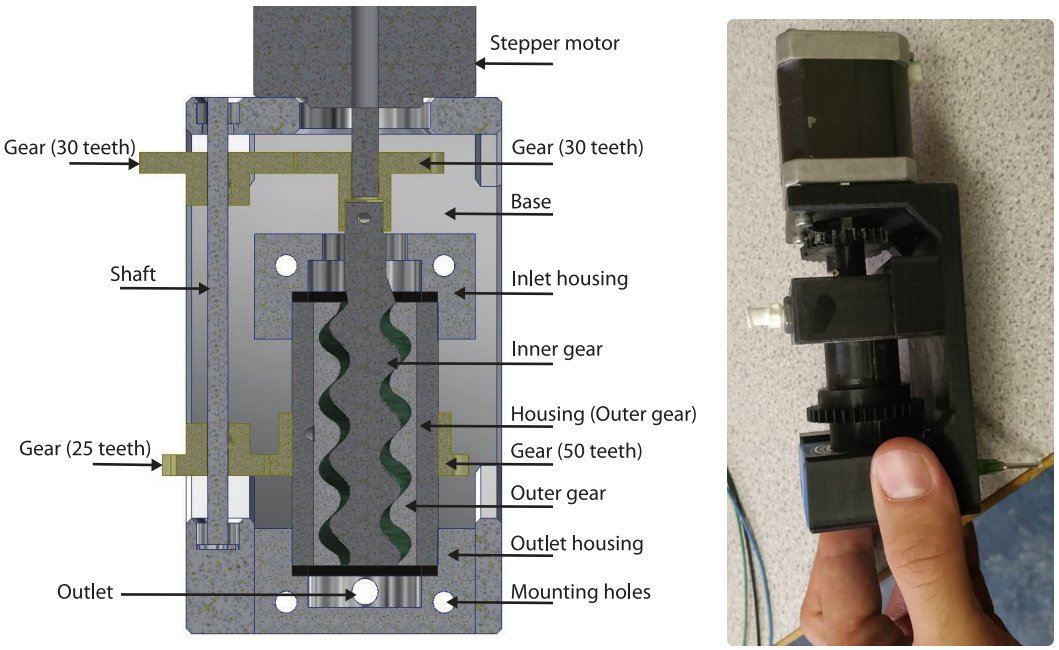

Figure 7.4: PCP with a synchronised drive of inner and outer gears. (Left) Design and explanation of the PCP with a synchronised drive of inner and outer gears. (Right)Functional prototype of the PCP with a synchronised drive of inner and outer gears.

the components. These limitations are against the defined requirements of easy-to-clean and cell-friendly extrusion. In other words, the excess number of components makes the PCP difficult to clean and assemble, and precision manufacturing obligation restricts the disposable PCP option. Therefore, the direction of the next prototype design will be defined as decreasing the number of components and making a single gear-driven PCP.

7.3.5 Concept 3: Inner gear actuated PCP

Various mechanisms were designed and prototyped in the previous three concepts to achieve defined requirements. While they were partially successful, they could not achieve the defined PCP requirements. This concept used previously gained experiences to design a novel PCP with the defined requirements.

The inner gear actuated PCP design and prototype can be seen in Figure7.5, and the name of this concept comes from the actuated part of the PCP. In concept two, the externally actuated PCP was designed; however, it was not satisfied with the desired rotation due to the greater rotation speed of the outer gear than the inner one. In addition, the contact point between gears was not enough to actuate the non-driven gear. In this design, the inner gear was actuated to rotate the outer gear, and the contact points were increased by selecting a

4:3 lobes arrangement to overcome the limitations of the second concept.

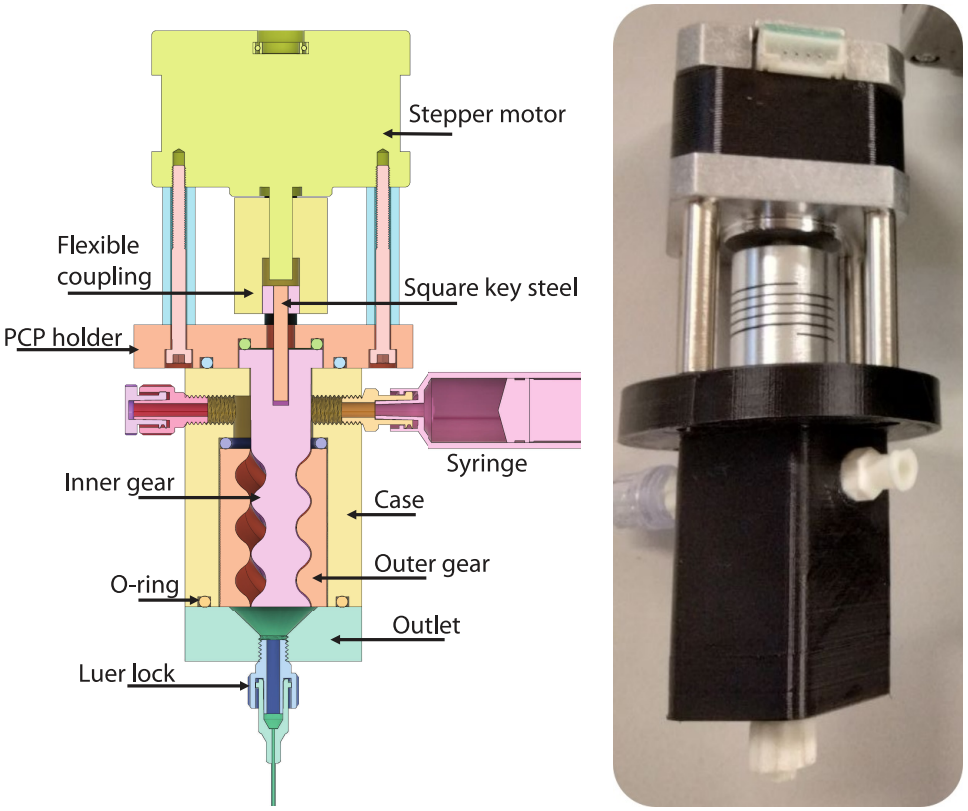

Figure 7.5: Inner gear actuated PCP. (Left)Design and explanation of the inner gear actuated PCP. (Right) Functional prototype of the PCP.

The PCP design consists mainly of the inner gear, outer gear, case and outlet. The main advantage of the design is the self-alignment of inner and outer gear due to the gear matching between them. The number of components was minimised to make it easy to clean and assemble, and this can be the design even disposable with the help of mass manufacturing by reducing the PCP cost. Apart from the main components, Luer-locks were used to enable easy syringe and needle connection, and a flexible coupling and square key steel were used to transfer power from the stepper motor to the inner gear. In addition, nitrile rubber o-rings were used between the case, outlet and PCP holder parts for sealing purposes.

The initial PCP evaluation was successfully conducted by rotating the inner gear to observe the outer gear rotation. Subsequently, the petroleum jelly was filled to the inlet of the PCP, and a successful dispensing action was observed without leakage. In the sealing performance evaluation, tap water was pushed through the inlet channel by closing other exits of the PCP. When the moving force was increased, a small amount of leakage was observed

between the PCP holder and the case. The leakage issue can be solved by changing the arrangement of the o-rings, and the compression force of the flexible coupling can help to press the o-rings to enable leakage-free sealing.

The preliminary 3D printing test of the PCP was conducted by printing 30 layers of the hollow square cube, as can be seen in Figure7.6. A syringe pump was used to feed the PCP, and the speed of synchronised driven motors was calculated based on the theoretical PCP flow rate and syringe pump specifications. The square cube was successfully printed, and results showed that the inner gear actuated PCP is a promising dispensing technology after further optimisation.

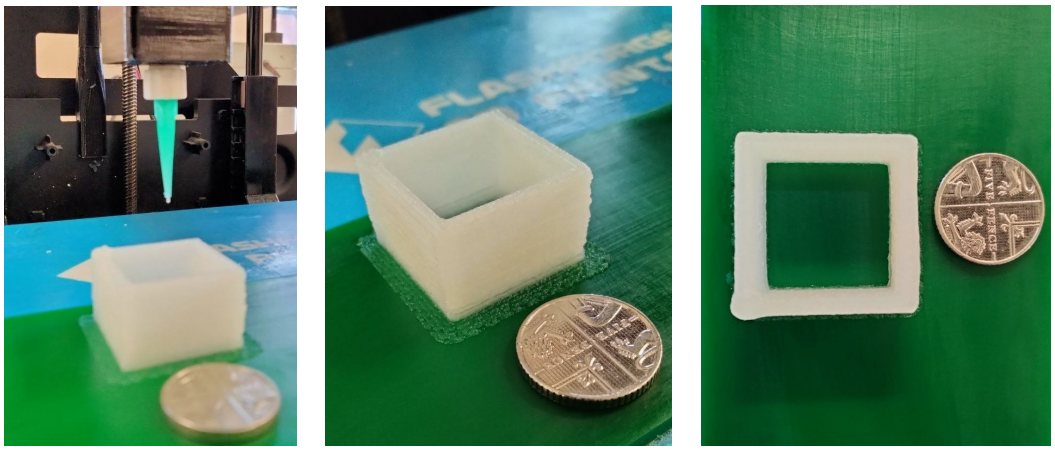

Figure 7.6: The results of the hollow cube 3D printing test of inner gear actuated PCP.

The design does not require any coupling, making it scalable and uncomplicated. In the design process, the design methods for additive manufacturing were used. Therefore, the PCP components were designed to print without support, and an angle of fewer than 45 degrees was used where applicable.

Together these results showed that the inner gear actuated PCP concept meets most of the defined PCP requirements except accuracy. The accuracy of the PCP needs to be tested against other EBB to validate the performance. Consequently, the inner gear actuated concept was approved for further development and validation.

7.3.6 PCP Concepts

In the previous sections, redesigning of a conventional PCP and three concepts were designed and developed. The development process enabled us to obtain a deep understanding

of PCP design, and the evolution of the concept development process can be seen in Figure 7.7. Consequently, the design layout of the most promising PCP concepts can be seen in Figure 7.8. The figure shows the design layouts of a conventional dispensing PCP (a) and developed concepts (b,c,d). In addition, a novel internal gear-driven PCP arrangement was conceptualised, as seen in the last layout (e) of Figure 7.8.

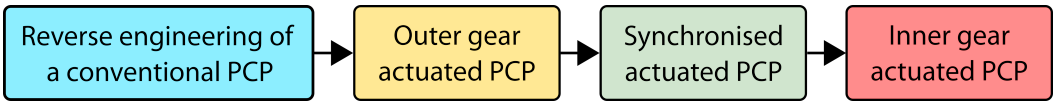

Figure 7.7: Evolution of the concept development process.

The internal gear-driven arrangement can solve the mentioned limitations of bioprinting applications by evenly driving the rotor of the PCP. The arrangements can also overcome the stator material selection limitation due to the applied force to the stator wall. The only limitation in the arrangement can be the high cost of precision manufacturing for the internal gear drive mechanism. However, this cost can be considered a one-time investment, and the critical components of the rotor and stator can be manufactured as single-use components using cost-efficient materials. In this way, the drive mechanism and single-use components can be assembled with a quick-release locking mechanism such as a toggle latch and snib lock. Therefore, an easy-to-clean and low-cost PCP can be obtained.

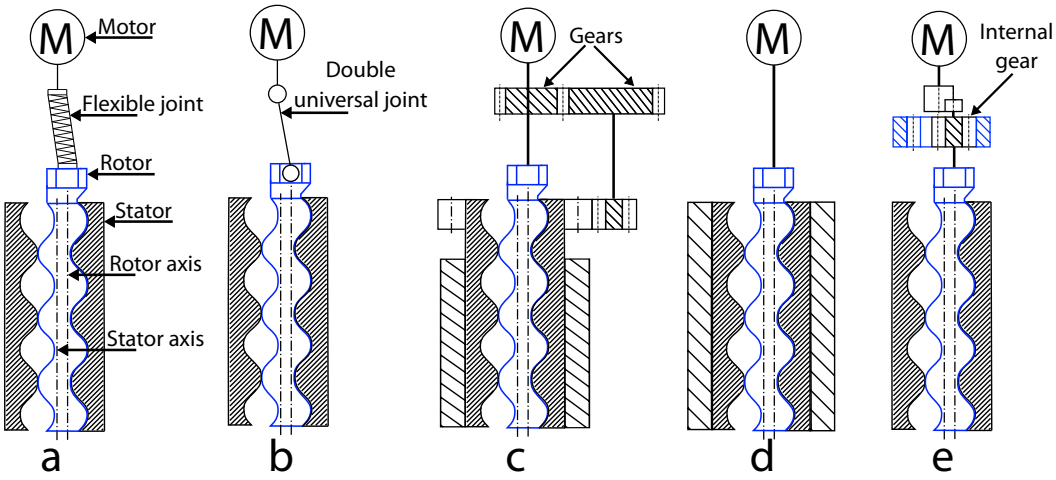

Figure 7.8: Design layouts of possible PCP drive arrangements, namely (a) conventional dispensing PCP, (b) redesigned PCP, (c) synchronised actuated PCP, (d) inner gear actuated PCP and (e) internal gear-driven PCP.

7.4 Conclusion

The purpose of this study was to develop a PCP concept for EBB applications. Therefore, a spiral development process was proposed to achieve a novel PCP with the help of AM, and the API was developed to enable quick design iterations. PCP requirements were determined through literature research, a user questionnaire, user interviews and redesigning of a conventional PCP. Subsequently, three PCP concepts were designed, prototyped and evaluated to meet the defined requirements, and the final concept was approved for the product validation phase.

The present study makes several noteworthy contributions to the product development process, including a framework of additive manufacturing enabled spiral development model and an API to provide quick design iterations. Consequently, the research extends our knowledge of the working mechanisms of PCPs by developing three different concepts and providing a critical evaluation of their limitations. In addition, a novel internal gear-driven PCP concept was proposed as a promising solution for future research.

This study provides the first comprehensive assessment of the working mechanism of PCPs, and a novel PCP concept for EBB applications has been successfully developed. In the next chapter, the required torque for the selected concept is calculated, and a syringe pump is developed and validated to use the approved final PCP concept. Subsequently, the final concept is prototyped to validate the concept by conducting flow rate measurements and a series of printing experiments.

8

INNER GEAR ACTUATED PCP PROTOTYPE

8.1 Introduction

The need for an advanced PCP-based extrusion unit was highlighted in the literature review. Subsequently, limitations and required specifications were investigated in Chapter 5 and Chapter 7. As a result of the PCP Concept Development Chapter 7, several possible concepts were proposed, and the inner gear-actuated PCP concept was chosen for the product development phase.

This chapter aimed to develop an extrusion unit by integrating a syringe pump and the inner gear PCP actuated. Therefore, a novel syringe pump was developed and validated against the Harvard PHD 2000 syringe pump and the open-source Replistruder 3 syringe pump. Subsequently, the inner gear actuated PCP concept was designed and developed. Subsequently, it was integrated into the developed syringe pump for the validation tests.

The first version of the Replistruder open-source pump series was introduced in the supplementary materials of the research of Hinton et al. (2015). In the subsequent research, advanced versions of this pump were proposed, including the Replistruder 2, 2.5, 3 and 4 (Hinton, 2016*a*,*b*, 2018; Tashman et al., 2021). In this study, Replistruder 3 was used as it was the latest version when the experiments had been conducted.

The extrusion unit was designed considering the design for additive manufacturing methods due to the selected FFF manufacturing method (discussed in Chapter 6). Pump validation was carried out by flow rate measurement, line printing, and 3D object printing methods. The rationale and details about validation experiments can be found in Section 8.3.6

There are two reasons behind the development of a syringe pump. First, the PCP requires a material feed for consistent operation. Second, the extrusion unit was designed using the

existing 3D printers. Therefore, a custom syringe pump was required. The name of the developed syringe pump is "Mf syringe pump", and the name of the developed inner gear actuated PCP is "Mf PCP". Therefore, they will be mentioned as the Mf syringe pump, Mf PCP, and the integrated pump will be mentioned as the extrusion unit.

8.2 Methodology

8.2.1 Prototype Evaluation

In the product prototype evaluation, the following features were considered:

- Design scalability
- Sealing performance of the PCP
- Power transfer from a motor to the rotor
- Adaptation to the existing 3D printers
- Easy to clean or disposable
- Easy modification for multi-material dispensing capability

Design scalability was necessary for PCP development due to overcoming cartridge volume restrictions. This criterion was satisfied using parametric modelling and designing a coupling-free PCP.

The sealing aspect was also considered in the concept prototype development phase. Similarly, it was the main objective in the product prototype development because a PCP cannot be fully operational without proper sealing.

Most existing 3D printers use stepper motors for gantry mechanisms and extrusion. For accurate extrusion, the motor torque should be enough to dispense material without skipping steps. Therefore, the power transfer between motors and pumps was carefully considered. In addition, this is the key aspect of developing an extrusion unit for existing 3D printers.

The cell-friendly extrusion was the main limitation in the commercial PCPs (see Chapter 2). Therefore, the easy-to-clean or disposable feature was the most crucial when developing the

PCP. The methods to satisfy this criterion were minimising the number of components and developing an easy-to-assemble design.

The last objective was to make the design easy to duplicate to enable multi-material extrusion. Therefore, the placement of the components was carefully considered to prevent conflict between the extrusion units.

8.2.2 Required Torque Calculation

The Mf syringe pump and Mf PCP are driven by stepper motors for easy adaptation to existing 3D printers. Stepper motors were chosen by calculating the required torque based on printing parameters and syringe specifications.

Layer thickness, needle diameter and printing speed are used to calculate the required flow rate and can be given as follows:

$$Q = L_t D_n V_p \tag{8.1}$$

where Q is the volumetric flow rate (m^3/s), L_t is the layer thickness (m), D_n is the needle diameter in m, and V_p is the printing velocity in m/s.

Hagen-Poiseuille equation is used to calculate the pressure drop of an incompressible Newtonian fluid flowing through a cylindrical tube of constant cross-section, and given as:

$$\Delta P = \frac{8\mu L Q}{\pi R^4} \tag{8.2}$$

where ΔP is pressure difference between two ends (Pa), μ is the dynamic viscosity $(kg/(ms)$, L is the needle length (m), Q is the volumetric flow rate (m^3/s), and R is the needle radius (m).

The force required to reach desired flow rate is calculated as:

$$F = PxA \tag{8.3}$$

where P is pressure and A is the area where the pressure is applied.

Finally, for a threaded rod driven mechanism, the required torque to push the syringe plunger for the given flow rate can be given as (Shigley, 2011):

$$T = \frac{F d_m}{2}\left(\frac{l + \pi f d_m}{\pi d_m - f l}\right) \tag{8.4}$$

where T is the torque, F is the load on the screw, d_m is the mean diameter of the threaded rod, f is the coefficient of friction of the threaded rod, l is the lead which is equal to pitch for single start screws.

Assumptions for these calculations are as follows:

- Atmospheric pressure disregarded due to negligible effect compared to pressure drop.
- Friction between plunger rubber and syringe wall was disregarded
- Fluid assumed as an incompressible and Newtonian fluid
- Flow is laminar

8.2.3 Experimental Setup

This study includes two experimental setups. The first is the experimental setup used in Chapter 5 to compare the flow rate and dispensing accuracy.

The second experimental setup consists of the Mf syringe pump, Mf PCP and Makerbot Replicator 2x experimental 3D printer (see Figure 8.1). This setup was used to evaluate the extrusion quality and ability to print a 3D object of the developed pumps. The extrusion quality experiment was conducted by printing a single line and six squares, and ImageJ software was used to measure the dimensions.

Makerbot printers do not use open-source firmware, which limits any customisation to the printer. Therefore, the control board of the 3D printer should be changed to adapt to the developed extrusion unit. For this reason, Duet 2 Wi-Fi was selected with the Makerbot platform because it satisfies the motor driving requirements and provides easy adjustment to the control.

Initially, the limit switches and motors were wired. Subsequently, the RepRap firmware 2 was set up on the board, and Wi-Fi communication was enabled for browser accessibility. Flow rate adjustment for synchronising driving was calculated based on Chapter 6, and the M567 command was accordingly set for tool mix ratios. In addition, RepRap firmware

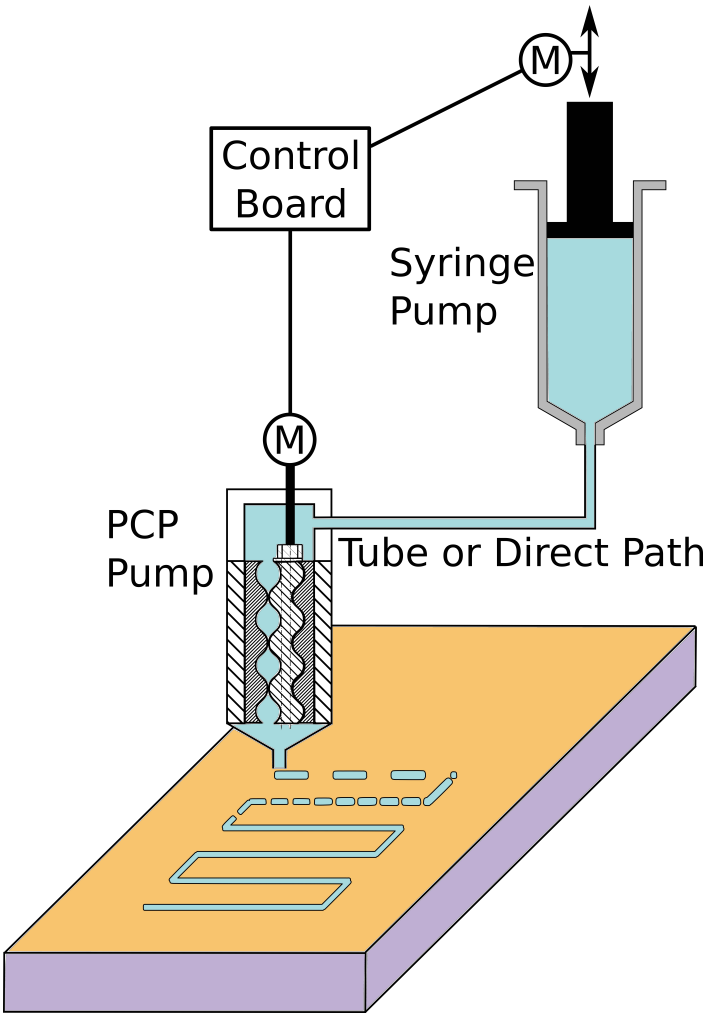

Figure 8.1: Illustration of the experimental setup for the extrusion unit's 3D printing validation tests.

was programmed to use with 3D printers and requires a temperature check before starting the extrusion. Therefore, the cold extrusion command of M302 was enabled to disable the temperature check. Otherwise, it was not possible to use extruders.

The printing began by filling a syringe and loaded into the syringe pump. Subsequently, the syringe pump was connected to the PCP via Luer-locks, and the inlet cavity of the PCP was filled. Therefore, the extrusion unit became ready for the printing experiments.

8.2.4 Implementation of the Control Board

Duet 2 Wi-Fi 32-bit control board (Duet, UK) was used to control the Makerbot Replicator 2x 3D printer and the stepper motors of the extrusion pumps. The schematic of the control board can be found in Section 3.4.1. This section mainly includes the G-codes edits to

control the extrusion units.

Firstly, RepRapFirmware 3.1.1. was installed using Makerbot Replicator 2x settings. The default firmware was developed to drive heated extrusion units of FFF technology, and if there is no signal from the thermistor, the printer will not work. Therefore, the "M302 P1" command was added to the configuration file to allow cold extrusion. Subsequently, the axis minimum and the maximum were defined using the "M208" command to prevent collision of extrusion units as they had different dimensions than the standard extruders. In addition, 3D-printed parts were designed and manufactured to arrange the end-stop positions of the X, Y and Z axis. Another adjustment was required to define the tools and to set the mixing ratio. Therefore, "M563" and "M567" commands were added to define the tool and set the tool mixing ratio, respectively.

The calibration of extruders for the correct dispensing amount was critical in the control board implementation. In addition, the steps per millimetre and mixing ratio settings required adjustment depend on the theoretical flow rate calculations of the developed extruders. Therefore, the following equations were used to calculate the theoretical flow rates of the extrusion units and to adjust the g-codes.

The RepRapFirmware drives the extruder based on the filament diameter. Therefore, the calculation of the volume for a $1mm$ extrusion is required to adjust the steps per millimetre value of the firmware (M92 code in the configuration) and can be calculated as:

$$V_{mm} = \pi r^2 h \tag{8.5}$$

where V_{mm} is the volume extruded per millimetre, r is the radius of a filament or syringe and h is the extruded length.

In the lead screw driven syringe-pumps, the required steps for a $1mm$ displacement can be calculated as follows:

$$Steps/mm_{syringe\ pump} = \frac{Steps\ per\ revolution}{Lead\ screw\ pitch}\ x\ Ratio\ of\ pulleys\ x\ Micro\ step\ ratio \tag{8.6}$$

In the firmware installation, the filament diameter was kept default as $1.75mm$. Therefore,

the steps per millimetre value can be adjusted using the following equation.

$$Adjusted\ steps/mm_{syringe\ pump} = \frac{V_{mm(syringe\ pump)}}{V_{mm(default)}}\ x\ Steps/mm_{syringe\ pump} \tag{8.7}$$

where $V_{mm(syringe\ pump)}$ is the extruded volume per millimetre of a syringe pump and $V_{mm(default)}$ the extruded volume per millimetre based on diameter defined in firmware configuration.

Similarly, the steps per millimetre adjustment for PCPs can be calculated by using the equations given in Section 6.2.5.

8.3 Results and Discussion

8.3.1 Torque Requirement for the Mf Pump

Electric motors drive PCPs, and in this research, the usage of a stepper motor was decided for easy adaptation to existing 3D printers. One main parameter to selecting the correct stepper motor is holding torque capability. To calculate the torque, bioprinting parameters are the key factors, including nozzle diameter, printing speed and layer thickness. In the calculations, the dynamic viscosity of glycerol was assumed as $1.487 Pa \cdot s (at 20 \deg C)$, and layer thickness was equated to the needle diameter (Ferreira et al., 2017). The inner diameter of the syringes can be seen in Table 8.1. In addition, a low-cost threaded rod of $8mm$ diameter and $1.25mm$ pitch was selected to drive the pump, and the torque was calculated based on these parameters. The threaded rod coefficient of friction is 0.25 for steel on steel in a dry condition (Shigley, 2011).

Table 8.1: Inner diameter of syringes.

	Name	Inner Diameter (mm)
1	5 ml BD Plastic	12.06
2	20 ml BD Plastic	19.13
3	60 ml BD Plastic	26.72
4	20 ml Samco Glass	19.7
5	50 ml Samco Glass	28

Figure 8.2 shows the relationship between the torque and needle diameter for three various volumes of plastic syringes. The printing speed was assumed as $50mm/s$ for the calculation.

Overall, the required torque decreases when the needle diameter decreases; similarly, a

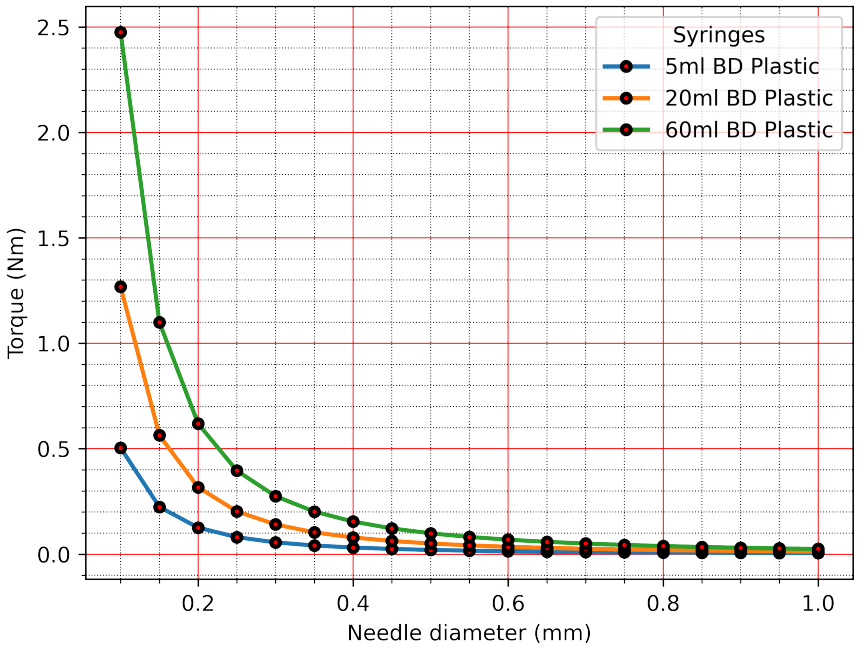

Figure 8.2: Relationship between the torque and needle diameter for $5ml, 20ml$, and $60ml$ plastic syringes (Printing speed = 50 mm/s, Layer thickness = Needle diameter).

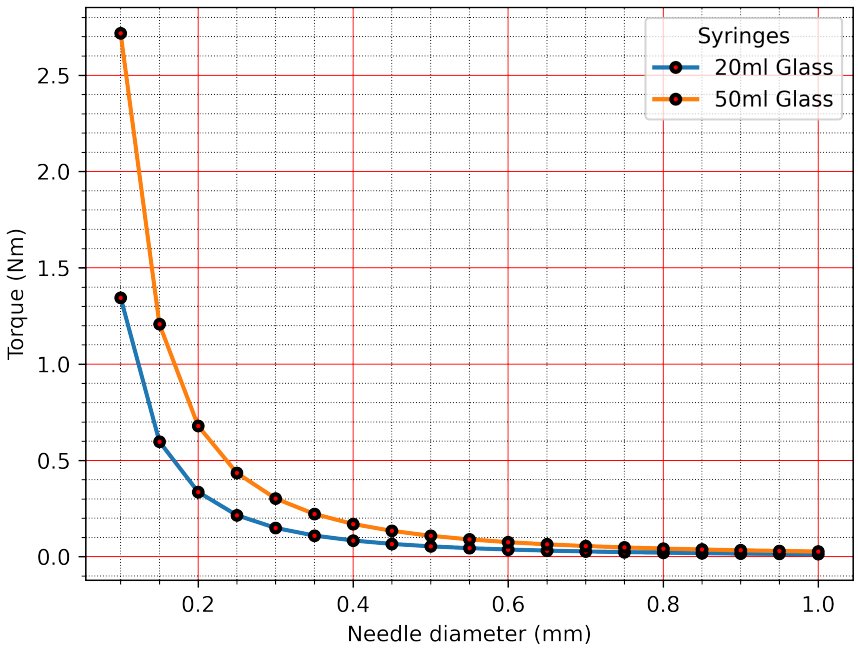

Figure 8.3: Relationship between the torque and needle diameter for $20ml$, and $50ml$ glass syringes (Printing speed = 50 mm/s, Layer thickness = Needle diameter).

large syringe diameter requires more torque. The highest torque is required for the 60*ml* syringe with a 0.1*mm* needle diameter, whereas the 5*ml* syringe requires $0.5N \cdot m$ torque. The 60*ml* syringe with a 0.1*mm* needle diameter requires the highest torque of almost $2.5N \cdot m$, whereas the 5*ml* syringe requires $0.5N \cdot m$ torque with the same size needle.

The same parameters were used to compare the 20*ml* and 50*ml* glass syringes. Figure 8.3 shows the relationship between the torque and needle diameter. Glass syringes have larger diameters than plastic ones. Therefore, a slightly larger torque of $2.7N \cdot m$ is required for the same volume of syringes.

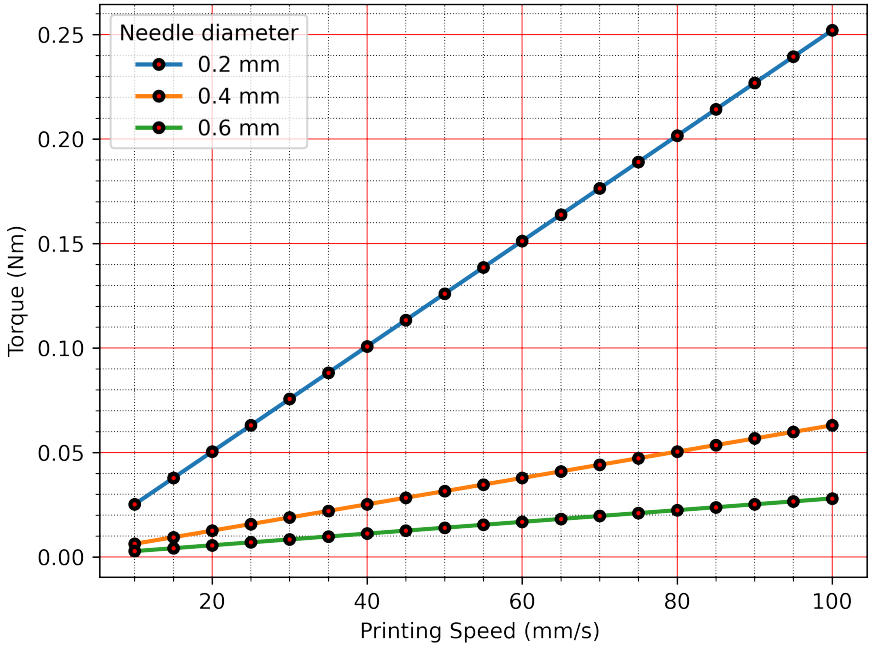

Figure 8.4: Relationship between the torque and printing speed for glycerol-filled 5*ml* plastic syringe with various needle diameters (Layer thickness = Needle diameter).

Figures 8.4 and 8.5 show the correlational analysis between torque and printing speed for glycerol. The required torque was calculated for 5*ml* and 20*ml* plastic syringes as they are commonly used in bioprinting. For the same reason, 0.2*mm*, 0.4*mm* and 0.6*mm* needles were selected, and layer thickness was equated to the needle diameter. The 5*ml* syringe with 0.2*mm* needle diameter at a $100mm/s$ printing speed requires the highest torque of slightly above $0.25N \cdot m$. Similarly, the 20*ml* syringe requires the highest torque of $0.62N \cdot m$ with the same parameters.

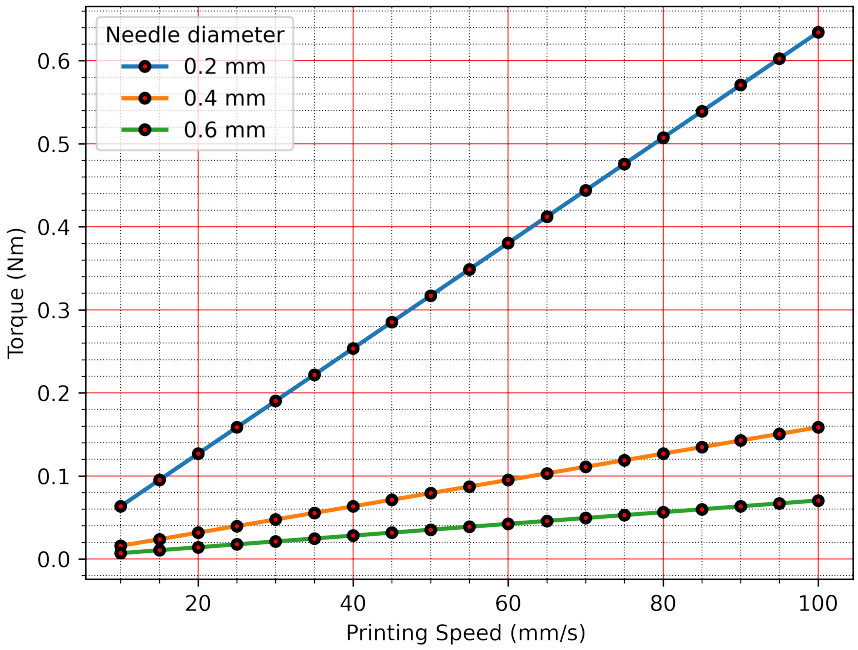

Figure 8.5: Relationship between the torque and printing speed for glycerol-filled 20*ml* plastic syringe with various needle diameters (Layer thickness = Needle diameter).

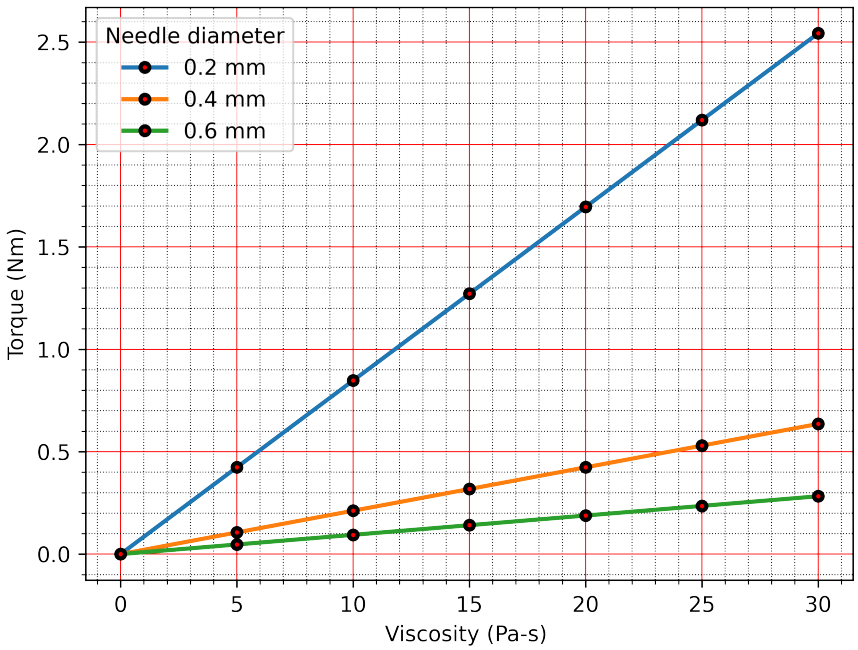

Figure 8.6: Relationship between the torque and viscosity for 5*ml* plastic syringe with various needle diameters (Printing speed = 50mm/s Layer thickness = Needle diameter).

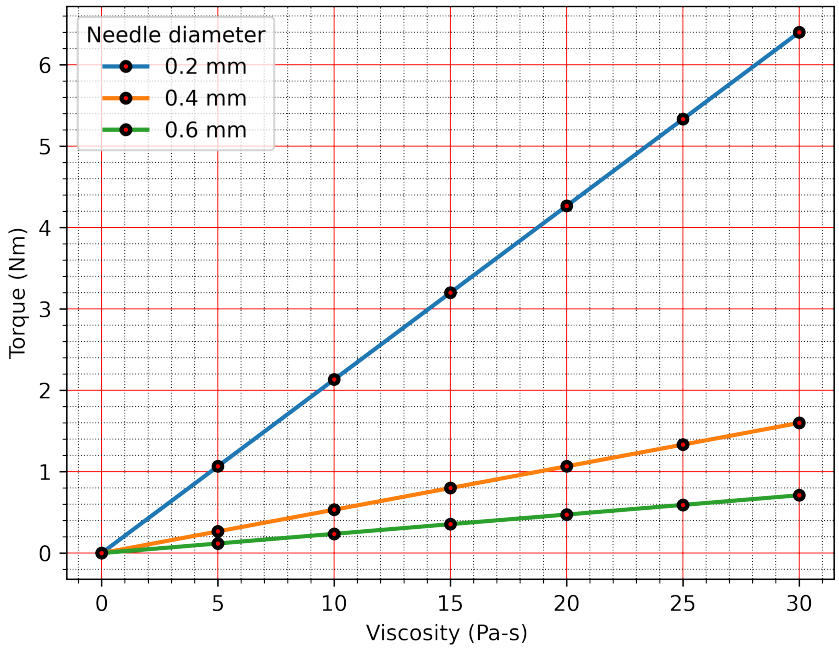

Figure 8.7: Relationship between the torque and viscosity for 20ml plastic syringe with various needle diameters (Printing speed = 50mm/s Layer thickness = Needle diameter).

Figures 8.6 and 8.7 illustrate the torque and viscosity relationship for 50mm/s printing speed. The required torque was calculated for 5ml and 20ml plastic syringes, and 0.2mm, 0.4mm and 0.6mm needles. The layer thickness was equated to the needle diameter, and the viscosity range was selected up to 30$Pa \cdot s$ according to literature (He et al., 2016). The 5ml syringe with 0.2mm needle diameter for a 30$Pa \cdot s$ dynamic viscosity requires the highest torque of slightly above 2.5$N \cdot m$. Similarly, the 20ml syringe requires the highest torque of 6.4$N \cdot m$ with the same parameters.

Figures 8.8 and 8.9 show torque and viscosity relationship for 10mm/s, 30mm/s, and 50mm/s printing speeds with a 0.2mm needle diameter. The required torque was calculated for 5ml and 20ml plastic syringes, the layer thickness was equated to the needle diameter, and the viscosity range was selected up to 30$Pa \cdot s$. The 5ml syringe at 10mm/s printing speed for a 30$Pa \cdot s$ dynamic viscosity requires the lowest torque of slightly above 0.5$N \cdot m$. Similarly, the 20ml syringe requires the lowest torque of 1.23$N \cdot m$ with the same parameters.

Together these results provide important insights into the relationships between the torque and printing parameters. The NEMA 17 type is the most common stepper motor used in 3D

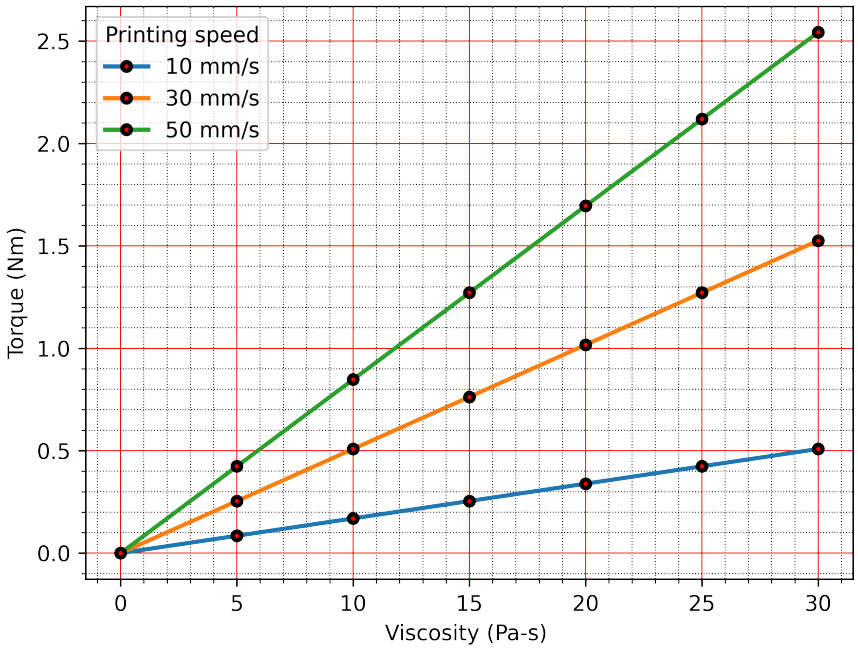

Figure 8.8: Relationship between the torque and viscosity for 5*ml* plastic syringe with various printing speeds (Layer thickness = Needle diameter).

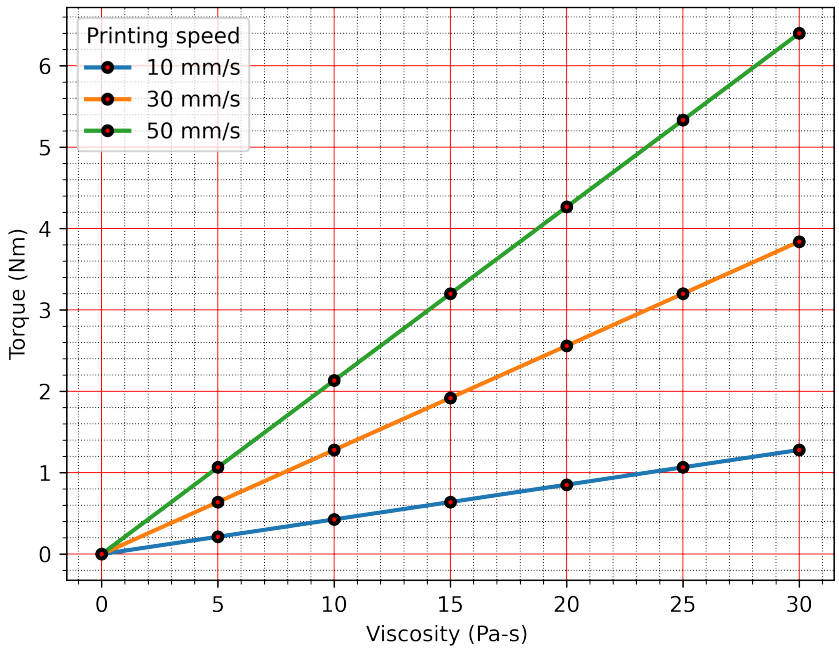

Figure 8.9: Relationship between the torque and viscosity for 20*ml* plastic syringe with various printing speeds (Layer thickness = Needle diameter).

printers. The average torque for a 40mm length motor is 0.44$N \cdot m$. While the higher torque could be provided (up to 0.8$N \cdot m$), longer length (60mm) and heavier (0.55kg) weight causes heavy extrusion unit and decreased the accuracy (Ooznest, 2022). Therefore, a 40mm, 0.44$N \cdot m$ NEMA 17 stepper motor was selected.

The 0.44$N \cdot m$ NEMA 17 stepper motor enables the extrusion of up to 30$Pa \cdot s$ viscosity fluid at 10mm/s printing speed with a 5ml syringe. Moreover, the use of gears or pulleys-belt arrangements increases the torque. Therefore, printing with a smaller nozzle, at a higher speed, with a large volume syringe or with a highly viscous fluid can be possible.

As mentioned in the literature review, the suitable viscosity range for bioprinting is between 0.3 and 30$Pa \cdot s$, and the average printing speed varies between 5 to 30mm/s (Suntornnond et al., 2016; Ozbolat et al., 2017; Naghieh and Chen, 2021; He et al., 2016). Therefore, the 0.44$N \cdot m$ torque motor with pulleys and belt mechanism can provide enough power for the developed pumps.

8.3.2 Design and Development of the Mf Syringe Pump

The Mf syringe pump was designed and developed for up to 20ml syringes in order to meet the defined requirements of bioprinting applications. Initially, a syringe pump prototype was designed and developed using the laser-cutting manufacturing method to decrease the prototyping time. Figure 8.10 shows the laser-cut version of the Mf syringe pump. However, it was not successful in terms of start and stop accuracy due to the use of acrylic material with a thickness of 3mm. The start and stop accuracy were initially tested by observation before moving into a detailed flow-rate experiment. In the observation of the laser-cut version, the extrusion process was initiated, and obvious bending of the acrylic components was observed. The reason for the low accuracy was the bending of the laser-cut parts due to the reaction force of the syringe pushing. For this reason, all laser-cut components were re-designed for 3D printing with higher thickness, and the Mf syringe pump was re-prototyped.

Figure 8.11 shows the components of the 3D printed version of the Mf syringe pump with numbered balloons, and corresponding names can be seen in Table 8.2. The table presents a detailed list of parts, including part name, product code, category, quantity, unit cost, and supplier information.

NEMA 17 (FL42STH47-1684A) stepper motor, with the holding torque of 0.44$N \cdot m$ and

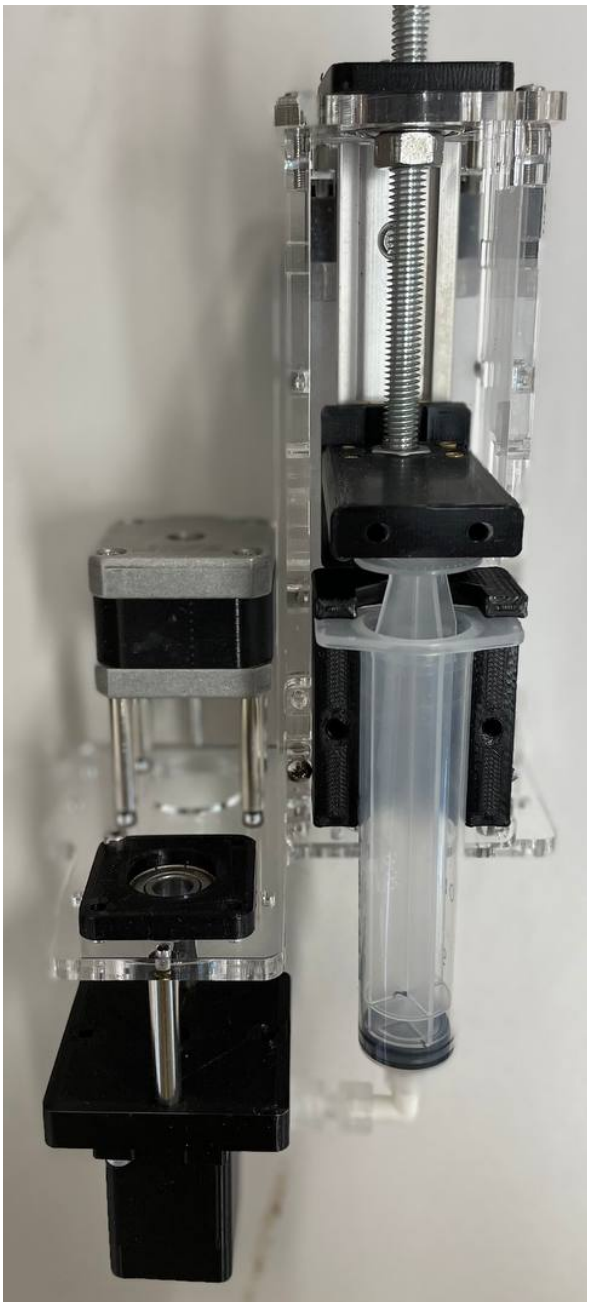

Figure 8.10: Laser-cut version of the Mf syringe pump prototype.

the step angel of 1.8°, was selected with the pulley and belt driving mechanism (1/3 ratio) based on the required torque calculation results. Therefore, $1.29 N \cdot m$ torque can be obtained to push the syringe. The stepper motor was located on the left side of the pump because the PCP was intended to attach to the left side to keep the centre of gravity in the middle of the extrusion unit. The pulleys and belt mechanism consist of pulleys with 16 and 48 teeth, and the timing belt is 6 mm wide, 213 mm long, and has 71 teeth. Therefore, the stepper motor torque was tripled and transferred to the M8 threaded rod.

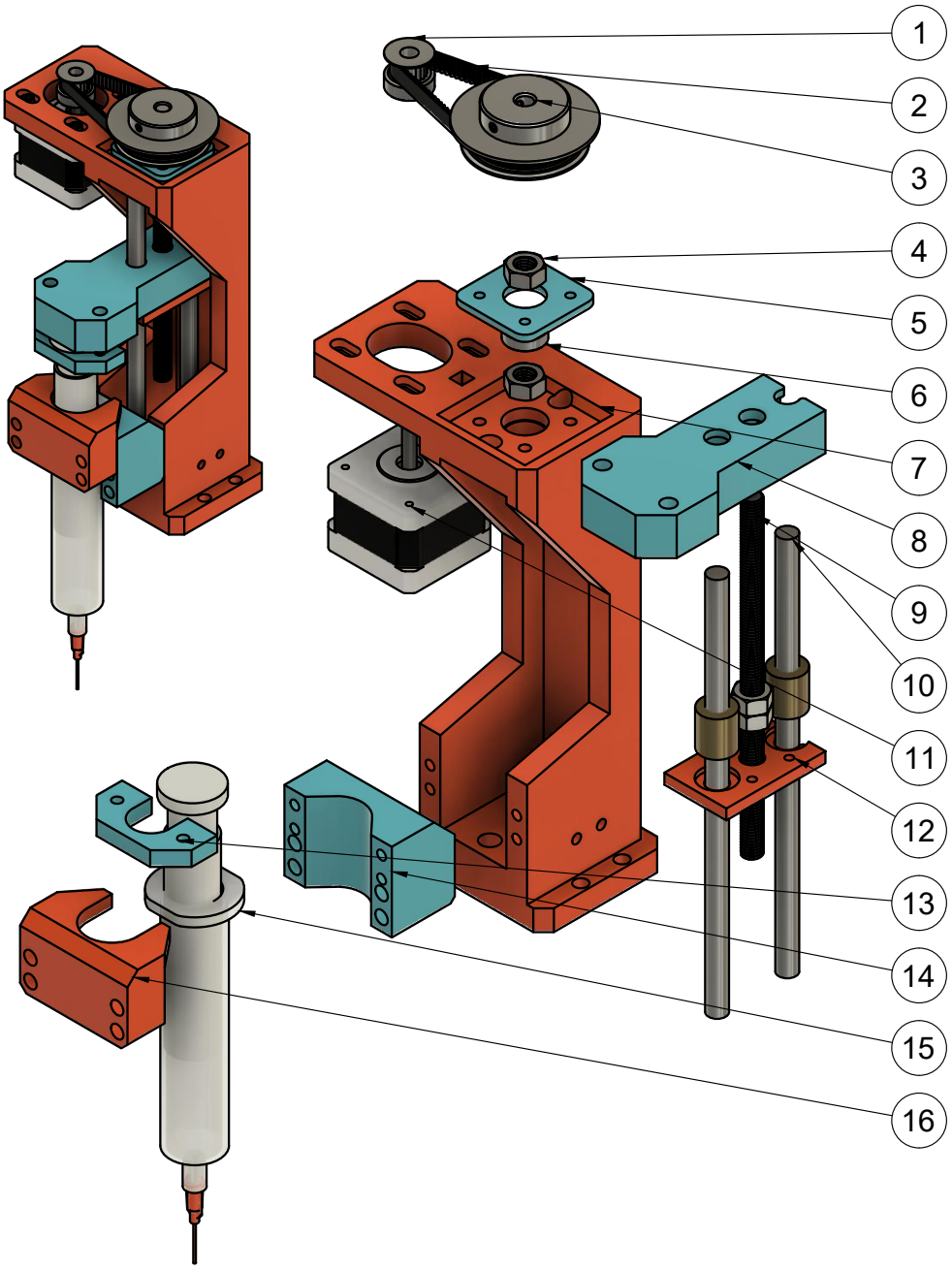

Figure 8.11: Exploded view of the Mf syringe pump without fasteners.

The threaded rod was selected to decrease the pump cost, and the wobbling limitation of the threaded rod was overcome by using two M8 nuts. These nuts were placed inside the pusher component and clamped with the pusher cover to obtain tightness between threads. The arrangement of rods and bushings was selected for the linear motion mechanism. While one bushing could provide the movement, two bushings were selected due to the possible bending force stemming from the reaction force of the syringe pusher.

Table 8.2: Parts list of the Mf syringe pump.

	Part Name	Product Code	Type	Qty	Cost (£)	Supplier
1	Belt Pulley	16PHTD3-10	-	1	13.73	HPC Gears
2	Belt	HTC3/213/6	-	1	4.40	HPC Gears
3	Belt Pulley 48 Tooth	48PHTD3-10	-	1	12.94	HPC Gears
4	M8 Nut	HPN-M8-A2	-	2	1.06	Accu
5	Top Cover	-	3D Printed	1	0.03	-
6	Ball Bearing	207-8238	-	1	7.98	RS Components
7	Main Plate	-	3D Printed	1	6.32	-
8	Pusher	-	3D Printed	1	1.05	-
9	M8 Threaded Rod	280-408	-	1	7.22	RS Components
10	8mm Rod	786-6015	-	1	6.75	RS Components
11	NEMA 17 Motor	1703HS168A	-	1	11.56	Ooznest
12	Pusher Cover	-	3D Printed	1	0.19	-
13	Retractor	-	3D Printed	1	0.16	-
14	Syringe Holder	-	3D Printed	1	1	-
15	20ml Glass Syringe	SYR2110	-	1	3.63	SLS
16	Syringe Fixer	-	3D Printed	1	0.65	-
			Total		£78.67	

The syringe holder and syringe fixer were designed according to the syringe diameter. These are the only components that require a design iteration due to the diameter adjustment of a different syringe. Heat inserts were used to assemble these components because they enable easy disassembly of the pump. Retractor was designed to enable retraction operation to prevent material leakage, and it was mounted to the pusher.

All components can be printed in 26 hours and 47 minutes using 373 grams of PLA. Therefore, the 3D printed components of the Mf syringe pump cost around £10 if the $1kg$ is £27 (PLA filament price based on RS Components).

8.3.3 Mf Syringe Pump Validation

The design and development of the Mf syringe pump were proposed in the previous section. The developed pump is validated in this section with the commercial Harvard 500 syringe pump and an open-source Replistruder 3 syringe pump using the same experimental setup described in Section 3.1.4. Figure 8.12 shows the result of the validation experiment by measuring the flow rate of three pumps.

The experiment aimed to compare the starting and stopping times of the selected pumps.

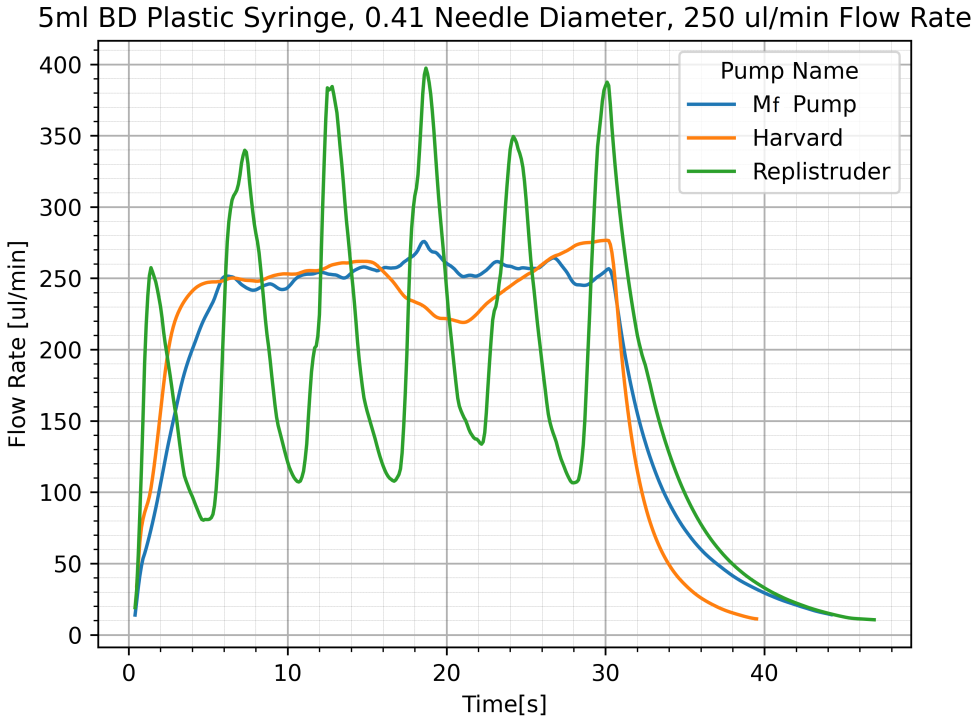

Figure 8.12: Flow rate measurement with glycerine to evaluate the performance of the developed syringe pump with the Harvard and Replistruder.

The flow rate was set to $250\mu l/min$ for $30seconds$, and this flow rate was selected based on user requirements. The sensor readings multiplied by 2.47 to fit the graph with the flow rate and a sensor reading below $5\%\mu l/min$ of measured value disregarded according to the sensor accuracy data sheet (Sensirion, 2021). Therefore, the graph was plotted with the sensor readings above the $5\mu l/min$ flow rate. Glycerine was used in the experiment due to its known insensitivity to minor fluctuations in environmental conditions, particularly in terms of viscosity (Ferreira et al., 2017). As it is stable to temperature variations, all experiments were conducted on the same day without constant monitoring of the environmental conditions. The experiment begins with filling the syringe with glycerine and removing the air bubbles kept inside the syringe. Subsequently, the syringe was placed in the used pump, and the theoretical volume was extruded and then measured with the flow rate sensor (see 3.4.3). Experiments were conducted five times for each pump and at $18°C \pm 1$. Figure 8.13 shows the Replistruder 3 and Harvard pumps used in the experiment.

As shown in Figure 8.12, the Replistruder 3 has the worst flow rate consistency. This could be because of the Replistruder pump design. In other words, the M3 threaded rod was used

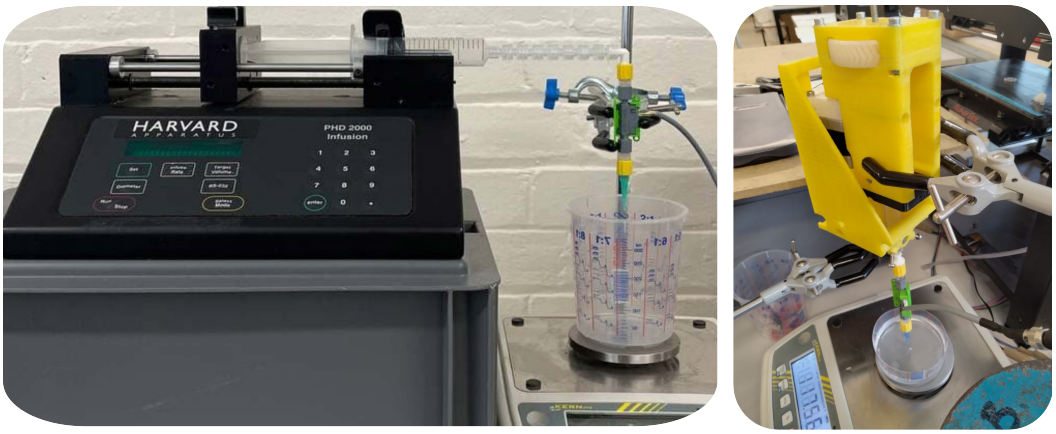

Figure 8.13: Harvard (A) and Replistruder 3 (B) pumps used to evaluate the developed Mf syringe pump with flow rate measurement.

to transfer force, and the selected diameter could cause a bending of the rod. As an extra evaluation not related to this experiment, it can be said that the use of gears also decreases the accuracy of the retraction action. Evidence proving the correctness of these assessments can also be seen with changes made to the subsequent design of the Replisturuder 4 (Tashman et al., 2021). The changes included changing the threaded rod from 3.5mm to 8mm and using a pulley-belt arrangement instead of gears. Consequently, the performance of the Mf pump could be better understood by comparing it against the Harvard pump.

The Harvard pump showed better performance in terms of starting and stopping accuracy. The starting time showed a 0.8*seconds* difference; the Harvard pump was reached in 5.1*seconds*, and the Mf pump reached the same flow rate at 5.9*seconds*. However, the stopping time difference was slightly longer at 4.3*seconds*; the Harvard pump could stop in 9.7*seconds* and the Mf pump in 14*seconds*. Regarding flow rate consistency, the Mf pump performed better than the Harvard pump.

The mean of the weight measurement for the PHD2000 pump was 0.1211*ml* with a standard deviation of 0.0021. Similar results were observed for the Mf syringe pump, with the measured mean value of 0.1248*ml* and a standard deviation of 0.0020.

Results show that the Mf pump can perform just as well as the Harvard pump. Therefore, the Mf pump can provide repeatable extrusion with precision and accuracy, and there is no inconvenience in using the Mf pump to feed the developed PCP. The only limitation of the Mf pump could be considered as the stopping accuracy.

8.3.4 Design and Development of the Inner Gear Actuated PCP

The inner gear actuated PCP was developed using a 4:3 lobe arrangement to enable rotation of the outer gear. The Mf PCP parameters can be seen in Table 8.3. In Figure 8.14, the bottom view of the 4:3 lobe arrangement can be seen with the exerted force from the inner gear to the outer gear. The PCP requirement aimed to select a minimum number of PCP lobe arrangements due to the decrease in the pump length and to increase the number of cavities. Therefore, the best option was the 4:3 lobe arrangement, which enables the required rotation of the gears, provides the minimum lobes and has more strength than the 3:2 lobe arrangement.

Table 8.3: Parameters of Mf PCP and the symbols of parameters (see Chapter 6).

	Name	Value
1	Generator Radius (r=e)	1 mm
2	Tolerance (w)	0.2 mm
3	Cusp Diameter (d)	4 mm
4	Stator Turn	1
5	Pump Height (P_s x Number of Stator Turn)	24 mm

The minimum dispensing amount of the PCP can be calculated based on the equation 6.23 and parameters given in Table 8.3. The theoretical minimum dispensing is 0.0043 ml/step based on selected parameters and the pulley and belt driving mechanism (1/3 ratio). Please note that micro-stepping is disregarded to obtain the required torque of $0.44N \cdot m$, and 200 steps/rotation is assumed.

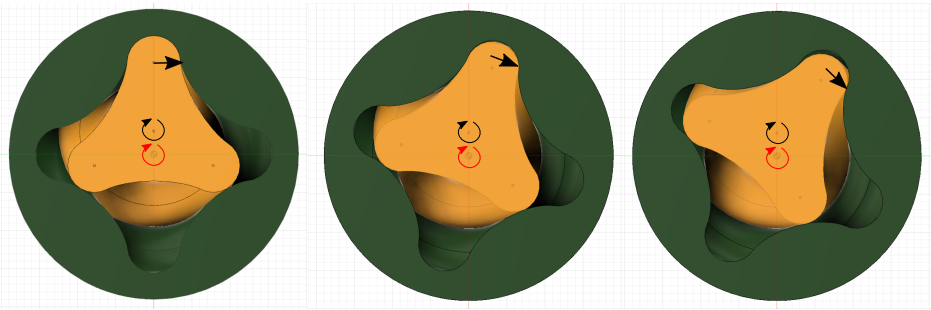

Figure 8.14: Cross-sectional view of 4:3 lobe PCP design. Circular arrows correspond to the rotor and stator axis, black and red, respectively, and a black straight arrow shows the contact point between the rotor and stator.

The exploded view of the final PCP design can be seen in Figure 8.15. The fasteners were disregarded in the figure to explain the design clearly, and components were numbered, and

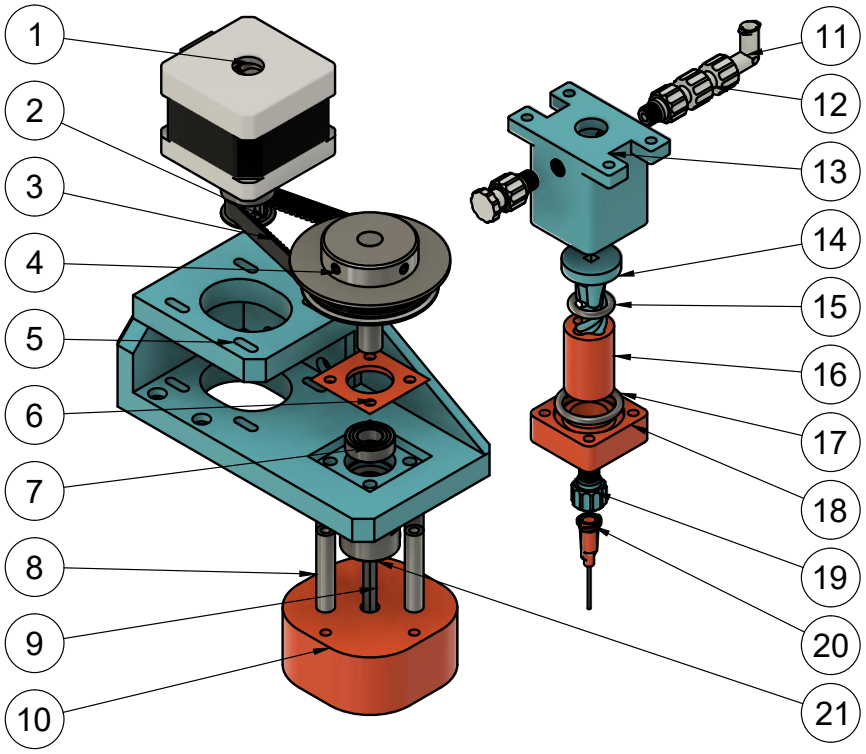

Figure 8.15: Exploded view of the Mf PCP pump with component numbering.

corresponding names were given in Table 8.4. The table presents a detailed list of parts, including part name, product code, category, quantity, unit cost, and supplier information.

In the PCP design, pulleys and belt arrangement were used to increase the torque for the same reason as in the Mf syringe pump. This also enables an increase in the material selection in terms of viscosity. NEMA 17 stepper motor rotates the pulleys, and power is transferred to the inner and outer gears. The flexible coupling was selected to overcome misalignment between shafts, and it can also provide the necessary compression force to the O-ring for sealing purposes. Two O-rings were used in the design, one for sealing above the PCP case and the second for sealing the gap between the outer gear and the PCP outlet.

Luer-locks were selected with $1/4-28UNF$ threads having an outside diameter of $6.35mm$. Therefore, the holes were designed as $5.5mm$ for tapping. Heat inserts had $4.22mm$ outside diameter, and $0.4mm$ narrower holes were designed to place the inserts.

8.3.5 Extrusion Unit Design

The extrusion unit consists of the developed Mf syringe and the Mf PCP pumps. Figure 8.16 shows the design and prototyping of the extrusion unit. Pumps were assembled using

Table 8.4: Parts list of the developed Mf PCP.

	Part Name	Product Code	Type	Qty	Cost (£)	Supplier
1	NEMA 17 Motor	1703HS168A	-	1	11.56	Ooznest
2	Belt Pulley	16PHTD3-10	-	1	13.73	HPC Gears
3	Belt	HTC3/213/6	-	1	4.40	HPC Gears
4	Belt Pulley	48PHTD3-10	-	1	12.94	HPC Gears
5	PCP Base	-	3D Printed	1	2.38	-
6	Bearing Cover	-	3D Printed	1	0.03	-
7	Ball Bearing	207-8238	-	1	7.98	RS Components
8	Spacer	HPS-6-30-BR-NI	-	4	9.08	Accu
9	Square Key Steel	HPCKS3-3-300	-	1	2.95	HPC Gears
10	PCP Holder	-	3D Printed	1	0.97	-
11	Elbow Luer Lock	WZ-45502-26	-	1	0.61	Cole-Parmer
12	Luer Extender	UY-45508-80	-	4	3.61	Cole-Parmer
13	PCP Case	-	3D Printed	1	0.62	-
14	PCP Inner Rotor	-	3D Printed	1	0.11	-
15	O-Ring	196-4967	-	1	0.05	RS Components
16	PCP Outer Rotor	-	3D Printed	1	0.11	-
17	O-Ring	196-4975	-	1	0.05	RS Components
18	PCP Outlet	-	3D Printed	1	0.19	-
19	Male Luer Lock	-	Inventory	1	-	-
20	Needle	-	Inventory	1	-	-
21	Flexible Coupler	SC-5-8	-	1	2.88	Ooznest
			Total		£74.25	

six M3 screws, and the syringe pump was connected to the PCP via Luer-locks.

The Makerbot printer has four holes for extruder assembly as default, and these holes were used to mount the extrusion unit on the gantry. The X, Y and Z limit switches were adjusted according to the extrusion unit dimensions to prevent collision during the homing operation.

8.3.6 Extrusion Unit Validation

The design of the extrusion unit and its components were explained in the previous sections. This section shows the performance of the developed extrusion unit, which was validated by printing single lines, squares, a hollow tube, an ear, a nose and a 3D Benchy. The selection of these geometries aimed to evaluate the performance of the PCP, each serving specific validation purposes:

- **Single-line printing:** Single-line printing was chosen to assess the starting and stop-

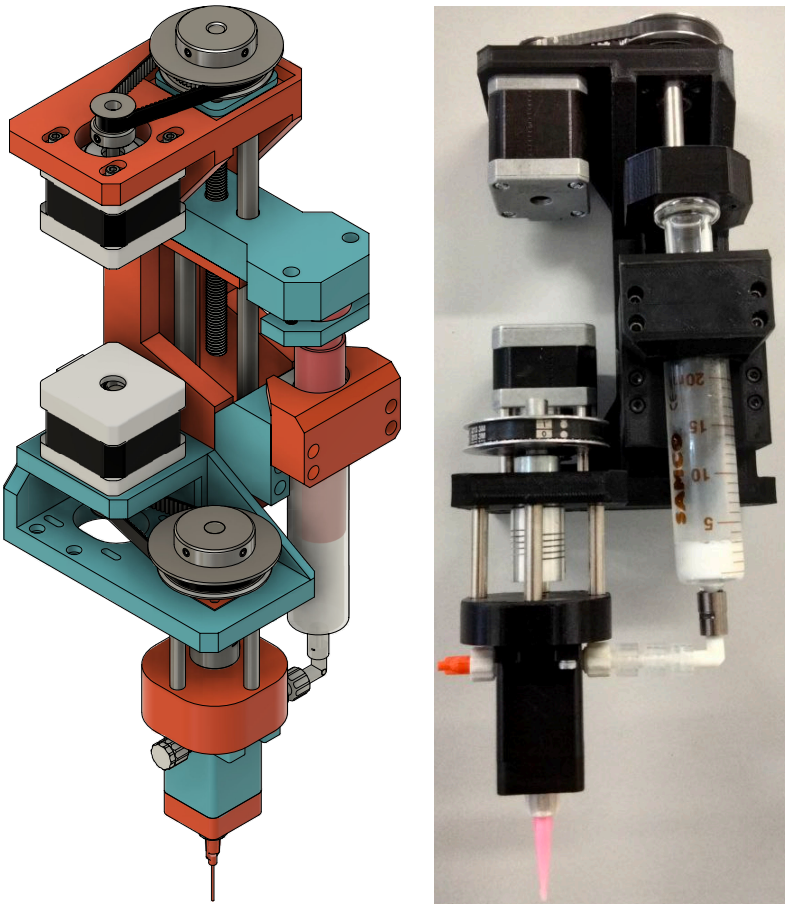

Figure 8.16: Design (Left) and prototype (Right) of the developed extrusion unit consisting of the Mf syringe pump and Mf PCP.

ping accuracy of pumps. The ability of the developed PCP to maintain accurate control during extrusion was tested using both the Mf syringe pump alone and with the Mf PCP attachment. The test involved moving the extrusion head by 40*mm*, 20*mm* with extrusion and 20*mm* without. The starting and stopping accuracy were evaluated by analysing the printed lines at the beginning and end. This approach was used to assess how the Mf PCP attachment affected the control over the extrusion process.

- **Squares printing:** The evaluation was extended to include printing square shapes, which helped us investigate the uniform extrusion ability of the pump across different directions and angles. Similar to the single-line tests, squares were printed with and without the Mf PCP attachment. The mean line thickness and standard deviation were measured to assess the performance of the Mf PCP attachment.

- **Hollow tube:** The hollow tube was included to evaluate the ability of the developed

pump and PCP attachment to print multiple layers. The single-line and squares printing trials were 2D, and the 3D hollow tube was selected as it is a common benchmark object in bioprinting (Ying et al., 2018).

- **Ear, nose and 3D Benchy:** Printing ear, nose, and 3D Benchy objects allowed for the assessment of the performance of the developed pump and PCP attachment. They demonstrated the unit's capability to produce typical benchmark shapes and manage intricate features, which included sloping surfaces, cylindrical shapes, curved overhangs, flat overhangs, and round horizontal holes (3D-Benchy, 2016; Fisch et al., 2020). The tests assessed the capabilities and adaptability of the developed unit to 3D printing.

Throughout these examinations, important parameters such as line thickness accuracy and the starting and stopping accuracy were evaluated. This methodology provided valuable data for evaluating the extrusion unit's performance and understanding the impact of the Mf PCP attachment on its capabilities. The details of the results can be seen in the following sub-sections.

Single-line Printing

Figure 8.17 shows the single-line printing experiment results. The Mf syringe pump is on the left, and the syringe pump with the PCP is on the right. In the experiment, the first 20mm was extruded with the extrusion head movement, and the extrusion was stopped in the second 20mm section by moving the extruder. Glycerol was used, and the aim was to compare the starting and stopping accuracy of the pumps. The Mf syringe pump was able to initiate the extrusion within 8.142mm, and it could stop after 17.664mm. On the other hand, the extrusion unit showed better performance with the Mf PCP attachment. The extrusion unit could start the extrusion immediately. However, the under-extrusion was observed during the first 1mm. Subsequently, the extrusion continued as expected, and the unit responded to the stop command after 1.045mm.

Squares Printing

Figure 8.18 shows the squares printing experiment results. The Mf syringe pump is on the left, and the syringe pump with the PCP is on the right. The extrusion was conducted with-

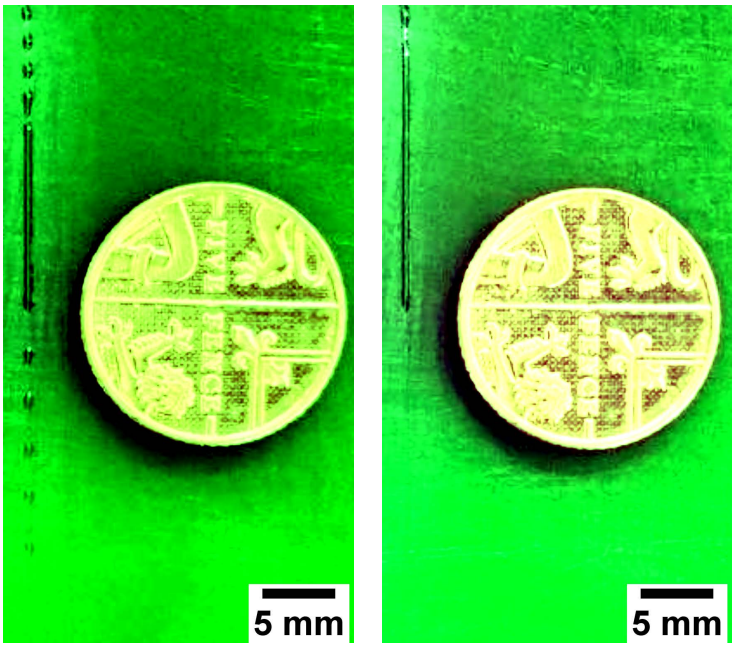

Figure 8.17: Extrusion of a single line for 20*mm* and moving the head without extrusion for 20*mm*. Mf syringe pump performance is on the left, and the syringe pump with the PCP is on the right.

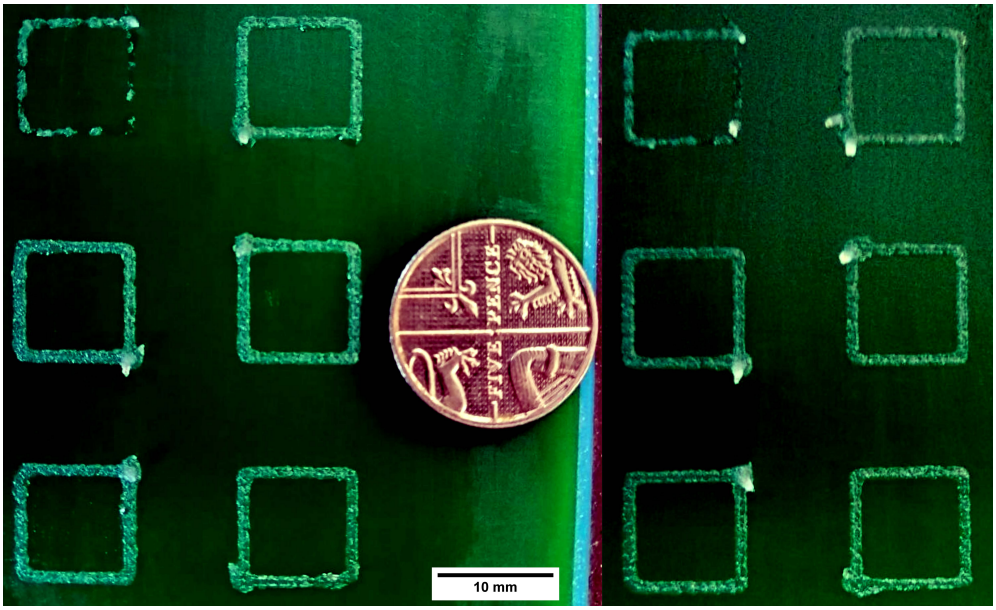

Figure 8.18: Extrusion of six squares without retraction and enabling the 1*mm* Z-hop (Z-axis movement between squares). Mf syringe pump performance is on the left, and the Mf syringe pump with the PCP is on the right.

out retraction, and the Z-hop (Z-axis movement between squares) was enabled. Petroleum jelly was used in the experiment, and the aim was to compare the line thickness and starting accuracy. The Mf syringe pump and the extrusion unit showed similar performance in terms

of line thickness. The measurement was taken from ten different locations, and the mean line thicknesses were 1.061*mm* and 1.06*mm* for the Mf syringe pump and the extrusion unit, respectively. The standard deviation was 0.073*mm* for the Mf syringe pump and 0.059*mm* for the extrusion unit. When the starting accuracy was compared, a similar result was observed in the single-line printing experiment. The Mf syringe pump could reach the full extrusion after 18.302*mm*, and 12.024*mm* was required for the extrusion unit.

Hollow Tube Printing

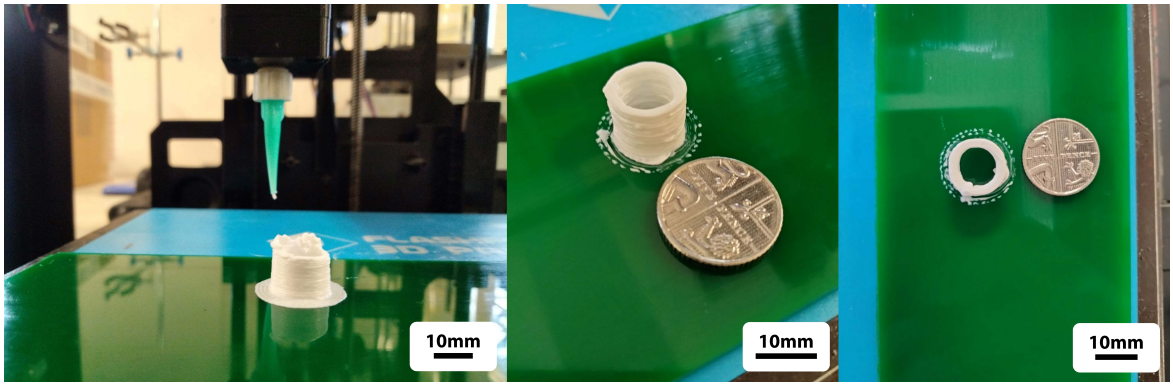

Figure 8.19: The hollow tube printing trial with a 18*G* needle. Mf extrusion unit was used to print a 10*mm* diameter hollow tube with 15 layers.

Figure 8.19 shows the printing of a hollow tube 10*mm* in diameter and printed in 15 layers. A tapered 18*G* needle was selected to decrease the required torque, as petroleum jelly is a highly viscous material. The tube was successfully printed without any retraction of the material, as the 3D printing path was continuous. As can be seen from the figure, there are some over-extruded sections on the wall. Therefore, the printing parameters require further adjustment to overcome this issue.

Ear, Nose and 3D Benchy Printing

Figure 8.20 shows the 3D object printing performance of the extrusion unit. A common benchmarking object used by the open-source desktop printing community is the 3D Benchy, and the printing of ear and nose objects can commonly be seen in the bioprinting literature (3D-Benchy, 2016). Therefore, the experiment aimed to 3D print these objects using petroleum jelly to show the performance of the developed unit. The objects were sliced with a 0.4*mm* layer thickness and printed using an 18*G* tapered needle at 15mm/s printing speed. The ear and nose were successfully printed except for the over-extrusion issue in the

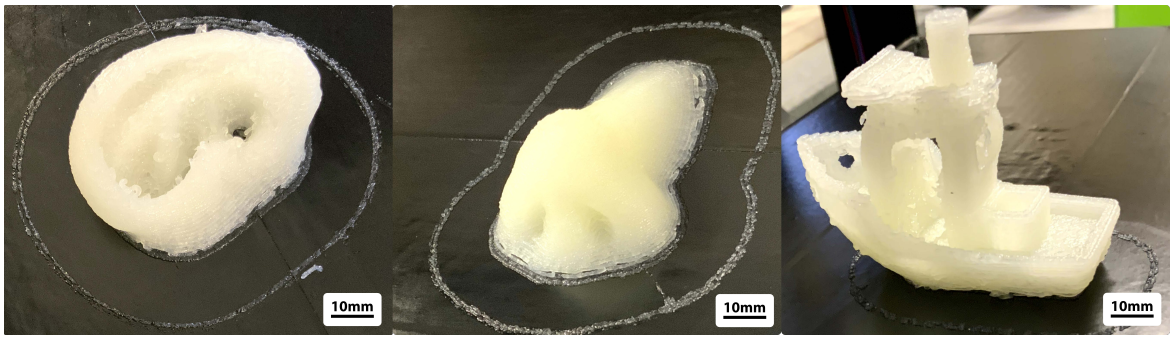

Figure 8.20: The printing trial of the most popular 3D objects with a 18*G* needle. The ear (left), nose (Middle) and benchy (Left). Mf extrusion unit was used to print the objects.

ear printing. The reason for the issue was the disabling of the retraction in the ear printing. Therefore, the nose was printed with a 1*mm* retraction and showed promising quality.

The 3D Benchy contains various aspects that are difficult to print geometrically, including sloping surfaces, cylindrical shapes, curved overhangs, flat overhangs, and round horizontal holes. The 3D Benchy printing can be considered as successful if the overhang areas are disregarded, as poor performance was observed due to the petroleum jelly viscosity. In other words, the vaseline could not withstand the load, and a bend was observed in the lower part of the roof. Besides, shape integrity was achieved for all 3D objects, and the chimney was successfully printed.

8.3.7 Cost Analysis

The cost analysis of the developed PCP extrusion unit prototype was conducted by comparing it with a commercial PCP. The main factors that affect the cost are the component cost, the number of components, and the manufacturing method. The component cost includes the developed PCP, not the control unit.

The results showed that the developed PCP prototype has a lower component cost than the commercial PCP. The component cost of the extrusion unit was 152.92 with the Mf syringe pump was £78.67, THE Mf PCP was £74.25 (see Figure 8.2 and 8.4). On the other hand, the commercial PCP typically costs around £3000, and the control unit £2500 (ELPRO, 2023*a*,*b*).

The cost analysis clearly indicates that the developed PCP prototype is a cost-effective solution. While a direct functionality comparison was beyond the scope of this study due to budget constraints, the cost of the developed PCP concept is significantly lower than that of

a commercial PCP. This makes it an economically viable alternative, particularly for settings where budget constraints are a major consideration. In addition, it is essential to recognise that this cost analysis aligns with our research aim of developing a novel low-cost fluid dispensing and deposition pump for EBB.

8.3.8 Evaluation of the Mf Pump Against Product Design Specification (PDS)

The product design specification (PDS) is a document that defines the requirements and criteria for the product development. Evaluating the developed product against the PDS is important to ensure that it meets the expectations. In this section, the Mf pump is evaluated against the PDS that was presented in Section 3.1.2. The PDS consists of the following specifications:

- Reduction in pump cost
- Reduction in the number of components
- Scalable minimum dispensing amount
- Scalable cartridge volume
- Use of biocompatible materials
- Disposable or easy-to-clean pump design

Table 8.5 shows the comparison of the target values and the Mf pump values for previously defined specifications.

Table 8.5: Evaluation of Mf Pump against Product Design Specification

Specification	Unit	Target Value	Mf Pump Value
Reduction in pump cost	GBP	< 3000	152.92
Reduction in the number of components	EA.	< 29	21
Scalable minimum dispensing amount	ml	0.001 to 0.06	0.0043
Scalable cartridge volume	ml	2.5 to 60	2.5 to 20
Use of biocompatible materials	Binary	Yes	Yes
Disposable or easy-to-clean pump design	Binary	Yes	Yes

The Mf pump has been successful in achieving a significant reduction in pump cost. The target value for the pump cost was less than £3000. However, the Mf pump was developed at a cost of £152.92, which is significantly lower than the target value. This cost reduction can be attributed to the use of cost-effective materials and manufacturing methods, as well as a simplified design that reduces manufacturing costs.

In terms of the number of components, the target was to keep the pump design at less than 29 components without fasteners. The Mf pump has surpassed this target by consisting of only 21 components. This meets the target and simplifies the assembly and maintenance process, making the pump more user-friendly.

The Mf pump was designed to deliver a minimum dispensing amount of 0.0043 ml (see Section 8.3.4). This does not meet the target minimum dispensing amount of 0.001 ml as specified in the PDS. This is an area where the Mf pump falls short of the target specification. While 0.0043 ml is still a relatively small amount, it may not provide the level of precision required for certain applications. However, the pump was designed to be scalable for a wide range of applications using parametric API; therefore, it has the potential for a smaller minimum dispensing amount. In addition, micro-stepping can be applied by selecting another stepper motor with higher torque, and a lower minimum dispensing amount can be obtained.

The Mf pump can be used with syringes of different volumes, ranging from 2.5 ml to 20 ml. However, the target specification for the scalable cartridge volume was 2.5 ml to 60 ml. Therefore, the Mf pump meets the lower end of the target range but not the upper end. This is a limitation of the current design, which could be improved by using a larger Mf syringe pump. In addition, the Mf PCP can be integrated into another large-scale pump, and this enables a wide range of possibilities for large-volume required applications.

The use of biocompatible materials (such as PLA) in the construction of the Mf pump ensures that it meets the specifications outlined in the PDS. This means that the pump can be safely used in bioprinting and other biomedical applications without causing adverse reactions. While the 3D printed components might not be useful to use in bioprinting, the design of the Mf PCP pump enables different manufacturing methods, such as injection moulding and CNC machining.

Finally, the Mf pump was designed to be disposable or easy to clean, per the PDS. This feature enhances the pump's usability and convenience, particularly in applications where sterility is crucial. The Mf PCP can be used just by replacing or cleaning the inner rotor, outer rotor, case, outlet and o-rings which can make the design disposable or easy to clean.

8.4 Conclusion

The present study was designed to develop and validate an extrusion unit containing a syringe pump and the selected inner gear actuated PCP concept in Chapter 7.

The syringe pump was successfully developed and validated against the PHD 2000 pump. The required motor torque was calculated for various printing parameters, and the syringe pump stepper motor was selected based on the result. While the literature contains several syringe pump development studies, they did not calculate the required torque Pusch et al. (2018); Klar et al. (2019); Booeshaghi et al. (2019); Samokhin (2020); Tashman et al. (2021); Bessler et al. (2019). Therefore, the study can be considered a valuable contribution to the literature.

The selected PCP concept was designed using a design for additive manufacturing methods, and it was prototyped and integrated into the syringe pump to obtain an extrusion unit. The extrusion unit was validated with the developed syringe pump; in other words, experiments were conducted with the syringe pump alone and by integrating the PCP. Single-line and squares were printed for validation, and the PCP-integrated extrusion unit performed better. In addition, common benchmarking 3D objects were printed to observe the 3D printing ability of the extrusion unit. The printing of the 3D objects showed acceptable results by considering the limitation of the petroleum jelly viscosity for overhang printing. In Section 8.3.7, the cost analysis was conducted on the extrusion unit, and it was found that it is much cheaper than a commercial PCP.

The last section 8.3.8 showed that the Mf pump met most of the specifications, such as reduction in pump cost, reduction in the number of components, reduction in the number of components, use of biocompatible materials, and disposable or easy-to-clean pump design. However, the Mf pump did not meet two specifications of the PDS, which were scalable minimum dispensing amount and scalable cartridge volume. Therefore, future work can focus on meeting these specifications of the Mf pump design to achieve better performance

and versatility for EBB applications.

9

CONCLUSIONS AND FUTURE WORKS

9.1 Introduction

This chapter summarises the main findings, contributions, limitations and recommendations of this research, which aimed to develop a novel, low-cost, scalable, easy-to-clean extrusion system based on the progressive cavity pump (PCP) principle for extrusion-based bioprinting (EBB) applications. The research was conducted using a spiral development model that involved a literature review, user survey, syringe pump evaluation, PCP concept development, and PCP validation. The research addressed two main assumptions: (1) current extrusion technologies could not meet the requirements of bioprinting, and (2) PCP could be used as an advanced dispensing unit for EBB. The research objectives were derived from these assumptions and were achieved through various methods and experiments. The research outcomes were evaluated against the existing literature and practice and were discussed in terms of their implications and limitations. The chapter concludes with suggestions for future research based on the findings and limitations of this study.

9.2 Main Findings and Contributions

This research has achieved the main aim of developing a novel, low-cost, scalable, easy-to-clean extrusion system based on the progressive cavity pump (PCP) principle for extrusion-based bioprinting (EBB) applications. The main findings and contributions of this research are as follows:

- The research identified the limitations and requirements of existing EBB technologies and PCPs through the literature review, user questionnaire, user interviews, and syringe pump evaluation. The research also proposed a product design specification (PDS) to guide the design and evaluation of PCP concepts.
  - The literature review revealed the current challenges and opportunities of EBB, such as material properties, printability and accuracy. It also reviewed the existing extrusion technologies, such as pneumatic, piston, screw, and PCP systems, and their advantages and disadvantages for EBB applications.
  - The user survey and interviews collected the opinions and expectations of 20 bioprinting experts from different countries and fields. The results showed that

the users preferred a low-cost, scalable, easy-to-clean, and cell-friendly extrusion system that can print various types of biomaterials with high accuracy.

  - The syringe pump evaluation assessed the performance of a commercial syringe pump and a custom-made large-volume syringe pump for EBB applications. The results showed that the syringe pumps had limitations in terms of extrusion accuracy and material compatibility. The results also highlighted the negative effects of plunger rubber compressibility and compressed volume on extrusion accuracy.
  - Based on the literature review, user questionnaire, user interviews, and syringe pump evaluation, a PDS was developed to define the technical specifications and requirements for a novel PCP concept for EBB applications. The PDS included four main user needs: low-cost, scalable, well-sealed, and cell-friendly.

- The study designed and validated a large-volume syringe pump (LVSP) to analyse the impact of compressibility in the plunger rubber on a plastic syringe and the influence of the compressed syringe volume on extrusion precision.
  - The large-volume syringe pump was designed and prototyped using additive manufacturing methods to overcome the volume restriction of conventional syringe pumps.
  - The LVSP was developed using the Duet control board, which provides complete control over the extrusion process and enables easy adaptation for PCP integration, as commercial pumps were challenging to integrate with.
  - The developed LVSP was validated by comparing its performance with a commercial syringe pump using flow rate experiments for accuracy. The study investigated how the compressibility of plunger rubber affects the accuracy of extrusion in a plastic syringe. It was discovered that there is a strong negative correlation between the compressibility of the rubber plunger in a plastic syringe and the accuracy of extrusion. This observation confirms the findings presented by previous research (Banović and Vihar, 2018).
  - Another finding of the study relates to the relationship between the volume of the syringe under compression and extrusion accuracy. The research showed a

negative correlation, indicating that as the volume within the syringe becomes compressed, extrusion accuracy is adversely affected.

- The study examined the theoretical and parametric modelling of PCPs and low-cost prototyping methods. API was developed for rapid PCP design iterations, and a DfAM methodology was used for PCP prototyping. The research also compared the manufacturing quality of FFF and SLS methods for PCP components.
  - The study presented theoretical modelling for rotor and stator components of PCPs based on the modified hypocycloid method. A tolerance factor, based on the work of Nguyen et al. (2014), was incorporated into this method. This adaptation leads to the development of an extended hypocycloid equation, which serves as the foundation for creating a parametric modelling API. Notably, this API represents one of the initial efforts to comprehensively explore the parametric modelling of PCPs, with a specific focus on enhancing prototyping efficiency. The resulting API was designed to speed up prototyping and is suitable for practical use in future PCP design research.
  - The manufacturing quality of FFF and SLS methods was compared for PCP components. The results showed that both methods could produce high-quality PCP components with similar dimensional accuracy. However, FFF method had lower cost, higher availability, and faster printing time than SLS method. Therefore, FFF method was selected and employed for PCP prototyping in this research.
  - FFF printing parameters were optimised, and results indicated the ideal settings for producing accurate and cost-effective PCP prototypes. These findings contribute to the understanding of how to achieve optimal results with FFF technology to use in the prototyping stage of PCP development.
- The research developed various PCP concepts, and initial evaluations were performed for these concepts to select the best design for EBB.
  - In addition to previously conducted literature research, user questionnaires and interviews, a conventional PCP was redesigned to determine PCP limitations.

This approach was employed to generate knowledge in this research area due to the lack of existing research.

  - Three different PCP concepts were designed, prototyped, and evaluated to meet the defined requirements. This comprehensive approach allowed for a critical assessment of each concept's capabilities and limitations. This study is a first in this field and has made significant contributions to the field of PCP development, specifically for extrusion-based additive manufacturing applications.
  - The research has significantly enhanced our understanding of the working mechanisms of PCPs. This enhanced understanding paves the way for future research and development in the field.

- The study demonstrated the development and validation of an extrusion unit containing the Mf syringe pump and the selected inner gear actuated PCP concept (Mf PCP). The Mf PCP is the first open-source PCP to be used in extrusion-based additive manufacturing in the academic literature. It can be regarded as the main contribution of this research.

  - The torque requirements were determined for the Mf pump based on the material viscosity, needle diameter and printing speed. The results showed that the torque increased with the increase of viscosity and needle diameter and decreased with the increase of printing speed. For instance, a $60ml$ syringe with a $0.1mm$ needle diameter requires the highest torque, nearly $2.5N \cdot m$, while a $5ml$ syringe needs only $0.5N \cdot m$ for the same needle size. The research also compared glass and plastic syringes, demonstrating that larger-diameter glass syringes require slightly more torque. Consequently, the stepper motor, a $0.43N \cdot m$ NEMA 17, was selected to use with developed pumps. The existing literature includes numerous studies on syringe pump development; however, it is noteworthy that none of these studies conducted an assessment of the required torque (Pusch et al., 2018; Klar et al., 2019; Booeshaghi et al., 2019; Samokhin, 2020; Tashman et al., 2021; Bessler et al., 2019). Consequently, this research can be regarded as a valuable addition to the scholarly body of work in this field.
  - The Mf syringe pump was validated with glycerol and compared with the PHD2000

commercial syringe pump. The results showed that the Mf syringe pump showed similar performance as the PHD2000. The PHD2000 exhibited excellent starting and stopping accuracy, with a 0.8 second difference in starting time (5.1 seconds for PHD2000, 5.9 seconds for Mf). However, the stopping time difference was slightly longer at 4.3 seconds (9.7 seconds for PHD2000, 14 seconds for Mf). In terms of flow rate consistency, the Mf pump outperformed the PHD2000 pump. The PHD2000 pump had a mean weight measurement of $0.1211ml$ with a standard deviation of 0.0021, while the Mf syringe pump showed similar results with a measured mean value of $0.1248ml$ and a standard deviation of 0.0020.

- The Mf PCP was integrated with the Mf syringe pump to form an extrusion unit that can handle highly viscous materials with high accuracy and low dead volume. The inner gear actuated PCP had a cross-sectional geometry of 4:3 lobes and a flexible coupling to reduce the misalignment between the rotor and stator.
- The validation tests of the extrusion unit were performed against Mf syringe pump only in terms of flow rate, start and stop accuracy, retraction capability and printing quality. The results showed that the extrusion unit outperformed the Mf syringe pump in all aspects. For example, the Mf syringe pump could reach the full extrusion after $18.302mm$, and $12.024mm$ was required for the extrusion unit. Similarly, the Mf syringe pump initiated extrusion at $8.142mm$ and stopped at $17.664mm$. On the other hand, the extrusion unit performed better with the Mf PCP attachment, starting the extrusion process immediately. However, there was a slight under-extrusion in the first $1mm$. After that, the extrusion continued as expected, and the unit stopped after extruding $1.045mm$ in response to the stop command.
- The cost analysis of the extrusion unit showed that it is much cheaper than the commercial syringe pump and the Replistruder. The extrusion unit has a total cost of £152.92, which is much lower than a commercial PCP, which typically costs around £3000, and the control unit £2500.
- The Mf pump met most of the product design specifications (PDS), such as low cost, easy-to-clean, biocompatibility, and disposable design, but did not meet the

specifications of the scalable minimum dispensing amount and scalable cartridge volume. These attributes collectively demonstrate the Mf pump's potential as a low-cost, scalable, and easy-to-clean PCP.

9.3 Limitations

The research also has some limitations and implications that need to be acknowledged and discussed. These are as follows:

- The research used petroleum jelly as a material for bioprinting, which may not represent the properties of real biomaterials. Petroleum jelly has a high viscosity and low flowability, which may affect the extrusion accuracy and resolution of the PCP. Moreover, petroleum jelly is not biocompatible or biodegradable, which limits its application in tissue engineering. Therefore, the research did not evaluate the effect of the PCP on the viability and functionality of living cells or tissues.
- The research did not evaluate the effect of material heating and UV light. These factors are important for bioprinting applications, as they can influence the material properties. For example, heating can reduce the viscosity and increase the flowability of some biomaterials. UV light can be used to crosslink some hydrogels.
- The research did not test the PCP with multi-material or hydrogel extrusion, which are important features for bioprinting applications. Multi-material extrusion can enable the fabrication of complex tissue constructs with heterogeneous composition and structure.
- The manufacturing process for the developed inner gear-actuated PCP was relatively simple, which may not achieve the precision attained used for conventional pumps. Therefore, it does not reflect the full performance of the concept.
- The surface finish of the pump may impact the bioprinting performance. A smooth surface is ideal for bioprinting, as it provides a good surface for the cells to enable viability.
- While the Mf pump met several key PDS, it did not meet the specifications of the scalable minimum dispensing amount and scalable cartridge volume. These limitations

could impact the versatility and adaptability of the pump for different application requirements. Further improvements and refinements in the design of the pump and functionality are needed to fully meet all the outlined specifications.

9.4 Recommendations for Future Research

The research also suggests some possible ways to improve or extend the study in the future. These are as follows:

- One direction can be to prototype inner gear-actuated PCP using precision manufacturing to see the full potential of the developed concept. This would require the following:
  - Optimise the design parameters of the PCP, such as the number of lobes, the cross-sectional geometry, the eccentricity and the clearance, to achieve maximum efficiency and minimum leakage.
  - Test the performance of the PCP with different materials, such as hydrogels, cells and pastes, to evaluate its versatility and compatibility for EBB applications.
  - Integrate the PCP with a multi-material extrusion system that can handle multiple syringes and nozzles.
  - Validate the functionality and reliability of the PCP-based extrusion system by printing complex 3D structures with various materials and evaluating their morphology, mechanical properties and biological performance.
- Another route for exploration can be prototyping a disposable PCP, especially for sterilisation-required bioprinting. This can be accomplished by mass-producing the inner gear-actuated PCP concept through injection moulding and elastomer coating. The reason for using disposable components in bioprinting is to address critical concerns about cell viability and cost. Using injection moulding ensures precise and uniform production of the PCP. The elastomer coating provides a compressible surface for the rotor or stator, resulting in a fully sealed PCP.
- Optimising the PCP parameters, such as rotor and stator geometry, size, and number of lobes, to improve accuracy and resolution depending on the application. This would

require developing a mathematical model or a control system to predict and adjust the PCP design according to the desired extrusion process characteristics.

- Integrating heating and UV light into the PCP design to enhance functionality. These factors are important for bioprinting applications, as they can influence the material properties. For example, heating can reduce the viscosity and increase the flowability of some biomaterials, and UV light can be used to crosslink some hydrogels.

REFERENCES

3D-Benchy (2016), 'About'. Available at: http://www.3dbenchy.com/about/ (Accessed: 20 June 2021).

Aage, N., Donaldson, J., Feng, Y., Y, G., Grann, H., Gravesen, J., Hlod, A., Steenstrup, T., Larsen, A. A., Malakpoor, K., Markvorsen, S. and Moreno, D. (2006), 'Mathematical problems for Moineau pumps'.

Abas, M., Naeem, K., Habib, T., Khan, I., Farooq, U., Khalid, Q. S. and Rahman, K. (2021), 'Development of prediction model for conductive pattern lines generated through positive displacement microdispensing system using artificial neural network', *Arabian Journal for Science and Engineering* **46**(3), 2429–2442.

Al-Safran, E., Aql, A. and Nguyen, T. (2017), 'Analysis and Prediction of Fluid Flow Behavior in Progressing Cavity Pumps', *Journal of Fluids Engineering* **139**(12), 121102.

Autodesk (2018), 'Moineau | fusion 360 | autodesk app store'. Available at: https://tinyurl.com/2tmhen3u (Accessed: 12 August 2021).

Banović, L. and Vihar, B. (2018), 'Development of an Extruder for Open Source 3D Bioprinting', *Journal of Open Hardware* **2**(1).

Belcher, I. (1991), An investigation into the operating characteristics of the progressive cavity pump, PhD thesis, Cranfield Institute of Technology.

Bessler, N., Ogiermann, D., Buchholz, M.-B., Santel, A., Heidenreich, J., Ahmmed, R., Zaehres, H. and Brand-Saberi, B. (2019), 'Nydus One Syringe Extruder (NOSE): A Prusa i3 3D printer conversion for bioprinting applications utilizing the FRESH-method', *HardwareX* **6**, e00069.

Blaeser, A., Duarte Campos, D. F., Puster, U., Richtering, W., Stevens, M. M. and Fischer, H. (2016), 'Controlling shear stress in 3D bioprinting is a key factor to balance printing resolution and stem cell integrity', *Advanced healthcare materials* **5**(3), 326–333.

Boehm, B. W. (1988), 'A spiral model of software development and enhancement', *Computer* **21**(5), 61–72.

Boland, T., Xu, T., Damon, B. and Cui, X. (2006), 'Application of inkjet printing to tissue engineering', *Biotechnology Journal: Healthcare Nutrition Technology* **1**(9), 910–917.

Booeshaghi, A. S., da Veiga Beltrame, E., Bannon, D., Gehring, J. and Pachter, L. (2019), 'Principles of open source bioinstrumentation applied to the poseidon syringe pump system', *Scientific reports* **9**(1), 1–8.

Buj-Corral, I., Bagheri, A. and Sivatte-Adroer, M. (2021), 'Effect of printing parameters on dimensional error, surface roughness and porosity of fff printed parts with grid structure', *Polymers* **13**(8), 1213.

Calvert, P. (2001), 'Inkjet printing for materials and devices', *Chemistry of materials* **13**(10), 3299–3305.

Canessa, E., Baruzzo, M. and Fonda, C. (2017), 'Study of moineau-based pumps for the volumetric extrusion of pellets', *Additive Manufacturing* **17**, 143–150.

Chen, X. B. and Kai, J. (2004), 'Modeling of positive-displacement fluid dispensing processes', *IEEE transactions on electronics packaging manufacturing* **27**(3), 157–163.

Chua, C. K. and Yeong, W. Y. (2014), *Bioprinting: principles and applications*, Vol. 1, World Scientific Publishing Co Inc.

Crump, S. S. (1992), 'Apparatus and method for creating three-dimensional objects'. US Patent no. US5121329A.

CustomPartNet (2008*a*), 'Inkjet printing process'. Available at: https://tinyurl.com/y7v3css7 (Accessed: 29 May 2022).

CustomPartNet (2008*b*), 'Stereolithography'. Available at: https://tinyurl.com/5n944kyz (Accessed: 29 May 2022).

Dababneh, A. B. and Ozbolat, I. T. (2014), 'Bioprinting technology: a current state-of-the-art review', *Journal of Manufacturing Science and Engineering* **136**(6), 61016.

Duet3D (2020), 'Duet 2 wifi/ethernet hardware overview'. Available at: https://tinyurl.com/y3h9hukx (Accessed: 12 July 2020).

ELPRO (2023*a*), 'Valve control for eco-pen series - eco-control ec200 2.0'. Available at: https://tinyurl.com/5n6ns5za (Accessed: 26 September 2023).

ELPRO (2023*b*), 'Volume dispenser up to 1,5 ml/min'. Available at: https://tinyurl.com/5694hhu4 (Accessed: 26 September 2023).

Fedorovich, N. E., Schuurman, W., Wijnberg, H. M., Prins, H.-J., Van Weeren, P. R., Malda, J., Alblas, J. and Dhert, W. J. (2012), 'Biofabrication of osteochondral tissue equivalents by printing topologically defined, cell-laden hydrogel scaffolds', *Tissue Engineering Part C: Methods* **18**(1), 33–44.

Ferreira, A. G., Egas, A. P., Fonseca, I. M., Costa, A. C., Abreu, D. C. and Lobo, L. Q. (2017), 'The viscosity of glycerol', *The Journal of Chemical Thermodynamics* **113**, 162–182.

Fisch, P., Holub, M. and Zenobi-Wong, M. (2020), 'Improved accuracy and precision of bioprinting through progressive cavity pump-controlled extrusion', *Biofabrication* **13**(1), 015012.

Gamboa, J., Aurelio, O. and Sorelys, E. (2003), 'New approach for modeling progressive cavity pumps performance', *SPE annual technical conference and exhibition* .

Gelber, M. K. (2015), 'Precision hot-melt freeform 3d printing for monolithic multilayer microfluidics', *PhD Thesis, University of Illinois at Urbana-Champaign* .

Gravesen, J. (2008), 'The geometry of the Moineau pump', *Computer Aided Geometric Design* **25**(9), 792–800.

Guillotin, B. and Guillemot, F. (2011), 'Cell patterning technologies for organotypic tissue fabrication', *Trends in biotechnology* **29**(4), 183–190.

He, Y., Yang, F., Zhao, H., Gao, Q., Xia, B. and Fu, J. (2016), 'Research on the printability of hydrogels in 3d bioprinting', *Scientific reports* **6**(1), 1–13.

Hinton, T. J. (2016*a*), 'Replistruder v2'. Available at: https://tinyurl.com/3xu9tep5 (Accessed: 17 June 2021).

Hinton, T. J. (2016*b*), 'Replistruder v2.5 syringe pump extruder'. Available at: https://tinyurl.com/2p93t4wa (Accessed: 17 June 2021).

Hinton, T. J. (2018), 'Replistruder v3.0'. Available at: https://tinyurl.com/3ayy2wr9 (Accessed: 17 June 2021).

Hinton, T. J., Jallerat, Q., Palchesko, R. N., Park, J. H., Grodzicki, M. S., Shue, H.-J., Ramadan, M. H., Hudson, A. R. and Feinberg, A. W. (2015), 'Three-dimensional printing of complex biological structures by freeform reversible embedding of suspended hydrogels', *Science advances* **1**(9), e1500758.

Hutmacher, D. W., Sittinger, M. and Risbud, M. V. (2004), 'Scaffold-based tissue engineering: rationale for computer-aided design and solid free-form fabrication systems', *TRENDS in Biotechnology* **22**(7), 354–362.

ISO/ASTM) (2015), *Additive manufacturing — General principles — Terminology*, ISO/ASTM 52900:2015 edn.

ISO/ASTM (2021), *Additive manufacturing — General principles — Fundamentals and vocabulary*, ISO/ASTM 52900:2021 edn.

Jisc (n.d.), 'Online surveys'. Available at: https://www.onlinesurveys.ac.uk/ (Accessed: 27 January 2019).

Karassik, I. J., Messina, J. P., Cooper, P. and Heald, C. C. (2001), *Pump handbook*, Vol. 3, McGraw-Hill New York.

Karyappa, R. and Hashimoto, M. (2019), 'chocolate-based ink three-dimensional Printing (Ci3DP)', *Scientific reports* **9**(1), 1–11.

Kawecki, F., Clafshenkel, W. P., Auger, F. A., Bourget, J.-M., Fradette, J. and Devillard, R. (2018), 'Self-assembled human osseous cell sheets as living biopapers for the laser-assisted bioprinting of human endothelial cells', *Biofabrication* **10**(3), 035006.

Khademhosseini, A., Langer, R., Borenstein, J. and Vacanti, J. P. (2006), 'Microscale technologies for tissue engineering and biology', *Proceedings of the National Academy of Sciences* **103**(8), 2480–2487.

Khalil, S., Nam, J. and Sun, W. (2005), 'Multi-nozzle deposition for construction of 3D biopolymer tissue scaffolds', *Rapid Prototyping Journal* **11**(1), 9–17.

Khoeini, R., Nosrati, H., Akbarzadeh, A., Eftekhari, A., Kavetskyy, T., Khalilov, R., Ahmadian, E., Nasibova, A., Datta, P., Roshangar, L. et al. (2021), 'Natural and synthetic bioinks for 3d bioprinting', *Advanced NanoBiomed Research* **1**(8), 2000097.

Klar, V., Pearce, J. M., Kärki, P. and Kuosmanen, P. (2019), 'Ystruder: Open source multifunction extruder with sensing and monitoring capabilities', *HardwareX* **6**, e00080.

Kumar, H. and Kim, K. (2020), 'Stereolithography 3d bioprinting', pp. 93–108.

Kumke, M., Watschke, H. and Vietor, T. (2016), 'A new methodological framework for design for additive manufacturing', *Virtual and physical prototyping* **11**(1), 3–19.

Langer, R. and Vacanti, J. P. (1993), 'Tissue engineering', *Science* **260**(5110), 920–926.

Leberfinger, A. N., Ravnic, D. J., Dhawan, A. and Ozbolat, I. T. (2017), 'Concise review: bioprinting of stem cells for transplantable tissue fabrication', *Stem cells translational medicine* **6**(10), 1940–1948.

Li, J., Chen, M., Fan, X. and Zhou, H. (2016), 'Recent advances in bioprinting techniques: approaches, applications and future prospects', *Journal of translational medicine* **14**(1), 1–15.

Li, W. (2019), 'Freeform extrusion fabrication of advanced ceramics and ceramic-based composites'.

Li, W., Ghazanfari, A., Leu, M. C. and Landers, R. G. (2017), 'Extrusion-on-demand methods for high solids loading ceramic paste in freeform extrusion fabrication', *Virtual and Physical Prototyping* **12**(3), 193–205.

Ligon, S. C., Liska, R., Stampfl, J., Gurr, M. and Muulhaupt, R. (2017), 'Polymers for 3d printing and customized additive manufacturing', *Chemical reviews* **117**(15), 10212–10290.

Malda, J., Visser, J., Melchels, F. P., Jüngst, T., Hennink, W. E., Dhert, W. J. A., Groll, J. and Hutmacher, D. W. (2013), '25th anniversary article: engineering hydrogels for biofabrication', *Advanced Materials* **25**(36), 5011–5028.

Mandrycky, C., Wang, Z., Kim, K. and Kim, D.-H. (2016), '3D bioprinting for engineering complex tissues', *Biotechnology Advances* **34**(4), 422–434.

Microsoft (n.d.), 'Skype technologies'. Available at: https://www.skype.com/ (Accessed: 5 February 2019).

Moineau, R. (1930), A new capsulism, PhD thesis, Doctoral Thesis. The University of Paris.

Mondschein, R. J., Kanitkar, A., Williams, C. B., Verbridge, S. S. and Long, T. E. (2017), 'Polymer structure-property requirements for stereolithographic 3d printing of soft tissue engineering scaffolds', *Biomaterials* **140**, 170–188.

Murphy, S. V. and Atala, A. (2014), '3d bioprinting of tissues and organs', *Nature biotechnology* **32**(8), 773–785.

Murphy, S. V., Skardal, A. and Atala, A. (2013), 'Evaluation of hydrogels for bio-printing applications', *Journal of Biomedical Materials Research Part A* **101**(1), 272–284.

Naghieh, S. and Chen, X. (2021), 'Printability–a key issue in extrusion-based bioprinting', *Journal of Pharmaceutical Analysis* **11**(5), 564–579.

Nair, K., Gandhi, M., Khalil, S., Yan, K. C., Marcolongo, M., Barbee, K. and Sun, W. (2009), 'Characterization of cell viability during bioprinting processes', *Biotechnology Journal: Healthcare Nutrition Technology* **4**(8), 1168–1177.

Nakamura, M., Kobayashi, A., Takagi, F., Watanabe, A., Hiruma, Y., Ohuchi, K., Iwasaki, Y., Horie, M., Morita, I. and Takatani, S. (2005), 'Biocompatible inkjet printing technique for designed seeding of individual living cells', *Tissue engineering* **11**(11-12), 1658–1666.

Nguyen, K., Nguyen, T. and Al-Safran, E. (2021), 'Modeling the performance of progressive cavity pump under downhole conditions', *Journal of Petroleum Science and Engineering* **198**, 108121.

Nguyen, T. (2020), *Artificial Lift Methods: Design, Practices, and Applications*, Springer Nature.

Nguyen, T., Al-Safran, E., Saasen, A. and Nes, O.-M. (2014), 'Modeling the design and performance of progressing cavity pump using 3-d vector approach', *Journal of Petroleum Science and Engineering* **122**, 180–186.

Nordson (2020), 'How does a progressive cavity pump work?'. Available at: https://tinyurl.com/mvz537x4 (Accessed: 23 January 2022).

Ojama, H. (2022), 'Visco bio-tulostuspään käyttöönotto ja testaus'.

Ooznest (2022), 'Nema17 stepper motors'. Available at: https://tinyurl.com/mtbd9x2u (Accessed: 17 May 2022).

Ozbolat, I. T. (2015), 'Bioprinting scale-up tissue and organ constructs for transplantation', *Trends in biotechnology* **33**(7), 395–400.

Ozbolat, I. T. and Hospodiuk, M. (2016), 'Current advances and future perspectives in extrusion-based bioprinting', *Biomaterials* **76**, 321–343.

Ozbolat, I. T., Moncal, K. K. and Gudapati, H. (2017), 'Evaluation of bioprinter technologies', *Additive Manufacturing* **13**, 179–200.

Park, E.-K. and Song, K.-W. (2010), 'Rheological evaluation of petroleum jelly as a base material in ointment and cream formulations: steady shear flow behavior', *Archives of pharmacal research* **33**(1), 141–150.

Paxton, N., Smolan, W., Böck, T., Melchels, F., Groll, J. and Jungst, T. (2017), 'Proposal to assess printability of bioinks for extrusion-based bioprinting and evaluation of rheological properties governing bioprintability', *Biofabrication* **9**(4), 044107.

Peltola, S. M., Melchels, F. P. W., Grijpma, D. W. and Kellomäki, M. (2008), 'A review of rapid prototyping techniques for tissue engineering purposes', *Annals of medicine* **40**(4), 268–280.

Pradel, P., Campbell, R. I. and Bibb, R. (2019), 'When design never ends - a future scenario for product developement', *Proceedings of the Design Society: International Conference on Engineering Design* **1**(1), 829–838.

Pradel, P., Zhu, Z., Bibb, R. and Moultrie, J. (2018), 'A framework for mapping design for additive manufacturing knowledge for industrial and product design', *Journal of Engineering Design* **29**(6), 291–326.

Preeflow (2023*a*), 'Preeflow datasheet'. Available at: http://tinyurl.com/3a9drhpy (Accessed: 26 December 2023).

Preeflow (2023*b*), 'Spare parts lists eco-pen300'. Available at: http://tinyurl.com/bd25n3fp (Accessed: 26 December 2023).

Pusch, K., Hinton, T. J. and Feinberg, A. W. (2018), 'Large volume syringe pump extruder for desktop 3d printers', *HardwareX* **3**, 49–61.

Ramadan, Q. and Zourob, M. (2021), '3d bioprinting at the frontier of regenerative medicine, pharmaceutical, and food industries', *Frontiers in Medical Technology* **2**, 607648.

Raman, R., Bhaduri, B., Mir, M., Shkumatov, A., Lee, M. K., Popescu, G., Kong, H. and Bashir, R. (2016), 'High-resolution projection microstereolithography for patterning of neovasculature', *Advanced healthcare materials* **5**(5), 610–619.

Raval, A. D. and Patel, C. (2022), 'Estimation of interface friction and concrete boundary layer for 3d printable concrete pumping', *Materials Today: Proceedings* **57**, 664–669.

Samokhin, A. S. (2020), 'Syringe Pump Created using 3D Printing Technology and Arduino Platform', *Journal of Analytical Chemistry* **75**, 416–421.

Sarcar, M., Rao, K. M. and Narayan, K. L. (2008), *Computer aided design and manufacturing*, PHI Learning Pvt. Ltd.

Sensirion (2021), 'Slf3s-0600f liquid flow sensor datasheet'. Available at: https://tinyurl.com/2hfj745a (Accessed: 18 November 2022).

Shakor, P., Nejadi, S. and Paul, G. (2019), 'A study into the effect of different nozzles shapes and fibre-reinforcement in 3d printed mortar', *Materials* **12**(10), 1708.

Shigley, J. E. (2011), *Shigley's mechanical engineering design*, Tata McGraw-Hill Education.

Shih, R. (2013), *Parametric Modeling with Autodesk Inventor 2014*, Sdc Publications.

Simontacchi, P., Blasi, R., Edeline, E., Sagnier, S., Ravier, N., Espinosa-Ramos, A., Breteau, J. and Altenhoefer, P. (2019), 'Prometheus: Precursor of new low-cost rocket engine family'.

Skalak, R. and Fox, C. F. (1988), *Tissue engineering: proceedings of a workshop, held at Granlibakken, Lake Tahoe, California, February 26-29, 1988*, Vol. 107, Alan R. Liss.

Suntornnond, R., Tan, E., An, J. and Chua, C. (2016), 'A Mathematical Model on the Resolution of Extrusion Bioprinting for the Development of New Bioinks', *Materials* **9**(9), 756.

Swanson, W., Turley, P., Leavitt, P., Karwoski, P., LaBossiere, J. and Skubic, R. (1999), 'High temperature modeling apparatus'. US Patent no. US6722872B1.

Tashman, J. W., Shiwarski, D. J. and Feinberg, A. W. (2021), 'A high performance open-source syringe extruder optimized for extrusion and retraction during FRESH 3D bioprinting', *HardwareX* **9**, e00170.

Thompson, M. K., Moroni, G., Vaneker, T., Fadel, G., Campbell, R. I., Gibson, I., Bernard, A., Schulz, J., Graf, P., Ahuja, B. and Martina, F. (2016), 'Design for additive manufacturing: Trends, opportunities, considerations, and constraints', *CIRP Annals* **65**(2), 737–760.

Ullman, D. (2009), *The Mechanical Design Process*, McGraw Hill.

Ullman, D. G. (1992), *The mechanical design process*, Vol. 2, McGraw-Hill New York.

Ulrich, K. T. and Eppinger, S. D. (2016), *Product design and development*, McGraw-hill.

Verbruggen, D. (2014), 'The road to better paste extrusion', *RepRap magazine* **3**, 26–29.

Viscotec (2016), '3d printing of abrasive materials'. Available at: https://tinyurl.com/5ynw2x74 (Accessed: 18 September 2022).

ViscoTec Pumpen- u. Dosiertechnik GmbH (2022), '3D Bioprinting with Alginate', *adhesion ADHESIVES + SEALANTS* **19**(1), 28–29.

Wang, G., Yao, L., Wang, W., Ou, J., Cheng, C.-Y. and Ishii, H. (2016), Xprint: A modularized liquid printer for smart materials deposition, *in* 'Proceedings of the 2016 CHI Conference on Human Factors in Computing Systems', CHI '16, Association for Computing Machinery, New York, NY, USA, p. 5743–5752.

Webb, B. and Doyle, B. J. (2017), 'Parameter optimization for 3D bioprinting of hydrogels', *Bioprinting* **8**, 8–12.

Weisstein, E. W. (2003), 'Hypocycloid', *https://mathworld. wolfram. com/* .

Wüst, S., Müller, R. and Hofmann, S. (2011), 'Controlled positioning of cells in biomaterials—approaches towards 3d tissue printing', *Journal of functional biomaterials* **2**(3), 119–154.

Xu, T., Binder, K. W., Albanna, M. Z., Dice, D., Zhao, W., Yoo, J. J. and Atala, A. (2012), 'Hybrid printing of mechanically and biologically improved constructs for cartilage tissue engineering applications', *Biofabrication* **5**(1), 015001.

Yahyaabadi, A., Driedger, M., Turenne, N., Connell, S., Parthasarathy, V., Carvey, A., Platero, V., Campos, J., Rososhansky, M. and Ferguson, P. (2020), 'Manitobasat-1: a novel approach for technology advancement', *IEEE potentials* **39**(4), 17–23.

Yang, S. and Zhao, Y. F. (2015), 'Additive manufacturing-enabled design theory and methodology: a critical review', *The International Journal of Advanced Manufacturing Technology* **80**, 327–342.

Yao, L., Ou, J., Wang, G., Cheng, C.-Y., Wang, W., Steiner, H. and Ishii, H. (2015), 'bioprint: A liquid deposition printing system for natural actuators', *3D Printing and Additive Manufacturing* **2**(4), 168–179.

Yeh, Y. C., Yamada, N., Watanabe, Y., Shiblee, M. N. I., Ogawa, J., Khosla, A., Kawakami, M., Akamatsu, T. and Furukawa, H. (2020), '(invited) 3d printing of soft-matter mono pump in infant ventricular assist device (VAD) for blood pumping', *ECS Transactions* **98**(13), 31–38.

Ying, G., Jiang, N., Yu, C. and Zhang, Y. S. (2018), 'Three-dimensional bioprinting of gelatin methacryloyl (gelma)', *Bio-Design and Manufacturing* **1**, 215–224.

Yue, K., Trujillo-de Santiago, G., Alvarez, M. M., Tamayol, A., Annabi, N. and Khademhosseini, A. (2015), 'Synthesis, properties, and biomedical applications of gelatin methacryloyl (gelma) hydrogels', *Biomaterials* **73**, 254–271.

Appendix 1: API code

```
# Author-Yusuf Furkan Ugurluoglu based on Cerambotics' code
import adsk.core
import adsk.fusion
import traceback
import math

defaultPartName = "Stator"
defaultLobes = 3
defaultGeneratorRadius = 0.16
defaultTolerance = 0.01
defaultCuspDiameter = 0.40
defaultMinorDiameter = 6.0
defaultTurns = 1.0
defaultHeight = 3.0
defaultPointNum = 80
defaultPosition = (0.0, 0.0, 0.0, math.pi / 6)

# global set of event handlers to keep them referenced for the
# duration of the command
handlers = []
app = adsk.core.Application.get()
if app:
    ui = app.userInterface

newComp = None


def createNewComponent():
    # Get the active design.
    product = app.activeProduct
    design = adsk.fusion.Design.cast(product)
    rootComp = design.rootComponent
    allOccs = rootComp.occurrences
    newOcc = allOccs.addNewComponent(adsk.core.Matrix3D.create())
    return newOcc.component


class PCPCommandExecuteHandler(adsk.core.CommandEventHandler):
    def __init__(self):
        super().__init__()

    def notify(self, args):
        try:
            unitsMgr = app.activeProduct.unitsManager
            command = args.firingEvent.sender
            inputs = command.commandInputs

            stator = Part()
            stator.partName = "Stator"
            for input in inputs:
                if input.id == "lobes":
```

```
                    stator.lobes = input.value
                elif input.id == "generatorRadius":
                    stator.generatorRadius = unitsMgr.evaluateExpression(
                        input.expression, "mm"
                    )
                elif input.id == "Tolerance":
                    Tolerance = unitsMgr.evaluateExpression(input.expression, "mm")
                elif input.id == "cuspDiameter":
                    stator.cuspDiameter = unitsMgr.evaluateExpression(
                        input.expression, "mm"
                    )
                elif input.id == "turns":
                    stator.turns = input.value
                # elif input.id == "pointNum":
                #     stator.pointNum = input.value
                elif input.id == "height":
                    stator.height = unitsMgr.evaluateExpression(input.expression, "mm")
                stator.position = (0, 0, 0, math.pi / stator.lobes / 2.0)
            stator.drawCylinder = True
            stator.build()
            # args.isValidResult = True

            rotor = Part()
            rotor.partName = "Rotor"
            rotor.lobes = stator.lobes - 1
            # rotor.pointNum = stator.pointNum
            rotor.turns = stator.lobes * stator.turns / rotor.lobes
            rotor.generatorRadius = stator.generatorRadius
            rotor.height = stator.height
            rotor.cuspDiameter = stator.cuspDiameter - Tolerance
            rotor.position = (
                stator.generatorRadius,
                0,
                0,
                math.pi / stator.lobes / 2.0,
            )
            rotor.build()

            args.isValidResult = True

        except:
            if ui:
                ui.messageBox("Failed:\n{}".format(traceback.format_exc()))


# %%
class PCPCommandDestroyHandler(adsk.core.CommandEventHandler):
    def __init__(self):
        super().__init__()

```

```
    def notify(self, args):
        try:
            # when the command is done, terminate the script
            # this will release all globals which will remove
            # all event handlers
            adsk.terminate()
        except:
            if ui:
                ui.messageBox("Failed:\n{}".format(traceback.
    format_exc()))


# %%
class PCPCommandCreatedHandler(adsk.core.CommandCreatedEventHandler):
    def __init__(self):
        super().__init__()

    def notify(self, args):
        try:
            cmd = args.command
            cmd.isRepeatable = False
            onExecute = PCPCommandExecuteHandler()
            cmd.execute.add(onExecute)
            onExecutePreview = PCPCommandExecuteHandler()
            cmd.executePreview.add(onExecutePreview)
            onDestroy = PCPCommandDestroyHandler()
            cmd.destroy.add(onDestroy)
            # keep the handler referenced beyond this function
            handlers.append(onExecute)
            handlers.append(onExecutePreview)
            handlers.append(onDestroy)

            # define the inputs
            inputs = cmd.commandInputs

            # Create Instructions group
            groupInstructions = inputs.addGroupCommandInput("group1",
    "Instructions")
            groupInstructions.isExpanded = False
            instructionsTextString = str(
                "Creates an extended hypocycloid based rotor and
    stator for progressive cavity pumps. "
            )

            instructionsText = groupInstructions.children.
    addTextBoxCommandInput(
                "instructions", "", instructionsTextString, 12, True
            )

            # user entered parameters
            groupEntries = inputs.addGroupCommandInput("group2", "
    Entered Parameters")
            groupEntries.isExpanded = True

            initLobes = adsk.core.ValueInput.createByReal(
    defaultLobes)
```

```
            lobeEntry = groupEntries.children.addIntegerSpinnerCommandInput(
                "lobes", "Stator Lobes", 2, 10, 1, defaultLobes
            )
            lobeEntry.tooltip = "At least 2, values greater than 10 may crash Fusion360"

            initGeneratorRadius = adsk.core.ValueInput.createByReal(
                defaultGeneratorRadius
            )
            majDEntry = groupEntries.children.addValueInput(
                "generatorRadius",
                "Generator Radius",
                "mm",
                initGeneratorRadius,
            )
            majDEntry.tooltip = "Controls the in plane size."
            initTolerance = adsk.core.ValueInput.createByReal(defaultTolerance)
            majDEntry = groupEntries.children.addValueInput(
                "Tolerance",
                "Tolerance",
                "mm",
                initTolerance,
            )
            majDEntry.tooltip = "Controls the in plane size."
            initCuspDiameter = adsk.core.ValueInput.createByReal(defaultCuspDiameter)
            cuspDEntry = groupEntries.children.addValueInput(
                "cuspDiameter", "Cusp Diameter", "mm", initCuspDiameter
            )
            cuspDEntry.tooltip = "Controls the in plane size."

            initTurns = adsk.core.ValueInput.createByReal(defaultTurns)
            TEntry = groupEntries.children.addValueInput(
                "turns", "Turns", "", initTurns
            )
            TEntry.tooltip = "Use negative values for LH pitch angle"

            initHeight = adsk.core.ValueInput.createByReal(defaultHeight)
            HEntry = groupEntries.children.addValueInput(
                "height", "Pump Height", "mm", initHeight
            )
            HEntry.tooltip = (
                "Adjust with lobes and turns to give the desired pitch angle"
            )

        except:
            if ui:
                ui.messageBox("Failed:\n{}".format(traceback.format_exc()))

```

```
199
200 # %%
201 class Part:
202     def __init__(self):
203         self._partName = defaultPartName
204         self._lobes = defaultLobes
205         self._generatorRadius = defaultGeneratorRadius
206         self._Tolerance = defaultTolerance
207         self._cuspDiameter = defaultCuspDiameter
208         self._height = defaultHeight
209         self._turns = defaultTurns
210         self._position = defaultPosition
211         self._drawCylinder = False
212         # self._pointNum = defaultPointNum
213
214     # properties
215     @property
216     def partName(self):
217         return self._partName
218
219     @partName.setter
220     def partName(self, value):
221         self._partName = value
222
223     @property
224     def generatorRadius(self):
225         return self._generatorRadius
226
227     @property
228     def R(self):
229         return self._generatorRadius
230
231     @generatorRadius.setter
232     def generatorRadius(self, value):
233         self._generatorRadius = value
234
235     @property
236     def cuspDiameter(self):
237         return self._cuspDiameter
238
239     @property
240     def D(self):
241         return self._cuspDiameter
242
243     @cuspDiameter.setter
244     def cuspDiameter(self, value):
245         self._cuspDiameter = value
246
247     @property
248     def majorDiameter(self):
249         return self.R * self.N + self.D
250
251     # @pointNum.setter
252     # def pointNum(self, value):
253     #     self._pointNum = value
254
```

```
    # @property
    # def pointNum(self):
    #     return self._pointNum

    @property
    def majorDiameter(self):
        return self.R * self.N + self.D

    @property
    def lobes(self):
        return self._lobes

    @property
    def N(self):
        return self._lobes

    @lobes.setter
    def lobes(self, value):
        self._lobes = value

    @property
    def height(self):
        return self._height

    @height.setter
    def height(self, value):
        self._height = value

    @property
    def position(self):
        return self._position

    @position.setter
    def position(self, value):
        self._position = value

    @property
    def turns(self):
        return self._turns

    @turns.setter
    def turns(self, value):
        self._turns = value

    @property
    def drawCylinder(self):
        return self._drawCylinder

    @drawCylinder.setter
    def drawCylinder(self, value):
        self._drawCylinder = value

    @property
    def isValid(self):
        valid = self.N > 1
        valid &= self.R > 0
```

```
        valid &= self.D > 0
        valid &= self.majorDiameter > 0
        # avoid N=3 overlapping trims of rotor
        # (where N=2 and cusp circles overlaps)
        valid &= self.R * self.N != self.D / 2.0
        valid &= (self.R * 10) > self.D
        # valid &= (self.pointNum / self.lobes) > 40
        valid &= self.height > self.R
        valid &= math.modulus(self.turns / int(self.turns)) == 0
        valid &= math.modulus(self.N / int(self.N)) == 0
        return valid

    def get_x_h(self, t):
        return (
            self.R * (self.N - 1) * math.cos(t)
            + self.R * math.cos((self.N - 1) * t)
            + self.position[0]
        )

    def get_y_h(self, t):
        return self.R * (self.N - 1) * math.sin(t) - self.R * math.
sin((self.N - 1) * t)

    def build(self):
        global newComp
        newComp = createNewComponent()
        newComp.name = self.partName

        if newComp is None:
            ui.messageBox("New component failed to create", "New
Component Failed")
            return

        # Set up cycloidal geometric parameters
        steps = defaultPointNum  # // self.lobes #int(self.pointNum /
 self.lobes)

        R = float(self.R)
        N = int(self.N)
        D = float(self.D)

        q = 2.0 * math.pi / (float(steps) * N)
        sweepAngle = self.turns * 360.0

        # Create a new sketch.
        sketches = newComp.sketches
        xyPlane = newComp.xYConstructionPlane
        xzPlane = newComp.xZConstructionPlane

        # Create path
        sketchVertical = sketches.add(xzPlane)
        sketchLines = sketchVertical.sketchCurves.sketchLines
        startPt = adsk.core.Point3D.create(
            self.position[0], self.position[2], self.position[1]
        )
        endPt = adsk.core.Point3D.create(
```

```
            self.position[0], self.position[2] - self.height, self.
position[1]
        )
        line1 = sketchLines.addByTwoPoints(startPt, endPt)
        path = newComp.features.createPath(line1)

        # Create point collection

        sketch = sketches.add(xyPlane)

        # Get the SketchCircles collection from an existing sketch.
        circles = sketch.sketchCurves.sketchCircles
        # Outer cylinder
        if self.drawCylinder:
            circles.addByCenterRadius(
                adsk.core.Point3D.create(0, 0, 0), self.majorDiameter
            )
        if self.N > 1:
            # Generate curve points
            for n in range(N):
                points = adsk.core.ObjectCollection.create()
                x0, y0 = None, None

                # print one lobe
                for i in range(0, steps):
                    t = (i + n * steps) * q
                    x_h = self.get_x_h(t)
                    y_h = self.get_y_h(t)
                    q = 2.0 * math.pi / (float(steps) * N)
                    try:
                        n_x = (
                            (D / 2)
                            * (math.cos(t) - math.cos((N - 1) * t))
                            / (math.sqrt(2) * math.sqrt(1 - math.cos(
N * t)))
                        )
                        n_y = (
                            (D / 2)
                            * (math.sin(t) + math.sin((N - 1) * t))
                            / (math.sqrt(2) * math.sqrt(1 - math.cos(
N * t)))
                        )

                        x = x_h + n_x
                        y = y_h + n_y

                        points.add(adsk.core.Point3D.create(x, y, 0))

                        if x0 is None or y0 is None:
                            x0 = x
                            y0 = y
                    except:
                        pass
                # Create spline section and profile
                crv = sketch.sketchCurves.sketchFittedSplines.add(
points)
```

```
                crv.isClosed = False

        for n in range(1, N + 1):
            c_x = self.get_x_h(q * (n * steps))
            c_y = self.get_y_h(q * (n * steps))

            circle = circles.addByCenterRadius(
                adsk.core.Point3D.create(c_x, c_y, 0), D / 2.0
            )
            if self.N > 1:
                trim_x = (R * N - D / 2.0) * math.cos(
                    q * ((n + 1) * steps)
                ) + self.position[0]
                trim_y = (R * N - D / 2.0) * math.sin(q * ((n + 1) *
steps))
                circle.trim(adsk.core.Point3D.create(trim_x, trim_y,
0))

        profile = sketch.profiles[0]

        # Sweep
        sweeps = newComp.features.sweepFeatures
        newSweep = adsk.fusion.FeatureOperations.
NewBodyFeatureOperation
        sweepInput = sweeps.createInput(profile, path, newSweep)
        sweepInput.orientation = (
            adsk.fusion.SweepOrientationTypes.
PerpendicularOrientationType
        )
        sweepInput.taperAngle = adsk.core.ValueInput.createByString("
0 deg")
        sweepInput.twistAngle = adsk.core.ValueInput.createByString(
            str(sweepAngle) + " deg"
        )
        sweep = sweeps.add(sweepInput)


# %%


def run(context):
    try:
        product = app.activeProduct
        design = adsk.fusion.Design.cast(product)
        if not design:
            ui.messageBox(
                "It is not supported in current workspace, please
change to MODEL workspace and try again."
            )
            return
        commandDefinitions = ui.commandDefinitions
        # check the command exists or not
        cmdDef = commandDefinitions.itemById("Rotor")
        if not cmdDef:
            cmdDef = commandDefinitions.addButtonDefinition(
                "Rotor", "Create PCP", "Create a PCP pump.", "./"
```

```
            )  # relative resource file path is specified

        onCommandCreated = PCPCommandCreatedHandler()
        cmdDef.commandCreated.add(onCommandCreated)
        # keep the handler referenced beyond this function
        handlers.append(onCommandCreated)
        inputs = adsk.core.NamedValues.create()
        cmdDef.execute(inputs)

        # prevent this module from being terminate when the script returns,
        # because we are waiting for event handlers to fire
        adsk.autoTerminate(False)
    except:
        if ui:
            ui.messageBox("Failed:\n{}".format(traceback.format_exc()))
```

Appendix 2:Polylactic Acid Filament Datasheet

FEATURES

- Tougher and less brittle compared to regular PLA
- Easy to print at low temperature
- Low warping
- Biodegradable unlike ABS filament – PLA is derived from crops such as corn and sugar cane
- Limited smell
- Good shelf life

RS PRO 2.85mm Black PLA 3D Printer Filament, 2.3kg

RS Stock No.: 125-4336

RS Professionally Approved Products bring to you professional quality parts across all product categories. Our product range has been tested by engineers and provides a comparable quality to the leading brands without paying a premium price.

Product Description

Poly Lactic Acid (PLA) is a biodegradable plastic made from renewable natural resources and one of the most popular materials for 3D printing. Plastics such as PLA are the most popular 3D printing material due to its simplicity, dimensional accuracy and low cost. PLA can be printed at a low temperature and does not require a heated bed and is one of the most environmentally friendly filaments available.

125-4336 - Black
125-4338 - White
125-4340 - Blue
125-4342 - Red
125-4344 - Silver

General Specifications

Printing Technology	FDM
Printing Material	PLA
Machine Specific	No
Colour	Black
For Use With	Common Desktop 3D Printers
Material Type	PLA
Application	General printing, Hobbyist Medical, Education, Prototyping,Jewellery,Architecture models, Aviation, Engineering, Automotive

Mechanical Specifications

Diameter	2.85mm
Weight	1kg
Specific gravity	1,24 g/cc
MFI	6,0 g/10 min
Tensile strength	110 MPa (MD) / 145 MPa (TD)
Elongation at break	160% (MD) / 100% (TD)
Tensile Modulus	3310 MPa (MD) / 3860 MPa (TD)
Impact strength	7,5 KJ/m²
Tolerance	± 0.10mm
Roundness	≥ 95%

Operation Environment Specifications

Printing Temperature	180 ˚C -210˚C
Melting Temperature	210˚C ± 10 ˚C
Melting Point	145 ˚C -160˚C
Vicat Softening Temperature	± 60˚C
Storage Temperature	15 ˚C -25˚C

Approvals

Compliance/Certifications	ASTM D1505, ASTM D882,ASTM D3418,IS0 306, 2011/65/EU and 2015/863